التصميم الأمثل للمنشآت اللوحيّة والقشريّة اعتماداً على التحليل اللا خطي بالعناصر المحدّدة

رسالة

مقدمة الى كلية الهندسة في جامعة بابل

كجزء من متطلبات نيل درجة ماجستير

في الهندسة المدنية

(الهندسة الإنشائية)

من قبل

حيدر مفيد عبد الحسين الصائغ

بكالوريوس هندسة مدنية

إشراف

أ. م. د. نمير عبد الأمير علوش

أ. م. د. عمّار ياسر علي

أيار ٢٠٠٥

بسم الله الرحمن الرحيم

ويسألونك عن الروح قل الروح من أمر ربي وما أوتيتم من العلم إلا قليلا

صدق الله العظيم

الخلاصة

هذا البحث معنيّ بالتصميم المرن-اللدن الأمثل للمنشآت اللو حيّة والقشريّة وبالاعتماد على التحليل المرن-اللدن اللاخطي هندسيا، باستخدام طريقة العناصر المحددة مع الطريقة التزايديّة التكراريّة. تم استخدام العنصر الطبقي المحني المكبوس ذي العقد التسع مع تحديد خمس درجات للحرية في كل عقدة متعلقة بالازاحات الثلاث ودورا نين للمتجه العمودي في كل عقدة. في حالة لاخطية المادّة، تم استخدام التحليل المرن-اللدن مع تعميم لقانون هوبر- ميسيز (Huber-Mises) كمحدد للخضوع.

تم استخدام تمثيل طبقي لتحديد شكل الاجهادات باتجاه السمك بواسطة مخطط للتكامل يتضمن قاعدة نقطة المنتصف لكل طبقة. درجات الحرية الدورانية ليست مرتبطة بميل السطح المنصّف، وعليه فان التشوه القصي بالاتجاه العرضي ليس مهملا بل تم أخذه بالتحليل. تم استخدام معامل تصحيح قص لتقريب طاقة الانفعال القصية العرضية.

اللاخطية الهندسية تم تمثيلها بواسطة مبدأ لاكرانج (Lagrange) الكلي المعروف. لقد تم العمل بصيغة لاكرانج الكلي وهي مناسبة بفرض هطول كبير مع دوران معتدل و بمنحى مشابه لفرضية فون كارمان (Von Karman).

في حالة الأمثلية الإنشائية و التي هي أمثلية مقيدة لا خطية، فقد تم استخدام طريقة هوك و جيفس (Hooke and Jeeves) المعدلة وباعتبار حجم المنشأ كدالة الهدف وأبعاده كمتغيرات التصميم مع قيود هندسية. التصميم اللدن أنجز باستخدام محدد فون ميسيز (Von Mises) للاذعان بدلالة محصلات الإجهاد مع إدخال تأثير القوّة المحورية.

العديد من الأمثلة المتعلقة بـ الألواح المطوية و القشريّات، والتي قد تمّ تحليلها سابقا من قبل باحثين آخرين، تمّ تحليلها باستخدام طريقة العناصر المحددة الحالية والنتائج أظهرت تقارب جيد و خاصة مع نتائج التجارب العملية ومع وجود فرق لا يتعدّى ٧٪. التصميم الأمثل للألواح المطوية و القشريات قد تمّ تناوله أيضا وبالاعتماد على تحليل خطّي ولا خطّي. لقد أظهرت النتائج بان التصميم الأمثل المعتمد على تحليل لا خطّي يعطي حجما أمثلا أقل من ذلك المعتمد على تحليل خطّي بمقدار(١-٢٥)%. إن هذه النسبة تختلف باختلاف التصرف الإنشائي لمنشآت الألواح والقشريات.

OPTIMAL DESIGN OF PLATE AND SHELL STRUCTURES BASED ON NONLINEAR FINITE ELEMENT ANALYSIS

A THESIS
SUBMITTED TO THE COLLEGE OF ENGINEERING
OF THE UNIVERSITY OF BABYLON
IN FULFILLMENT OF PARTIAL REQUIREMENTS
FOR THE DEGREE OF MASTER OF SCIENCE
IN
CIVIL ENGINEERING
(STRUCTURAL ENGINEERING)

BY
HAIDER MUFEED ABDUL-HUSSEIN AL-SAEQ
(B.Sc)

SUPERVISED BY

Asst. Prof. Dr. Nameer A. Alwash **Asst. Prof. Dr. Ammar Y. Ali**

MAY ٢٠٠٥

ABSTRACT

This research deals with the optimal elastic-plastic design of plate and shell structures based on elastic-plastic geometrically nonlinear incremental-iterative finite element analysis. The nine-node degenerated curved shell element is used in which five degrees of freedom are specified at each nodal point, which are three displacements and two rotations of the normal at the node. In the case of the material nonlinearity, an elastic-plastic analysis is employed using a generalization of Huber-Mises law as the yield criterion.

A layered model is employed to determine the stress profile through the thickness direction. A mid-point rule integration scheme is adopted for each layer. The rotational degrees of freedom are not related to the slope of the mid-surface, so transverse shear deformation is permitted and taken into account. A correction shear factor is introduced in order to approximate the transverse shear strain energy.

The formulation of the geometrical nonlinearity problem is carried out using the well-known total Lagrangian principle. A specific and suitable total Lagrangian formulation is adopted in which large deflections and moderate rotations (in the sense of the Von Karman hypothesis) are considered.

For the structural optimization problem, which is dealt with as a constrained nonlinear optimization, the so-called Modified Hooke and Jeeves method is employed by considering the volume of the structure as the objective function and dimensions as the design variables with geometrical constraints. A plastic design is carried out using the Von-Mises yield criterion in terms of stress resultants with the effect of axial force being incorporated.

Several examples for the analysis of folded plates and shells, those analyzed previously by others, are worked out using the present finite

element analysis and the results show good agreement especially with experimental works with maximum difference of ٧٪. Optimal design of folded plates and shells are also carried out based on linear and nonlinear analysis. The results show that the optimal design based on nonlinear analysis gives optimal volume smaller than that based on linear analysis by amount (١-٢٥) %. This ratio differs with the different structural behaviour of plates and shells.

ACKNOWLEDGMENT

First of all, Praise to ALLAH, lord of the whole creation

I would like to express my deepest thanks and appreciation to my supervisors **Dr. Nameer A. Alwash** and **Dr. Ammar Y. Ali** for their valuable suggestions, encouragement, time and kind support at every stage of this work, without their help, this mission would not have been accomplished.

Also I wish to thank my parents for their constant support, assistance and understanding.

I extent my thanks to the staff of Civil Engineering Department and Internet Centre at University of Babylon. Special thanks to my cousin Hasanain and friends Hasanain and Ihsan for their aid. Finally, I would like to thank all friends and colleagues who helped in this work.

HAIDER,
MAY ٢٠٠٥

NOTATION

Symbol	Description
a	Flow vector
A	Hardening parameter
$\{a\}_i^n$	Displacement field at nth increment in the ith iteration
$\bar{a}_{ij}$	Anisotropic parameters in the flow vector **a**
b_i	Bound of the *i*th constraint
$\mathbf{b_i}$	*i*th base point
$[B]$	Strain- nodal variables matrix
$[B]_L$	Nonlinear part of $[B]$ matrix
$[B]_o$	Infinitesimal part of $[B]$ matrix
$[D]$	Elastic constitutive matrix
$\{d\}$	Nodal displacements vector
$d\{\delta\}$	Displacement variation
$d\lambda$	A non-negative scalar
$[D]_{ep}$	Elastoplastic constitutive matrix
$d\varepsilon$	Total strain increment
$d\varepsilon'$	Elastic strain increment
$d\varepsilon^p$	Plastic strain increment
$d\bar{\sigma}$	Effective stress increment
$d\bar{\varepsilon}_p$	Effective strain increment
E_1	Young's modulus in the ١ direction
E_2	Young's modulus in the ٢ direction
$\mathbf{e_i}$	Unit vector in the direction of the i-axis
E_{sh}	Initial slope of strain hardening region
E_x	Young's modulus in the x-direction
E_y	Young's modulus in the y-direction
$\{f\}^n$	External applied force vector in the nth increment
$f(x_1, x_2, \ldots)$	Objective function
$f(\mathbf{b_i})$	Objective function at the *i*th base point
$f(\sigma)$	Yield function
G_{12}	Shear modulus in the ١-٢ plane
G_{13}	Shear modulus in the ١-٣ plane
G_{23}	Shear modulus in the ٢-٣ plane
g_i	*i*th constraint
h	Step length

H	Height
h^k	Thickness of shell in ζ direction at nodal point k
H'	Hardening parameter
i, j	Unit vectors along the x, y-directions
$[J]$	Jacobian matrix
K_1	Shear correction factor in the ۱-۳ plane
K_2	Shear correction factor in the ۲-۳ plane
$[K]_{i-1}^{n}$	Tangential stiffness matrix at the beginning of the ith iteration in the nth increment
$[K]_{o}^{o}$	Initial stiffness matrix
$[K]_{1}^{n}$	Tangential stiffness matrix after the first iteration in the nth increment
$[\overline{K}]$	Tangential stiffness matrix for geometrically nonlinear problem
$[K]_{\sigma}$	Geometric stiffness matrix
L	Total number of layers
M_p	Plastic moment
M'_p	Changed plastic moment
M_x	Moment about y-axis
M_{xy}	Torsion in the x-y plane
M_y	Moment about x-axis
N_p	Squash load
$N^k(\xi,\eta)$	Two-dimensional interpolation function corresponding to node k
N_x	Axial force in the x-direction
N_y	Axial force in the y-direction
$\{p\}^n$	Equivalent internal force vector in the nth increment
$\mathbf{P_i}$	*i*th pattern point
Q	Potential of plastic flow
R	Radius of curvature, Radius of shell
r'	Radial distance
S	Elastic section modulus in beam
t	Thickness
u	Displacement in global x-direction
$u_{i,mid}^{k}$	*i*th component of the displacement of node k
$(u_i)_{\beta_1^k}$	*i*th component of displacement at node k resulting from β_1^k rotation
$(u_i)_{\beta_2^k}$	*i*th component of displacement at node k resulting from β_2^k rotation
u_{oi}^{k}	Displacement of the *k*th nodal point in the Cartesian coordinates
u'	Displacement in local x'-direction
v	Displacement in global y-direction

V_1, V_2, V_3	Unit vectors along the x', y', z' axes normalised from V_1', V_2', V_3' respectively.
V_1^k, V_2^k, V_3^k	Nodal Cartesian coordinate system at node k
V_{3i}^k	*i*th component of the unit normal vector to the middle surface at node k
v'	Displacement in local y'-direction
w	Displacement in global z-direction
w'	Displacement in local z'-direction
x, y, z	Global Cartesian coordinate system
x', y', z'	Local Cartesian coordinate system
x_1^*, x_2^*	Coordinates of the optimum point
$\bar{x}_i^k$	*i*th component of the global Cartesian coordinate in the direction of V_3^k vector at node k
$x_{i,mid}^k$	*i*th component of the global Cartesian coordinate system of node k
x_j	*j*th design variable
$x_{i,top}^k$	*i*th component of global x_i coordinate at top of node k
$x_{i,bot}^k$	*i*th component of global x_i coordinate at bottom of node k
Z	Plastic section modulus in beam
α_{ij}	Anisotropic parameters in general Huber-Mises yield function
$\bar{\alpha}_{ij}$	Anisotropic parameters in Huber-Mises yield function with $\sigma_3 = 0$
β_1^k	Rotation about V_2^k vector
β_2^k	Rotation about V_1^k vector
χ	Curvature
χ_y	Curvature at which the yield starts
$\Delta\{a\}_i^n$	Displacement change occurring during the *i*th iteration in the nth increment
$\Delta\zeta^i$	Thickness of *i*th layer in the natural coordinate system
Δh_j	Thickness of the *j*th layer
Δx_i^k	Difference between top and bottom for the *i*th component of global coordinates at node k
δ_1^k	Displacement in the V_1^k-direction
δ_2^k	Displacement in the V_2^k-direction
δx	Length of infinitesimal segment
ζ^i	ζ-coordinate at center of the *i*th layer
ε'	Total strain vector
ε_f'	In-plane strain
ε_s'	Transverse shear strain
$\{\varepsilon\}_o$	Linear contribution to the strain vector

$\{\varepsilon\}_L$	Nonlinear contribution to the strain vector
$\varepsilon_{x'}$	Axial strain in the local x' direction
$\varepsilon_{y'}$	Axial strain in the local y' direction
ξ, η, ζ	Natural coordinate system
$\gamma_{x'y'}$	Shearing strain in the local $x' - y'$ plane
$\gamma_{x'z'}$	Shearing strain in the local $x' - z'$ plane
$\gamma_{y'z'}$	Shearing strain in the local $y' - z'$ plane
υ_{12}	Poisson's ratio in the ١-٢ plane
υ_{21}	Poisson's ratio in the ٢-١ plane
$\{\psi\}_i^n$	Residual forces in the nth increment at the ith iteration
$\sigma_1, \sigma_2, \sigma_3$	Principal stresses
$\{\sigma\}^n$	Current stress field satisfying the yield condition
$\bar{\sigma}$	Effective stress
σ^i	Stress at the middle of the *i*th layer
σ_{uts}	Ultimate tensile stress
σ_{Yu}	The upper yield point stress
σ_Y	Yield stress
θ	Rotation of infinitesimal segment
$[\theta]$	Direction cosine matrix

Note: Any other notation may be explained where it appears.

LIST OF CONTENTS

LIST OF FIGURES

LIST OF TABLES

CHAPTER ONE
INTRODUCTION

١.١ General

One of the oldest problems that have long occupied the attention of the structural engineer is the search for structures that cover long spans and large areas without intermediate supports, using a minimum quantity of materials.

When a plane roof surface is not necessary to meet functional requirements of the structure, a singly or doubly curved roof will normally be found to be the most economical of materials. These nonlinear, non-planar systems owe their economy to their unique capacity to resist applied loads primarily by direct in-plane stress, as apposed to flexural and shear stresses, so, shells are an example of strength through form as opposed to strength through mass; therefore, a minimum of materials is used to the maximum structural advantage. Their popularity in contemporary construction is due to the resulting economy coupled with the availability of a large variety of forms with high architectural flexibility and aesthetic appeal. A shell sustains the applied loads primarily by direct; in-plane or membrane forces (compression or tension). Bending even when present normally assumes only a place of secondary importance. While a plain element like a roof slab undergoes bending only when subjected to vertical loads including self-weight.

The twin attributes of a shell, which recommend its use in roofs, are economy and aesthetics. [٢] To visualize the affectivity of shell roofs and folded plates, an ordinary simply supported beam may be studied. When a load is applied, only one cross section of the beam is subjected to the maximum design moment, and consequently, if the member is prismatic,

only one cross section of the beam is working at the maximum allowable stress at design load. What is worse is that at design load, only the extreme fiber of that unique section is stressed to the maximum; all the other fibers are under-stressed. Now, if this beam is bent (giving it a certain curvature), its strength and stiffness is very much improved because this increases its depth and consequently its moment of inertia. Hence, the capacity of a flat thin surface structure is very much increased if it is folded or bent.

١.٢ Nonlinear Analysis of Plates and Shells

The finite element method is an approximate numerical procedure for analyzing large structures and continua. The finite element method has become popular with the advancements in digital computers since they allow engineers to solve large systems of equations quickly and efficiently. The finite element method is a very useful tool for the solution of many types of engineering problems such as the analysis of structures, heat transfer and fluid flow. The method is also an important analysis tool in the design of airframes, ships, electric motors, heat engines and spacecrafts. [١٨]

Three approaches to the finite element representation of general shell structures have traditionally been used, namely the "*faceted*" form, with flat elements, elements formulated on the basis of curved shell theory and degenerated isoparametric elements. Among all of the shell elements, the Ahmed type "degenerated" isoparametric shell element based on an independent rotational and translational displacement interpolations has become popular in recent years. [٢]

The nonlinear stress-strain response of anisotropic material is of interest to designers. The Huber-Mises yield criterion has been generalized by Hill [١٤] for anisotropic metals. Hill theory has been

extended to consider strain-hardening behaviour. The tangential/initial stiffness approach and an associated flow rule have been used to define the elastic-plastic incremental constitutive relation.

The changes in the geometrical configuration of the structure may be considered as a second source of nonlinearity. It was proposed that the most appropriate formulation to take account of geometrical nonlinearity problems in the degenerated shell element is the total Lagrangian coordinates with large deflections and moderate rotations.

١.٣ Optimization

Since ١٩٧٠, structural optimization has been the subject of intensive research and several, different approaches for optimal design of structures have been advocated [٣٢]. The aim of optimization of structural systems is to find out the best combination of *design variables* that minimize an *objective function* (cost, weight, etc) without sacrificing the functional and performance *constraints*. The simplest approach to design such structures is to perform analyses for all possible combinations of design variables. However, it is almost impossible to perform such analyses since a huge number of combinations has to be considered in actual cases. Therefore, many kinds of structural optimization techniques have been proposed in the past years. [١٠]

Structural optimization problems are characterized by various objective and constraint functions that are generally nonlinear functions of the design variables. These functions are usually implicit, discontinuous and non-convex. The mathematical formulation of structural optimization problems with respect to the design variables, the objective and the constraint functions depend on the type of application. However, all optimization problems can be expressed in standard

mathematical terms as a nonlinear programming problem (NLP), which in general form can be stated as follows:

min $f(x_١ , x_٢ , x_٣ , \ldots . x_n)$

subject to $g_i (x_١ , x_٢ , x_٣ , \ldots . x_n) \leq b_i$ $(i= ١, ٢, \ldots m)$

where:

$(x_١ , x_٢ , x_٣ , \ldots . x_n)$: vector of design variables

$f(x_١ , x_٢ , x_٣ , \ldots . x_n)$: objective function to be minimized

$g_i (x_١ , x_٢ , x_٣ , \ldots . x_n)$: behavioural constraints

b_i: the bounds of the constraints.

n: No. of the design variables.

m: No. of the constraints.

١.٤ Scope and Aims

Folded plates and shells are efficient and economic structures under conditions of heavy loads to be transmitted and to cover large areas. The economy of plates and shells is mainly the results of saving in materials they use.

The present work has two main aims, namely:

١- To present a better understanding of the behaviour of different types of plate and shell structures. To achieve this aim, a theoretical work using a finite element, elastic-plastic geometrically nonlinear analysis is carried out to study the behaviour of metal plates and shells by using a degenerated layered shell element.

٢- To perform an optimal design of plate and shell structures based on that nonlinear analysis. To carry out the structural optimization, the modified Hooke and Jeeves method is used while the Von-Mises yield criterion in terms of stress resultants is used as a design technique.

The thesis consists of six chapters. The present introductory chapter is being the first. Chapter two is concerned with the review of literature; outlines of some previous research work on optimal design and nonlinear analysis of plates and shells are presented. The formulation of degenerated layered shell element and elastic-plastic constitutive relations are presented in chapter three.

Chapter four is devoted to the optimal design formulation. In chapter five, several numerical examples are presented for both nonlinear analysis and optimal design and verified with previous analytical and experimental studies. Finally, chapter six gives the conclusions and suggestions for future studies.

CHAPTER TWO
LITERATURE REVIEW

٢.١ Nonlinear Analysis of Plates and Shells

Reddy and Huang [٢٤] analyzed axisymmetric annular plates with varying thickness using large deflection bending by annular finite-element. The more general Reissner plate equations were used in the formulation. Shear deformation, geometrical nonlinearity and material orthotropy were included in that work. Both static and free vibration analysis were preformed.

Owen and Figueuras [٢٩] employed a semiloof curved shell element for the elastic-plastic analysis of plates and shells by means of the finite element displacement method. In that work, the elastio-plastic analysis is based on the Huber-Mises criterion, which is extended for anisotropic materials. The yield function is generalized by introducing anisotropic parameters of plasticity, which are updated during the material strain hardening history. The analysis is applicable to both perfectly plastic and work hardening materials. The middle surface of the structure was assumed to be a surface of material symmetry and linear geometrical behaviour was assumed.

In their second paper, Owen and Figueuras [٣٠] studied the anisotropic elasto-plastic finite element analysis of thick and thin plates and shells using a degenerate three-dimensional continuum element and a thick shell formulation accounting for shear deformation. A layered approach was used. Plastic yielding was based on the Huber-Mises yield surface. The assumption of a constant transverse shear strain was made, and a correction shear factor was used to approximate the real shear strain

energy component. The formulation is similar to that used in the present study.

Gorgi [٢١] investigated the nonlinear analysis of plates with plastic orthotropy. Different longitudinal and transverse stress-strain relations beyond the elastic limit were considered. The inelastic strains and the nonlinear terms due to lateral large deflection were considered as a combination of equivalent lateral loads, edge moments and in-plane forces. Also, the incremental constitutive relations were employed in that analysis.

Moshaiov and Vorus [٢٤] implemented a boundary integral equation formulation for the elasto-plastic plate bending analysis using a boundary element method with initial plastic moments to solve the integral equations. The plasticity as well as the external lateral load appeared in a domain integral. The solution was obtained by an incremental loading procedure with initial incremental plastic moments calculated by an iterative method.

Nasr and Pereira [٢٦] performed a stability analysis of plates and doubly curved shallow shells using the finite element method and some applications of MSC/NASTRAN. The finite element formulation was based on a variation formulation using Reissner's two-field variable variation principle with the transverse displacement w and Airy stress function as field variables. Euler-Lagrange equations and boundary conditions were used. A rectangular flat element with sixteen degrees of freedom stiffness matrix was used by eliminating some degrees of freedom. The study also included the case of pre-loaded plates and shallow shells.

McGowan and Anderson [٢٢] carried out an analytical formulation of curved anisotropic plates by solving nonlinear equilibrium equations that included transverse shear deformation effects. In their work, they

compared the use of classical plate theory (CPT) and first order shear-deformation plate theory (SDPT). The nonlinearity included was the nonlinear strain-displacement relations for large strains. The so-called "segmented-plates" analysis was used by approximating the geometry of curved plates by sub-dividing or discretizing it into a series of flat-plate elements that are joined to form the complete curved plate as illustrated in Figure (٢.١)

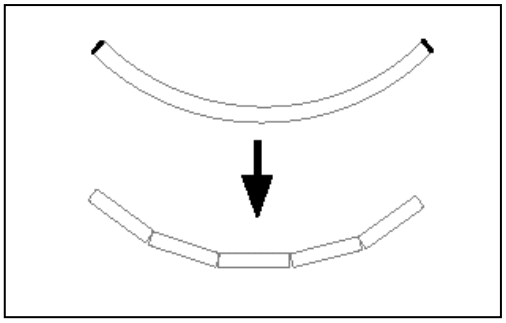

Figure (٢.١) Segmented Representation of Curved-Plate Geometry Used by McGowan and Anderson [٢٣]

Karkush [١٩] extended the application of the incremental finite strip method to study the nonlinear behaviour of prismatic, simple span folded plates and cylindrical shell structures. In that study, the combined effect of material and geometrical nonlinearities was taken into consideration as used in the present study. The formulation for the incremental plasticity approach was based on Von-Mises' yield criterion and Prantdl-Reuss flow rule.

Ciarlet and Coutand [٦] worked out a theoretical study about nonlinear elastic analysis of flexural shells and plates, using a formal asymptotic analysis of the three-dimensional equations of nonlinear elasticity with the thickness as the small parameter which leads to the two-dimensional equations of a flexural shell. These equations take the form of vibration equations with the deformation of the middle surface of the shell as unknown. The boundary conditions were considered as clamped and the

middle surface of the shell was considered as a portion of a cone or a cylinder, so, the study has no general applications.

Rahmatalla [٢٣] presented a ٤-node geometrically nonlinear degenerated shell element for modelling and analysis of fabric. The analysis assumptions imposed indicated that the shell is thin and all fibers remain straight (modified Mindlin-Reissner assumption). The stress normal to the midsurface was assumed to vanish(also called the plane stress condition). Selective reduced integration was used to avoid membrane and transverse shear locking. A layered approach was employed to tackle the through-thickness behaviour. The hyper elastic material modelling was based on the so-called Ciarlet strain energy function.

Nath and Sandeep [٢٧] studied the geometrically nonlinear behaviour of doubly curved, thin isotropic shells in rectangular platform. They solved the Von Karman-Donnell type nonlinear practical differential equations by linearization and using a quadratic extrapolation technique. The research focused on the analyses of clamped and simply supported doubly curved shallow shells considering uniformly distributed normal loading on rectangular domain as shown in Figure (٢.٢)

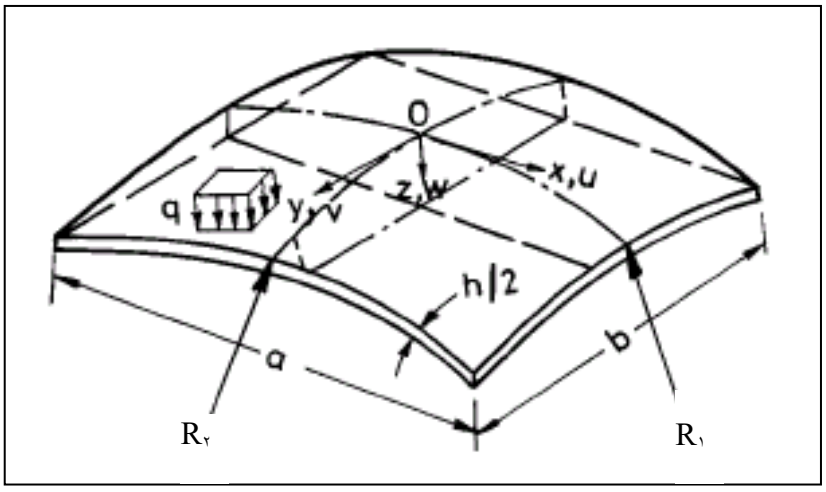

Figure (٢.٢) Geometry of Shell Considered by Nath and Sandeep [٢٣]

Uchiyama and Yamada [٤٣] implemented a degenerated nine-node shell element and an interpolation formulation for stress resultant vectors to the nonlinear finite element analysis of elastic pre- and post-buckling deflection of pressurised shallow spherical shells. In that study, the mixed variational formulation was used and by which the element does not exhibit locking phenomena even in thin-walled shells. The nine-node shell element was based on the four-node shell element by Simo et al. and the interpolation formulation for stress resultant vectors by Sansour and Buffer.

Stegmann et al [٤٠] employed a degenerated linear ٤-node element for geometrically nonlinear (GNL) analysis of layered shell structures. The element employed the MITC (Mixed Interpolation of Tensorial Components) approach proposed by Dvorkin and Bathe in order to eliminate the problem of shear locking. The element used full numerical integration both in-plane and through the thickness. The element formulation was based on the degenerated solid approach and Mindlin-type element. Founding on the observation that the transverse shearing strains are computed correctly at the mid-sides of the four-node element, the B-matrix was corrected so that transverse shearing strains are computed in these four mid-sides points instead of the Gauss-points.

Ahmed et al [١] presented a finite element nonlinear analysis of axisymmetric metal sheets using shell element. The proposed element is a simple three-node shell element with only three degrees of freedom per node, which are the axial displacement, tangential displacement and circumferential rotation. The element was capable of taking into consideration both membrane and bending effects. The material nonlinearity was considered by using rigid-plastic strain hardening material model. The proposed finite element shell formulation was based

on the Reissner-Mindlin axisymmetric shell theory for thin shells. The behaviour was assumed geometrically linear.

Sofistik [٣٩] presented a layered model software which employed nonlinear analysis of plates and shells. The layered approach allowed the layering of the material properties in the shell element and can be implemented for laminated steel, glass and wood plates or other composite plates. The layered technique can also be implemented for the nonlinear calculation of elements consisting of homogeneous material. The nonlinearity included was the material nonlinearity and this was done by assuming a linear material behaviour for each layer. The program was also extended to the nonlinear analysis of reinforced concrete plates and shells.

Sze and Kim [٤١] presented an improved triangular degenerated and solid shell element for linear and geometric nonlinear shell analysis. The study included a comparison between the two types of elements, namely: the six-node degenerated shell element with five d.o.f.s/ node and the twelve-node solid-shell element with three d.o.f.s/node. The element formulation was not modified by the Kirchhoff or zero transverse shear constraints so that they were applicable to thick and composite/sandwich plates and shells.

Gosling and Roy [١٧] presented a formulation for elasto-plastic geometrically nonlinear analysis for shell structures. In that formulation, virtual deformations of the shell were assumed to obey the Kirchoff-Love hypothesis, namely that the normals to the middle-surface are rigid bodies, and remain normal to the deformed middle-surface. The yield criterion used was the yield surface given by Ivanov. In the plastic range, the potential energy of the shell was modified to take account of the softening in the system by modifying Young's modulus. Total Lagrangian approach was implemented.

Hossain et al [١٥] studied the geometrically nonlinear finite element formulation for laminated composite shells. The used doubly curved laminated shell element was based on a geometrically exact stress resultant based on shell theory where the shell may undergo finite rotations. The presented finite element model was based on curvilinear coordinates and this is quite different from the usual isoparametric concept, in which the shell equations are formulated in global Cartesian coordinates with the same interpolation functions for both geometry and displacement fields. The total Lagrangian formulation was employed for arbitrary large displacements and rotations in cases of thin and moderately thick shells.

Colliat et al [٧] studied the nonlinear thermo-mechanical analysis of flat shell cellular structures. The objective for that work is the development of predictive models capable of describing the inelastic behaviour of cellular structures; build either of folded plates and/or non-smooth shells, under sustained long term effect of high temperature. A modified version of the so-called “Ibrahimbegovic” shell element was used to model the whole structure in an inelastic geometrically linear analysis. In that element, the compatibility of the displacement degrees of freedom was achieved by including the so-called drilling rotations, where the bending action in one shell element is coupled with the membrane action of its neighbour. The failure mechanism adopted was that of Saint-Venant in terms of stress resultants.

Kerja and Schmidt [٢٠] implemented finite element simulations to study the ultimate load carrying capacity of thin-walled structures in the geometrically nonlinear and elasto-plastic behaviour. The study included the complex interaction of the different types of nonlinearities, e.g. large deflections and rotations, elasto-plastic hardening material behavior, and also, gradual stiffness degradation due to material damage evolution.

٢.٢ Optimal Design of Plates and Shells

Cruz [٨] presented an analysis and design method for the optimal design of composite sandwich cover panels subjected to compressive loading which are used for transport aircraft wing applications. An analytical approach was used to solve for axial stress resultant including the transverse shear effect. The objective function used in that study was the weight per unit area of the cover panel. The design variables were related to face sheet and core thicknesses and plies directions. Constraints were placed on the axial stress resultant and relative thicknesses of layers. The study also included the effect of changing the lower and upper limits of constraints on the final optimal design.

Gotsis [١٣] worked out the structural optimization of thin shell structures that are subjected to stress and displacement constraints. In the static finite element stage, a triangular element was developed by modifying the membrane stiffness matrix in the local coordinates system and adding a fictitious rotational stiffness matrix. In the optimization part, and instead of the iterative solution, a stress ratio formula, which redesigns the thickness of each finite element of the structure, was solved by an analytical method. The modified method was used to design a thin, cylindrical shell structure with minimum weight.

Zhiming [٤٥] presented the optimal design, nonlinear bending and stability of shallow shells of revolution with variable thickness. The problem was investigated by means of a modified iterative method proposed earlier by the same author. Analytical solutions for nonlinear bending shallow shells of revolution with variable thickness, such as spherical and conical shells were presented. The optimal design of plates and shells, in which the volume is minimized or the critical load of the shell is maximized, was investigated. When the volume of the shell and

the arch height of the shell are given, the variable thickness problem was solved. In addition, the paper gave the constraints of optimization for circular plates under nonlinear bending.

Ostwald [٢٨] presented the multiobjective optimization of thin-walled sandwich cylindrical shells subjected to axial compression. The optimization problem was considered as bicriterial one, with the weight of the shell as the first objective function, and the flexibility as second (the flexibility was defined as the susceptibility of the shell to deflection). The optimization was carried out using the so-called "Pareto optimality", in which a set of optimal comprise solutions is generated and then, the best optimal solution is chosen from this set. The thicknesses of the layers were considered as design variables. The linear theory of shell stability was employed to calculate the critical load. The constraints were imposed on stability, stresses, deflection and technological requirements.

McGowan and Anderson [٢٣] prepared a design-optimization study of composite cylindrical shells subjected to uniform axial compression. The design was based on nonlinear analysis including material nonlinearity with prismatic flat or curved-plate elements that are rigidly connected along their longitudinal edges. The analysis included the effects of anisotropy and through-the-thickness or transverse shear deformation. The objective function was the mass of the structure. The design variables were the thicknesses of the face sheets and the core. The design constraints were considered as stresses and strains.

Rich [٣٥] presented an optimization strategy for the optimal design of composite shells. The study focused on the optimal design of balanced symmetric cylinders. The design was based on linear static analysis with large rotations. The implemented element was a quadrilateral flat four-node element with six degrees of freedom at each node using linear and cubic-linear shape functions. The constraints of the nonlinear

optimization problem were solved by sequential linear programming (SLP). The objective function was the weight of the cylinder and the design variables were related to shell wall thickness, in-plane stiffness and bending stiffness. The design constraints were introduced to prevent buckling.

Tong et al. [٤٢] performed an analytical model, finite element solutions and optimal shape control of composite thin plates which are made of piezoelectric materials i.e. materials that develop strain under applied voltage and which include structural deflection. Two dimensional finite element approach was developed by assuming that the in-plane displacements are negligible. The four-node twelve d.o.f. DKQ (Discrete Kirchhoff Quadrilateral) element was implemented in the elastic analysis. The nodal variables were the transverse displacement w and its derivatives at the four corner nodes. The optimization is constrained to obtain a prescribed deflection shape.

Kruzelecki and Trzeciak [٢١] investigated the problem of optimal design of rotationally symmetric inelastic shells loaded by hydrostatic pressure. The objective of the study was to obtain such geometry of a shell and a shape of a middle surface which lead to the minimum volume of shell material (or weight) under a constant given critical pressure. Additionally, and as an equality constraint, the internal capacity of the shell was considered. The hypothesis of the locality of buckling was utilized and the optimal structure was sought in the class of the shell of uniform stability. The inelastic material behaviour was defined by a tangent modulus. A parametrical optimization was performed.

Dippery and Srivastava [٩] studied the optimal design of pressure vessels to predict the stresses in the vessel. The design was based on a linear analysis with stress limits as allowable stress magnitudes. The objective function was the weight of the vessel as a measure of

fabrication costs. The constraints were established to satisfy stress limits of the American Society of Mechanical Engineering (١٩٩٨). The study also included notes about locating the weld in an area of lower bending stress or in an area where it may requires less weld material in a two-dimensional problem.

Rozvany and Olhoff [٣٧] prepared a study about topology optimization of structures and composite continua. The study included a formulation for optimal structural design of plate-like structures via plate theory and ٣-D theory of elasticity, based on finite elements. The influence of geometrical nonlinearity was examined. The objective function and design variables were related to sizes and shapes under displacements, buckling and stress constraints.

Wang et al [٤٤] used a structural optimization method in MSC/NASTRAN to size substructures and to reduce the weight of a composite sandwich cryogenic tank which used to carry liquid oxygen (LOX) and hydrogen ($LH_٢$) fuel. The face sheet and honeycomb core thicknesses of the sandwich structure were used as design variables in the optimization. Gradient-based nonlinear constrained optimization procedures were used to minimize the weight of the structure. Constraints imposed were related to strain and thicknesses of the different parts of the structure. Static linear and geometrically nonlinear finite element analysis were performed.

Rigo [٣٦] presented the optimal design of marine structures (ships and naval structures). To perform a rational analysis, the structures were modelled by using stiffened plate and stiffened cylindrical shell elements in the linear elastic analysis of orthotropic structures using the so-called “stiffened plate” method to provide a fast and reliable assessment of the stress pattern existing in the stiffened structure. The nonlinear constrained optimization problem was solved by iterative approach. The objective of

the design was the minimum cost including raw material, labour and overhead costs. The design variables were the plate thickness and dimensions of the longitudinal stiffeners. Three types of constraints were distinguished: structural, technological and geometrical.

Lund and Stegmann [٢٢] presented the structural optimization of composite shell structures. The procedure was based on ideas from multi-phase topology optimization where the material stiffness (or density) is computed as a weighted sum of the materials used. In that work, the stiffness of each layer of the composite was computed from a weighted sum of a finite number of "plausible" constitutive matrices. The design objective was chosen as the maximum stiffness. The design variables were related to layer thicknesses and fiber angles (see Figure (٢.٣)) with constraints on the total mass.

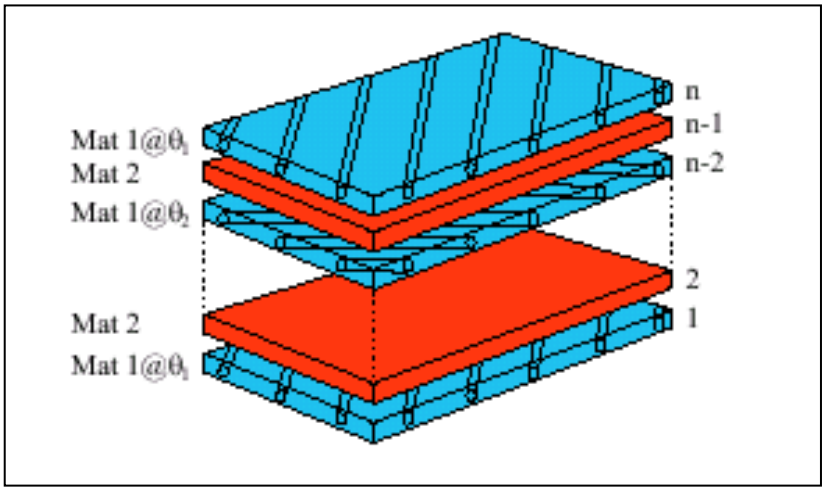

Figure (٢.٣) Laminated Structure Considered by Lund and Stegmann [٢٣]

The present study deals with the formulation of material and geometrical nonlinearity of plate and shell structures (in the sense of Von Karman hypothesis). For optimization, the modified Hooke and Jeeves method is employed by considering the volume of the plate or shell as the objective function and the dimensions as the design variables with geometrical constraints.

CHAPTER THREE

FINITE ELEMENT FORMULATION

٣.١ General

With the increasing use of high speed computers and the emphasis on numerical methods for engineering analysis, the finite element method has developed simultaneously.

The development of appropriate methods for the analysis of shell structures is increasingly demanded to insure the integrity of structural design. Analytical solutions to shell structures are limited in scope and in general are not applicable to arbitrary shapes, load conditions, irregular stiffening and support conditions, cut-outs and many other aspects of practical design. The finite element method has consequently become prominent in the analysis of such shells in view of the ease with which such complexities can be dealt with. [١٤]

Problems in finite element are usually tackled by one of three approaches: the displacement method, the equilibrium (force) method and the mixed method. Displacements are assumed as primary unknown quantities in the displacement method; stresses are assumed as primary unknown quantities in the equilibrium method; some stresses and some displacements are assumed as unknown quantities in the mixed method.

In this chapter, the elastic- plastic and geometrically nonlinear analysis using the nonlinear finite element displacement formulation of a layered degenerated shell element is presented.

٣.٢ Shell Element Formulation

There are various attempts to produce efficient, accurate and reliable shell elements. Three distinct classes of shell elements have been used. [١٦]

١. Flat, plate-like elements which are sometimes called facet elements because they approximate the curved shell by a faceted surface.
٢. Curved shell elements founded on some shell theory.
٣. Degenerated shell elements based on three-dimensional continuum theory.

In flat shell elements, the in-plane stretching and bending behaviour within each element is completely uncoupled, the coupling only appears indirectly through the degrees of freedom at the nodal points linking adjacent elements. Although there are certain shortcomings in such an approach, facet elements are very efficient for the approximate analysis of many shell structures.

Curved shell elements based on shell theories are also quite popular but suffer from various limitations associated with the lack of consistency in many shell theories and also with the difficulties in finding appropriate deformation idealizations which allow truly strain-free rigid body movements .

In the late sixties, Ahmad developed a degenerated, Mindlin-type, curved shell element which is quite efficient and simple. Since then many improvements in Mindlin-type plate and shell elements have been made. This approach avoids the complexities of fully general shell theories by discretizing directly the three dimensional equations continuum mechanics. This approach has been recently applied to the geometric and material nonlinear analysis of shells, as well as to combined geometric and material nonlinearities [١٤]

٣.٣ Degenerate Isoparametric Elements

٣.٣.١ General

Figure (٣.١.a) shows a three dimensional solid element. Two basic assumptions are adopted in this process:

١. It is assumed that, even for thick shells, “normal” to the middle surface remain practically straight after deformation.

٢. The strain energy corresponding to stresses perpendicular to the middle surface is disregarded, i.e. the strain components normal to the shell mid-surface is constrained to be zero.

Five degrees of freedom are specified at each nodal point, these correspond to its three displacements and two rotations of the normal at the node. The definition of independent rotational and displacement degrees of freedom permits transverse shear deformation to be taken into account, since rotations are not tied to the slope of the mid-surface. This approach is equivalent to using a general shell theory and reduces to the hypotheses of Reissner and Mindlin when applied to plates. [١٤]

In the present chapter, the derivation of the degenerated shell element is described according to the theory of the three dimensional degenerated curved shell.

٣.٣.٢ Coordinates Systems

The four coordinate systems used in the degenerated shell element formulation, as shown in Figure (٣.١), are now defined:

٣.٣.٢.١ Global Cartesian Coordinate System (x, y, z or x_i)

The global Cartesian coordinate system is used to define the nodal coordinates and displacements as well as the global stiffness matrix and applied load vector. The following notation is used (see Figure (٣.١))

$x_i \ (i = 1,2,3)$ and $x_1 = x \ , x_2 = y \ , x_3 = z$

$u_i \ (i = 1,2,3)$ and $u_1 = u \ , u_2 = v \ , u_3 = w$

٣.٣.٢.٢ Natural Coordinate System $(\xi \ , \eta \ , \zeta)$

The shape functions N_i are expressed in terms of the curvilinear coordinate system. The middle surface of the shell element is defined by the ξ and η coordinates. The ζ-direction is only approximately normal to

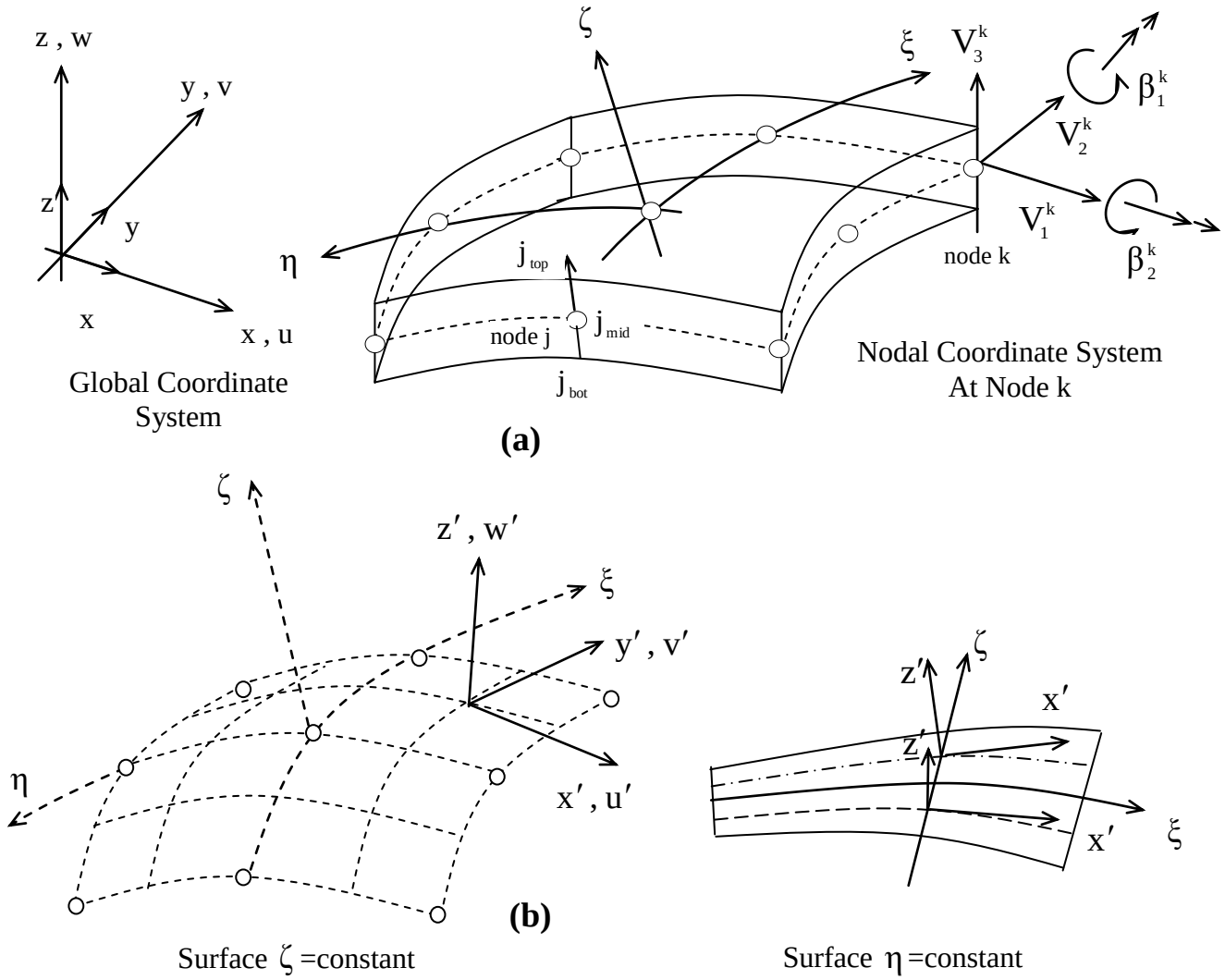

Figure (٣.١) Coordinate Systems: a- Global, Nodal and Curvilinear Systems b- Local System of Axes

the shell middle surface and varies from -١ to +١ in the thickness direction.

٣.٣.٢.٣ Local Cartesian Coordinate System (x', y', z' or x_i')

The local coordinate system is used to define local stresses and strains at any point within the shell element. At such a point the z'-direction is taken to be normal to the surface ζ = constant**.** The vector $V_3^{'}$ defines the z'-direction and it is obtained from the cross product of the vectors which are tangential to the ξ and η-directions so that:

$$V_3' = \xi \times \eta = \begin{bmatrix} \partial x/\partial \xi \\ \partial y/\partial \xi \\ \partial z/\partial \xi \end{bmatrix} \times \begin{bmatrix} \partial x/\partial \eta \\ \partial y/\partial \eta \\ \partial z/\partial \eta \end{bmatrix}^T \quad \text{----- (٣.١)}$$

The vector V_1' which is in the x' direction can be simply taken to coincide with the tangent to the ξ direction as:

$$V_1' = \xi = \left[\frac{\partial x}{\partial \xi} \quad , \quad \frac{\partial y}{\partial \xi} \quad , \quad \frac{\partial z}{\partial \xi} \right]^T \quad \text{----- (٣.٢)}$$

and vector V_2' in the y'-direction is defined by the cross product of the V_3' and V_1' :

$$V_2' = V_3' \times V_1' \quad \text{----- (٣.٣)}$$

The local coordinate system varies through the shell. It is useful to define the direction cosine matrix $[\theta]$, which enables transformations between the local and global coordinate systems to be undertaken:

$$[\theta] = \begin{bmatrix} \partial x/\partial x' & \partial x/\partial y' & \partial x/\partial z' \\ \partial y/\partial x' & \partial y/\partial y' & \partial y/\partial z' \\ \partial z/\partial x' & \partial z/\partial y' & \partial z/\partial z' \end{bmatrix} \quad \text{----- (٣.٤)}$$

The direction cosine matrix in (٣.٤) is now defined by the expression:

$$[\theta] = [V_1 \quad , \quad V_2 \quad , \quad V_3] \quad \text{----- (٣.٥)}$$

where V_1, V_2, V_3 are unit vectors along the x', y', z'-axes and normalized from V_1', V_2', V_3' respectively.

٣.٣.٢.٤ Nodal Cartesian Coordinate System $\left(V_1^k , V_2^k , V_3^k\right)$

The nodal Cartesian coordinate system is the local Cartesian coordinate system associated with each nodal point of the shell element and its origin is at the shell mid-surface. The vector V_3^k is constructed from the nodal coordinates of the top and bottom surfaces at node k, so that:

$$V_{3i}^k = \Delta x_i^k \Big/ \left(\left[\Delta x_1^k\right]^2 + \left[\Delta x_2^k\right]^2 + \left[\Delta x_3^k\right]^2 \right)^{0.5} \qquad (i = 1,2,3)$$ -----

(٣.٦)

where:

$$\Delta x_i^k = x_{i,top}^k - x_{i,bot}^k \qquad (i = 1,2,3)$$ -----

(٣.٧) The vector V_1^k is perpendicular to V_3^k and parallel to the global x-z plane, so that:

$$V_1^k = j \times V_3^k \Big/ \left| j \times V_3^k \right|$$ ----- (٣.٨)

or if V_3^k is in the y-direction,

$$V_1^k = V_3^k \times i \Big/ \left| V_3^k \times i \right|$$ ----- (٣.٩)

where i and j are the unit vectors along the x, y-directions respectively. The vector V_2^k is normal to the plane defined by V_1^k and V_3^k as:

$$V_2^k = V_3^k \times V_1^k \Big/ \left| V_3^k \times V_1^k \right|$$ -----

(٣.١٠)

where the superscripts refer to the nodal number. The vector V_3^k defines the direction of the normal at node k, which is not necessarily perpendicular to the mid-surface at k. Vectors V_1^k and V_2^k define the rotations (β_2^k and β_1^k respectively) of the corresponding normal. The advantage of this definition for the vector V_3^k (not necessarily perpendicular to the shell mid-surface) shows that, as a consequence, there are no gaps or overlaps along element boundaries. The definition used for the V_1^k provides an easy identification of its direction in general curved structures.

٣.٣.٣ Element Geometry

In the degenerated shell element, each node has five degree of freedom, i.e. three translational displacements in the directions of the global axes and two rotations with respect to axes in the plane of the middle surface as shown in Figure (٣.١). The Cartesian coordinates at any point of the shell can be uniquely given in terms of nodal coordinates and thickness. Firstly, the coordinates of a point at the vector V_3^k can be expressed as:

$$\bar{x}_i^k = x_i^k + \frac{\zeta}{2} h\, V_{3i}^k \qquad (i = 1,2,3) \qquad \text{-----}$$

(٣.١١)

Therefore,

$$x_i = \sum_{k=1}^{n} N^k(\xi,\eta)\cdot \bar{x}_i^k$$

$$x_i = \sum_{k=1}^{n} N^k(\xi,\eta)\cdot x_i^k + \frac{\zeta}{2}\sum_{k=1}^{n} N^k(\xi,\eta)\cdot h^k V_{3i}^k \qquad (i = 1,2,3) \qquad \text{-----} \ (٣.١٢)$$

Alternatively, the global coordinates of pairs of points on the top and bottom surface at each node (see Figure (٣.١)) are usually introduced to define the element geometry. Thus,

$$x_i = \sum_{k=1}^{n} N^k(\xi,\eta)\left[\frac{1+\zeta}{2} x_{i,top}^k + \frac{1-\zeta}{2} x_{i,bot}^k\right]$$

where x_i = Cartesian coordinate of any point in the element.($x_١$=x, $x_٢$=y, $x_٣$=z),

x_i^k = Cartesian coordinate of nodal point k,

h^k = Thickness of shell in ζ-direction at nodal point k,

V_{3i}^k = *i*th component of the unit normal vector to the middle surface,

$N^k(\xi,\eta)$ = the two-dimensional interpolation function corresponding to node k.

ζ = The distance from the middle surface.

Suitable shape functions for the degenerated shell elements are given in Table (٣.١). [٢]

Bilinear ٤-node element	$N_i = (1+\xi\xi_i)(1+\eta\eta_i)/4$
Serendipity ٨-node:	
Corner nodes	$N_i = (1+\xi\xi_i)(1+\eta\eta_i)(\xi\xi_i+\eta\eta_i-1)/4$
Mid-side nodes	$N_i = \xi_i^2(1+\xi\xi_i)(1-\eta^2)/2+\eta_i^2(1+\eta\eta_i)(1-\xi^2)/2$
Lagrangian ٩-node	$N_i = [\xi\xi_i(1+\xi\xi_i)/2+(1-\xi^2)(1-\xi_i^2)]\times$ $[\eta\eta_i(1+\eta\eta_i)/2+(1-\eta^2)(1-\eta_i^2)]$

Table (٣.١): Shape Functions for Mid-Surface Interpolation of Shell Element

٣.٣.٤ Hierarchical Formulation

A hierarchical formulation is adopted in the present work to implement the new ٩-node degenerated shell element. The shape functions of the eight boundary nodes are the Serendipity shape functions:

(a) for corner nodes

$$N_i = (1+\xi\xi_i)(1+\eta\eta_i)(\xi\xi_i+\eta\eta_i-1)/4 \qquad \text{----- (٣.١٣)}$$

(b) for midside nodes

$$N_i = \xi_i^2(1+\xi\xi_i)(1-\eta^2)/2+\eta_i^2(1+\eta\eta_i)(1-\xi^2)/2 \qquad \text{----- (٣.١٤)}$$

and the hierarchical shape function for the ٩^{th} central node is the bubble function,

$$N_9 = (1-\xi^2)(1-\eta^2) \qquad \text{-----}$$

(٣.١٥)

٣.٣.٥ Displacement Field

The displacements at any point in the shell element are defined by the three Cartesian components of mid-surface node displacements u_{oi}^k and two rotations (β_1^k, β_2^k) of the nodal vector V_3^k about the orthogonal direction normal to it (see Figure (٣.٢)). The displacements of a point on the normal resulting from the two rotations are calculated as illustrated in Figure (٣.٢).

$$\delta_1^k = h\,\beta_1^k$$
$$\delta_2^k = h\,\beta_2^k$$ -----

(٣.١٦)

Where

δ_1^k is a displacement in the V_1^k direction and

δ_2^k is a displacement in the V_2^k direction

The corresponding displacement components u_i are obtained by

$$\left(u_i\right)_{\beta_1^k} = \delta_1^k\, V_{1i}^k$$
$$\left(u_i\right)_{\beta_2^k} = \delta_2^k\left(-V_{2i}^k\right)$$ ----- (٣.١٧)

The displacements u_i^k, along the thickness at each nodal point are:

$$u_i^k = u_{oi}^k + x_3'\left[\theta_{x_1'}^k\left(\frac{\partial x_i}{\partial x_1'}\right)^k + \theta_{x_2'}^k\left(\frac{\partial x_i}{\partial x_2'}\right)^k\right]$$

$$= u_{oi}^k + \frac{\zeta}{2}h_k\left(V_{1i}^k\beta_1^k - V_{2i}^k\beta_2^k\right)$$ -----

(٣.١٨)

Thus:

$$u_i = \sum_{k=1}^{n} N^k(\xi,\eta)u_i^k$$

$$= \sum_{k=1}^{n} N^k(\xi,\eta)u_{oi}^k + \frac{\zeta}{2}\sum_{k=1}^{n} N^k(\xi,\eta)h_k\left(V_{1i}^k\beta_1^k - V_{2i}^k\beta_2^k\right)$$

$$= \overline{N}^k(\xi,\eta,\zeta)\,d^k \qquad (i=1,2,3)$$ ----- (٣.١٩)

and

$$\left\{d^k\right\} = \left[u_{o1}^k, u_{o2}^k, u_{o2}^k, \beta_1^k, \beta_2^k\right]^T$$ -----

(٣.٢٠) where u_{oi}^k is the displacement of the *k*th nodal point in the Cartesian coordinate, and β_1^k and β_2^k are the rotations about V_2^k and V_1^k respectively. It is noticed that [١٦]

$$\theta^k_{x'_1} = \beta^k_1$$
$$\theta^k_{x'_2} = -\beta^k_2$$

(٣.٢١)

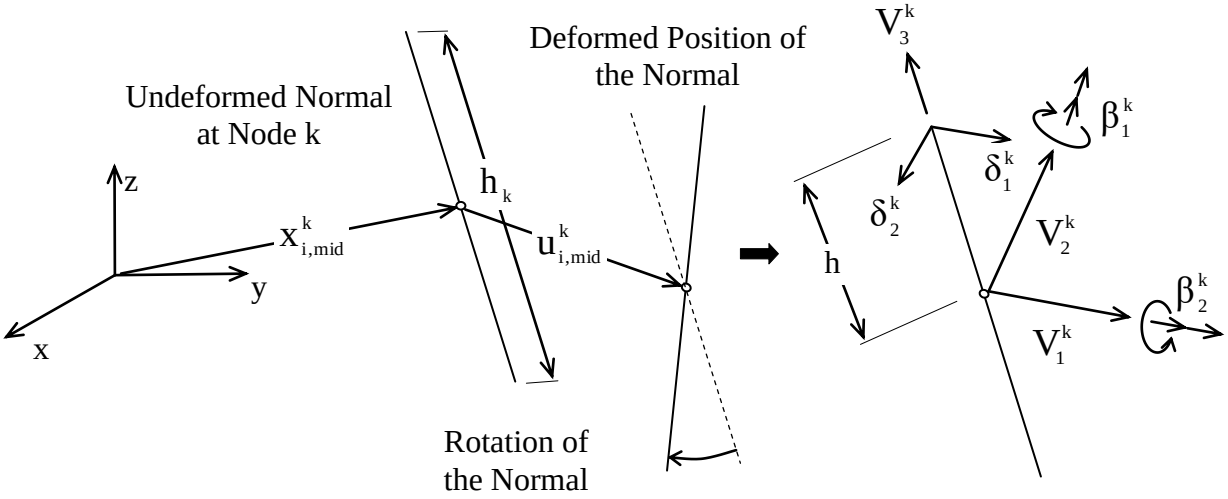

Figure (٣.٢) Displacements of a Point on the Normal at Node k

In expression (٣.١٦) a linear relation is employed, which assumes that the rotations (the incremental angles) are small; to admit large increments of rotations, this expression should be replaced by a nonlinear rotation-displacement relationship. It should be noted that in the implementation of the finite element method, V^k_3 is not necessarily normal to the shell mid-surface.

٣.٣.٦ Definition of Strains

The Mindlin and Reissner – type assumptions are used to derive the strain components defined in terms of the local coordinate system of axes $x'_i (x'_1 = x' , x'_2 = y' , x'_3 = z')$, where x'_3 is perpendicular to the material surface layer (ζ = constant) . The following assumptions need also to be made:

١. The deflections are small.

٢. Strain energy associated with stresses perpendicular to the local $x' - y'$ surface is neglected – the normal strain component is constrained to be zero and eliminated from the constitutive equations.

The five significant strain components are:

$$\{\varepsilon'\} = \begin{Bmatrix} \varepsilon'_f \\ \varepsilon'_s \end{Bmatrix} = \begin{Bmatrix} \varepsilon_{x'} \\ \varepsilon_{y'} \\ \gamma_{x'y'} \\ \gamma_{x'z'} \\ \gamma_{y'z'} \end{Bmatrix} = \begin{Bmatrix} \partial u'/\partial x' \\ \partial v'/\partial y' \\ \partial u'/\partial y' + \partial v'/\partial x' \\ \partial u'/\partial z' + \partial w'/\partial x' \\ \partial v'/\partial z' + \partial w'/\partial y' \end{Bmatrix} \quad \text{----- (٣.٢٢)}$$

where ε'_f is the in-plane strain vector defined in the local coordinates. ε'_s is a transverse shear strain vector, and u', v' and w' are the displacement components in the local system x'_i. These local derivatives of the displacements u, v and w are given by the following operation:

$$\begin{bmatrix} \partial u'/\partial x' & \partial v'/\partial x' & \partial w'/\partial x' \\ \partial u'/\partial y' & \partial v'/\partial y' & \partial w'/\partial y' \\ \partial u'/\partial z' & \partial v'/\partial z' & \partial w'/\partial z' \end{bmatrix} = [\theta]^T \begin{bmatrix} \partial u/\partial x & \partial v/\partial x & \partial w/\partial x \\ \partial u/\partial y & \partial v/\partial y & \partial w/\partial y \\ \partial u/\partial z & \partial v/\partial z & \partial w/\partial z \end{bmatrix} [\theta] \text{--}$$

(٣.٢٣)

where $[\theta]$ is the transformation matrix (matrix of direction cosines):

$$[\theta] = \begin{bmatrix} \partial x/\partial x' & \partial x/\partial y' & \partial x/\partial z' \\ \partial y/\partial x' & \partial y/\partial y' & \partial y/\partial z' \\ \partial z/\partial x' & \partial z/\partial y' & \partial z/\partial z' \end{bmatrix} \quad \text{----- (٣.٢٤)}$$

The derivatives of the displacements with respect to the global coordinates are given by:

$$\begin{bmatrix} \partial u/\partial x & \partial v/\partial x & \partial w/\partial x \\ \partial u/\partial y & \partial v/\partial y & \partial w/\partial y \\ \partial u/\partial z & \partial v/\partial z & \partial w/\partial z \end{bmatrix} = [J]^{-1} \begin{bmatrix} \partial u/\partial \xi & \partial v/\partial \xi & \partial w/\partial \xi \\ \partial u/\partial \eta & \partial v/\partial \eta & \partial w/\partial \eta \\ \partial u/\partial \zeta & \partial v/\partial \zeta & \partial w/\partial \zeta \end{bmatrix} \quad \text{-----}$$

(٣.٢٥) where $[J]$is the Jacobian matrix:

$$[J] = \begin{bmatrix} \partial x/\partial \xi & \partial y/\partial \xi & \partial z/\partial \xi \\ \partial x/\partial \eta & \partial y/\partial \eta & \partial z/\partial \eta \\ \partial x/\partial \zeta & \partial y/\partial \zeta & \partial z/\partial \zeta \end{bmatrix} \quad \text{----- (٣.٢٦)}$$

The strain matrix [B] relating the strain components in the local system to the element nodal variables can then be constructed as:

$$\{\varepsilon'\} = [B] \cdot \{d\} \quad \text{----- (٣.٢٧)}$$

where $\{\varepsilon'\}$ is the strain components defined by (٣.٢٢) and $\{d\}$ is nodal displacements vector defined by (٣.٢٠). The matrix [B] constitutes of five rows and a number of columns equal to the number of element nodal variables.

٣.٣.٧ Definition of Stresses

For a specially orthotropic material that possesses three mutually perpendicular axes of elastic symmetry , two of which (١,٢) are tangential to the material surface layer and the third (٣) is normal to it , and assuming that a state of plane stress exists and that the change of shell thickness during deformation is negligible , the constitutive relations will be :

$$\sigma_{1,2,3} = [D]\varepsilon_{1,2,3} \quad \text{----- (٣.٢٨)}$$

Where:

$$\sigma_{1,2,3} = [\sigma_1 ,\ \sigma_2 , \tau_{12} , \tau_{13} , \tau_{23} \ ]$$
$$\varepsilon_{1,2,3} = [\ \varepsilon_1 ,\ \ \varepsilon_2 , \gamma_{12} , \gamma_{13} , \gamma_{23}] \quad \text{----- (٣.٢٩)}$$

$$[D]=\begin{bmatrix} E_1/1-\upsilon_{12}\upsilon_{21} & \upsilon_{12}E_2/1-\upsilon_{12}\upsilon_{21} & 0 & 0 & 0 \\ \upsilon_{12}E_2/1-\upsilon_{12}\upsilon_{21} & E_2/1-\upsilon_{12}\upsilon_{21} & 0 & 0 & 0 \\ 0 & 0 & G_{12} & 0 & 0 \\ 0 & 0 & 0 & K_1G_{13} & 0 \\ 0 & 0 & 0 & 0 & K_2G_{23} \end{bmatrix} \text{--- (٣.٣٠)}$$

where E_1 and E_2 are Young's moduli in the ١ and ٢-directions respectively, υ_{12} and υ_{21} are Poisson's ratios, where υ_{ij} is the ratio of normal strain in direction j to normal strain in the direction i due to normal stress in direction i. G_{12} , G_{13} and G_{23} are the shear moduli in the ١ – ٢ , ١ – ٣ and ٢ – ٣ planes respectively and K_1 and K_2 are the shear correction factors in ١ – ٣ and ٢ – ٣ planes respectively which are equal to ٥/٦. [١٦]

٣.٣.٨ Layered Model

For laminated plates and shells of composite material it is necessary to use numerical integration to evaluate the stiffness contribution from each layer. This is also necessary for the representation of the gradual through-thickness plastification of the plate or shell. [١٤] Layers of different thickness can be employed. The natural coordinate ζ which varies from -١ to ١, is determined at the middle point of each layer, as illustrated in Figure (٣.٣), and the strain, stress components and stiffness contributions are all computed at the midsection of each layer. Consequently, the volume integral may be split into integrals over the area of the shell midsurface and through the thickness (h), thus, the stiffness may be written as:

$$K=\int_v [B]^T[D][B]\,dv=\int_s\left(\int_{-h/2}^{h/2}[B]^T[D][B]\,dz\right)ds \qquad \text{----- (٣.٣١)}$$

By using an isoparametric mapping, then:

$$K=\int_{-1}^{+1}\int_{-1}^{+1}\left(\int_{-1}^{+1}[B]^T[D][B]\,|J(\xi,\eta,\zeta)|\,d\zeta\right)d\xi\,d\eta$$

$$=\int_{-1}^{+1}\int_{-1}^{+1}\left[\sum_{j=1}^{L}[B]_j^T[D]_j[B]_j|J(\xi,\eta,\zeta_j)|\frac{2\Delta h_j}{h}\right]d\xi\,d\eta \qquad \text{----- (٣.٣٢)}$$

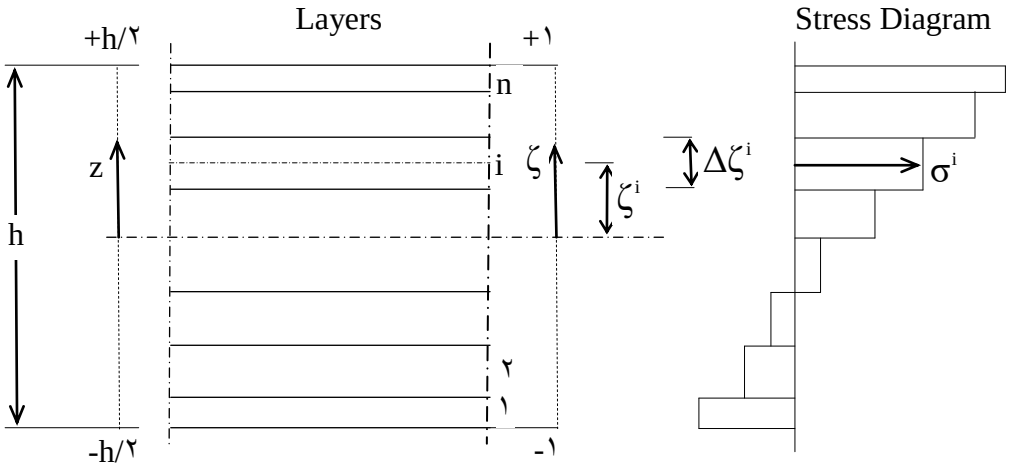

Figure (٣.٣) Layered Model and the Corresponding Stress Representation

where ? J(φ , η , ζ_j) ? is the determinant of the Jacobian matrix for layer j, Δh_j is the thickness of layer j and L is the total number of layers .The stress resultants are obtained by integrating the corresponding stress components with respect to the thickness coordinate.

٣.٣.٩ The Inclusion of the Nonlinear Behaviour

In this work, two types of nonlinear behaviour are accounted for. Firstly material nonlinearity due to an elastic-plastic material response which is considered and where anisotropy effects are included in the yielding behaviour. The second source of nonlinearity considered is that brought about by changes in the geometrical configuration of the structure. [١٤]

٣.٣.١٠ General Numerical Procedure for Nonlinear Analysis

During the general stage of the incremental-iterative solution of a finite element elastic-plastic problem, the equilibrium equations will not be exactly satisfied and a system of residual forces $\{\psi\}$ will exist such that:

$$\{\psi\}_i^n = \{f\}^n - \{p\}_i^n = \{f\}^n - \int_v [B]^T \{\sigma\}_i^n \, dv \neq 0 \qquad \text{---- (٣.٣٣)}$$

in which $\{f\}^n$ and $\{p\}^n$ are respectively the external applied force and the internal equivalent force vectors, $[B]$ is the strain-displacement matrix

(constant for infinitesimal deformation problems), $\{\sigma\}^n$ is the current stress field satisfying the yield condition, v denotes the volume of the solid, the superscript n signifies the load increment number, and subscript i the iteration cycle number within that increment.

An iteration sequence must be performed for each load increment in order to obtain a displacement field, $\{a\}_i^n$, which provides a stress field $\{\sigma\}_i^n$ in (٣.٣٣) such that the residuals $\{\psi\}_i^n$ vanish. In particular, the displacements are updated in each iteration according to:

$$\{a\}_i^n = \{a\}_{i-1}^n + \Delta\{a\}_i^n \qquad \text{---- (٣.٣٤)}$$

where $\Delta\{a\}_i^n$ denotes the displacement change occurring during the iteration. Several options exist for the choice of the displacement search direction. If the tangential stiffness approach is employed, the iterative displacement change is evaluated according to:

$$\Delta\{a\}_i^n = -\left[[K]_{i-1}^n\right]^{-1} \{\psi\}_{i-1}^n \qquad \text{---- (٣.٣٥)}$$

in which $[K]_{i-1}^n$ is the tangential stiffness matrix of the structure evaluated at the beginning of the i^{th} iteration. The updated displacements $\{a\}_i^n$ obtained from (٣.٣٤) are used to evaluate the current stresses $\{\sigma\}_i^n$ and hence the residual forces from (٣.٣٣). The iteration process is repeated until these residual forces are deemed to be sufficiently close to zero.

It should be noted that assembly and inversion of the full equation system is required for each iteration. A variant on the above algorithm is offered by the initial stiffness scheme in which the original structural stiffness matrix $[K]_o^o$ is employed at each stage of the iteration process. This reduces the computational cost per iteration but unfortunately also reduces the rate of convergence of the process. In practice the optimum algorithm is generally provided by updating the stiffnesses at selected iterative intervals only [١٤]. In this work, two possibilities are considered:

(a) the structural stiffness matrix is updated at the beginning of a load increment and maintained constant during iteration to equilibrium, so that $[K]^n_{i-1}$ in (٢٩) is replaced by $[K]^n_o$. (b) the stiffnesses are updated after the first iteration of each load increment only (i.e. $[K]^n_1$ is used in (٣.٣٥)). It was noticed that the type of the algorithm used has no strong effect on the results.

٣.٣.١١ Relation Between Elastic-Plastic Stresses and Strains:

The total strain increment $d\varepsilon$ is the sum of the elastic and plastic components, so that:

$$d\varepsilon = d\varepsilon' + d\varepsilon^p \quad \text{----} \quad (٣.٣٦)$$

where $d\varepsilon'$ is the elastic strain increment and $d\varepsilon^p$ is the plastic strain increment.

The plastic strain increment is given by the flow rule:

$$d\varepsilon^p = d\lambda \frac{\partial Q}{\partial \sigma} = d\lambda \ a \quad \text{---- (٣.٣٧)}$$

where $d\lambda$ is a non-negative scalar. For an associated flow, the potential Q is taken as identical to a yield function $f(\sigma)$. The function $f(\sigma)$ may be defined in a similar manner to the Huber-Mises yield function for isotropic materials and in terms of the general three dimensional case, it as follows:

$$f(\sigma) = \bar{\sigma} = \{\left[\alpha_{12}(\sigma_1 - \sigma_2)^2 + \alpha_{23}(\sigma_2 - \sigma_3)^2 + \alpha_{31}(\sigma_3 - \sigma_1)^2\right] + 3\left[\alpha_{44}\tau_{12}^2 + \alpha_{55}\tau_{13}^2 + \alpha_{66}\tau_2^2\right]\}^{1/2} \quad \text{---- (٣.٣٨)}$$

in which $\bar{\sigma}$ is termed the effective stress and α_{12} etc. are anisotropic parameters to be determined experimentally. According to the previous assumption, the transverse normal stress σ_3 is neglected for plates or shells. Thus, it is possible to write:

$$f(\sigma)=\bar{\sigma}=\left(\bar{\alpha}_1\sigma_1^2+2\bar{\alpha}_{12}\sigma_1\sigma_2+\bar{\alpha}_2\sigma_2^2+\bar{\alpha}_3\tau_{12}^2+\bar{\alpha}_4\tau_{13}^2+\bar{\alpha}_5\tau_{23}^2\right)^{1/2} \quad \text{---- (٣.٣٩)}$$

where $\bar{\alpha}_1$, $\bar{\alpha}_{12}$, $\bar{\alpha}_2$, $\bar{\alpha}_3$, $\bar{\alpha}_4$ and $\bar{\alpha}_5$ are anisotropic parameters which can be determined experimentally and the subscripts ١, ٢, ٣ refer to the directions of the three principal axes of anisotropy. The differential form of the general Huber-Mises law can be written as

$$a^T d\sigma - A d\lambda = 0 \quad \text{---- (٣.٤٠)}$$

where the flow vector $a=\partial f/\partial\sigma$ is defined as follows:

$$a=\frac{\partial f}{\partial\sigma}=\left[\frac{\partial f}{\partial\sigma_x},\frac{\partial f}{\partial\sigma_y},\frac{\partial f}{\partial\tau_{xy}},\frac{\partial f}{\partial\tau_{xz}},\frac{\partial f}{\partial\tau_{yz}}\right]^T \quad \text{---- (٣.٤١)}$$

in which,

$$\begin{aligned}
\frac{\partial f}{\partial\sigma_x}&=\frac{1}{\bar{\sigma}}\left(\bar{a}_1\sigma_x+\bar{a}_{12}\sigma_y+\bar{a}_{13}\tau_{xy}\right)\\
\frac{\partial f}{\partial\sigma_y}&=\frac{1}{\bar{\sigma}}\left(\bar{a}_{12}\sigma_x+\bar{a}_2\sigma_y+\bar{a}_{23}\tau_{xy}\right)\\
\frac{\partial f}{\partial\tau_{xy}}&=\frac{1}{\bar{\sigma}}\left(\bar{a}_{13}\sigma_x+\bar{a}_{23}\sigma_y+\bar{a}_3\tau_{xy}\right)\\
\frac{\partial f}{\partial\tau_{xz}}&=\frac{1}{\bar{\sigma}}\left(\bar{a}_4\tau_{xz}+\bar{a}_{45}\tau_{yz}\right)\\
\frac{\partial f}{\partial\tau_{yz}}&=\frac{1}{\bar{\sigma}}\left(\bar{a}_{45}\tau_{yz}+\bar{a}_5\tau_{yz}\right)
\end{aligned} \quad \text{----}$$

(٣.٤٢)

and

$$A = -\frac{1}{\lambda}\frac{\partial f}{\partial k}dk$$ ----

(٣.٤٣)

where the $\bar{a}'s$ are parameters of anisotropy, $\bar{\sigma}$ is the Huber-Mises yield function and k is a hardening parameter. Manipulation of (٣.٣٦) - (٣.٤٣) leads to the following elastic-plastic incremental stress-strain relationship:

$$d\sigma = [D]_{ep}\, d\varepsilon$$ ----

(٣.٤٤)

with

$$[D]_{ep} = [D] - \frac{[D]a\, a^T [D]}{A + a^T [D]a}$$ ----

(٣.٤٥)

where the matrix $[D]$ is the constitutive matrix (for elastic response) defined before and the hardening parameter A or H' can be deduced to be:

$$A = H' = \frac{d\bar{\sigma}}{d\bar{\varepsilon}_p}$$ ---- (٣.٤٦)

where $\bar{\varepsilon}_p$ is the accumulated effective plastic strain. For linearly hardening materials the hardening parameter H' is constant. The hardening parameter H' can be determined experimentally, (see appendix A).

٣.٤ Geometric Nonlinearity

Two basically different formulations [١٤] can be employed for the description of large deformation problem: (a) A total Lagrangian approach in which the current (٢nd Piola Kirchhoff) stresses and (Green-Lagrange)

strain fields are referred to the original geometric configuration and the displacement field gives the current configuration of the system in relation to its initial position. (b) Updated Lagrangian approach in which the current configuration of the system is used to define the current (Cauchy) and (Almansi) strain state. Both the Green-Lagrange and Almansi strains reduce to the usual definition of engineering strains for infinitesimal deformation problems.

The most appropriate formulation for numerical solution depends on the type of analysis being considered. For the degenerated shell element employed in this work a specific and appropriate total Lagrangian formulation is adopted in which large deflections and moderate rotations (in the sense of Von Karman hypothesis) are accounted for. Reference of the problem variables to the original configuration is advantageous for quadratic degenerate shell elements, since the computationally expensive transfer of quantities between local and global axes need then be performed only once. The strain-displacement matrix is calculated once during the nonlinear process and its nonlinear part is updated using the current displacements by a simple matrix product. The constitutive relations defined previously in terms of engineering stresses and strains are considered valid for the new stress/strain quantities measured in the original configuration. [١٤]

Taking the variation of equation (٣.٣٣) with respect to a displacement variation $d\{\delta\}$ gives the tangential stiffness matrix for a geometrically nonlinear problem to be:

$$\left[\overline{K}\right]\cdot d\{\delta\}=\int_v \left[B\right]^T d\{\sigma\}dv + \int_v d\left[B\right]^T \{\sigma\}dv \quad \text{----}$$

(٣.٤٧)

The strain-displacement matrix $\left[B\right]$may be separated into the usual infinitesimal part $\left[B\right]_o$ and nonlinear contribution $\left[B\right]_L$ so that:

$$[B]=[B]_o+[B]_L \quad \text{---- (٣.٤٨)}$$

Consequently $d[B]^T = d[B]_L^T$ defining the initial stress or geometric stiffness matrix, $[K]_\sigma$ as:

$$[K]_\sigma \cdot d\{\delta\}=\int_v d[B]_L^T \{\sigma\}dv \quad \text{----}$$

(٣.٤٩)

then use of (٣.٢٨) and (٣.٤٩) in (٣.٤٧) results in:

$$[\overline{K}]=[K]+[K]_\sigma \quad \text{---- (٣.٥٠)}$$

in which $[K]$ is given by the usual expression:

$$[K]=\int_v [B]^T [D][B]dv \quad \text{---- (٣.٥١)}$$

For elastic-plastic problem, the elastic matrix $[D]$ in (٣.٥١) must be replaced by $[D]_{ep}$.

Introducing Von Karman assumptions, which imply that derivatives of u' and v' with respect to x', y' and z' are small, and noting that the derivatives of w' with z' may be neglected, the Green-Lagrange strains may be expressed in local coordinates as: [٥]

$$\{\varepsilon\}=\begin{Bmatrix}\varepsilon_{x'}\\ \varepsilon_{y'}\\ \gamma_{x'y'}\\ \gamma_{x'z'}\\ \gamma_{y'z'}\end{Bmatrix}=\begin{Bmatrix}\partial u'/\partial x'\\ \partial v'/\partial y'\\ \partial u'/\partial y'+\partial v'/\partial x'\\ \partial u'/\partial z'+\partial w'/\partial x'\\ \partial v'/\partial z'+\partial w'/\partial y'\end{Bmatrix}+\begin{Bmatrix}(1/2)(\partial w'/\partial x')^2\\ (1/2)(\partial w'/\partial y')^2\\ (\partial w'/\partial x')(\partial w'/\partial y')\\ 0\\ 0\end{Bmatrix}=\{\varepsilon\}_o+\{\varepsilon\}_L \quad \text{---- (٣.٥٢)}$$

From (٣.٥٢), the nonlinear contribution to the strain vector can be written as:

$$\{\varepsilon\}_L=\frac{1}{2}[S][R] \quad \text{----}$$

(٣.٥٣) where

$$[S]^T = \begin{bmatrix} \partial w'/\partial x' & 0 & \partial w'/\partial y' & 0 & 0 \\ 0 & \partial w'/\partial y' & \partial w'/\partial x' & 0 & 0 \end{bmatrix} \quad \text{---- (٣.٥٤)}$$

$$[R] = \begin{bmatrix} \partial w'/\partial x' \\ \partial w'/\partial y' \end{bmatrix} = [G]\{\delta\} \quad \text{---- (٣.٥٥)}$$

The term $[G]$ is a matrix with two rows and a number of columns equal to the total number of element nodal variables. The first row contains the contribution of each nodal variable to the local derivative $\partial w'/\partial x'$(corresponding shape function derivatives) and the second row contains similar contributions for $\partial w'/\partial y'$.

Taking the variation of (٣.٥٣) gives:

$$d\{\varepsilon\}_L = \frac{1}{2} d[S]\cdot[R] + \frac{1}{2}[S]\cdot d[R] = [S]\cdot d[R] = [S]\cdot[G]\cdot d\{\delta\} \quad \text{---- (٣.٥٦)}$$

and then by definition:

$$[B]_L = [S]\cdot[G] \quad \text{---- (٣.٥٧)}$$

In the present finite element analysis, matrices $[B]_o$ and $[G]$ are initially calculated and stored. Using the current displacements and (٣.٥٥), matrix $[S]$ is formed and then $[B]_L$ is obtained from (٣.٥٧). The incremental strain-displacement matrix $[B]$is evaluated by summing $[B]_o$ to the current value of $[B]_L$ [١٤]. In order to determine the tangential stiffness matrix given by (٣.٥٠), for use in the nonlinear algorithm, it only now remains to explicitly evaluate the geometric matrix, $[K]_\sigma$. Substituting from (٣.٥٧) in (٣.٤٩) results in:

$$[K]_\sigma \cdot d\{\delta\} = \int_v [G]^T d[S]^T \{\sigma\} dv \quad \text{---- (٣.٥٨)}$$

The term $d[S]^T \{\sigma\}$ can be written, with the aid of (٣.٥٤) and (٣.٥٥), as:

$$d[S]^T \{\sigma\} = [\sigma]\cdot[G]\cdot d\{\delta\} \quad \text{---- (٣.٥٩)}$$

in which

$$[\sigma]=\begin{bmatrix} \sigma_{x'} & \tau_{x'y'} \\ \tau_{x'y'} & \sigma_{y'} \end{bmatrix} \quad \text{---- (٣.٦٠)}$$

Substituting (٣.٥٩) in (٣.٥٨) gives the geometric stiffness matrix which is a symmetric matrix of the form,

$$[K]_\sigma = \int_v [G]^T [\sigma][G] dv \quad \text{----}$$

(٣.٦١) Matrix $[G]$ was previously defined in (٣.٥٥), and $[\sigma]$is seen from (٣.٦٠) to be composed of components of the current Piola-Kirchhoff stress vector.

٣.٥ Finite Element Computer Code

The program used in the present study, is that prepared by Hinton & Owen [١٤] for the elastic-plastic geometrically nonlinear analysis of both thick and thin plates and shells by the ٩-node degenerated shell element. The layered approach described in section ٣.٣.٨ is adopted. This program is developed in the present study including subroutine for auto mesh generation. Also, such program will be included and called in the optimal design process which is written in the present study as will be explained later in chapter four. The structure of the program is shown schematically in Figure (٣.٤) where, in particular, the order in which the various subroutines are called by the controlling or master segment is indicated.

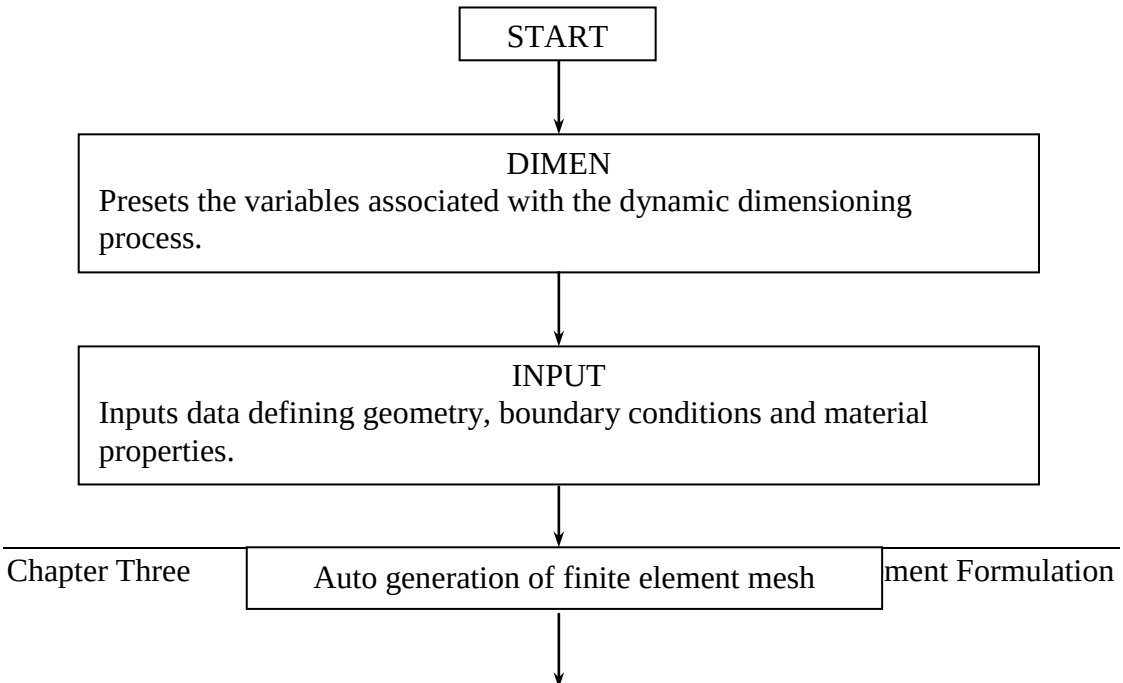

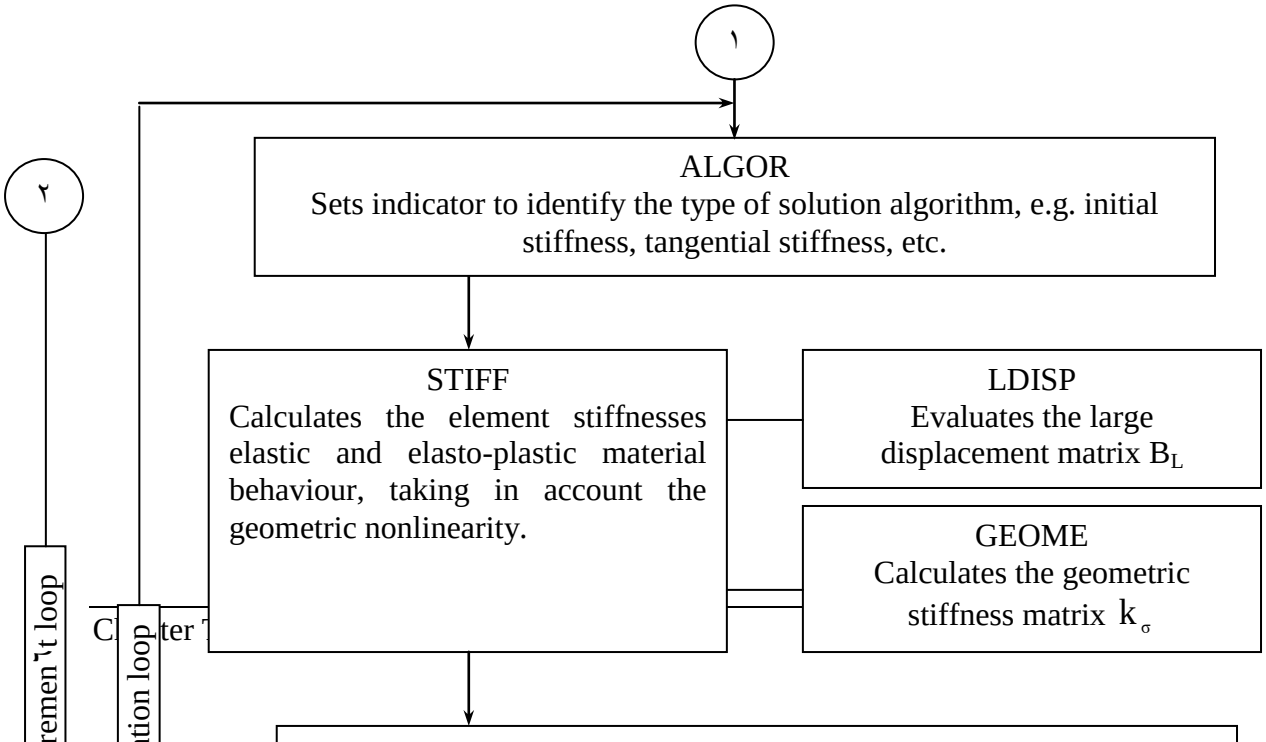
١
ALGOR
Sets indicator to identify the type of solution algorithm, e.g. initial stiffness, tangential stiffness, etc.
STIFF
Calculates the element stiffnesses elastic and elasto-plastic material behaviour, taking in account the geometric nonlinearity.
LDISP
Evaluates the large displacement matrix B_L
GEOME
Calculates the geometric stiffness matrix k_σ
٢

CHAPTER FOUR

OPTIMAL DESIGN FORMULATION

٤.١ Optimization

٤.١.١ General

Optimization is defined as finding the optimum value (maximum or minimum) of a function called the *objective function* $f(x_1, x_2, x_3, \ldots x_n)$ of n real variables called the *design variables*. The optimization is *constrained* when certain limitations are imposed on the design variables, while the optimization is *nonlinear* when the mathematical expressions relating the design variables in constraints or in the objective function are of nonlinear nature.

If for example, the function refers to the profit obtained by producing quantities x_i of products p_i, it may well be that the desire is to maximize the function. If on the other hand it refers to costs involved in an operation or volume of materials, it should probably be to minimize the function. From the mathematical point of view, there is little point in considering both maximization and minimization, since maximizing f is equivalent to minimizing – f. It is normal to confine the problem to minimization. In the present work, the nonlinear constrained optimization by the modified Hooke and Jeeves method will be implemented. Structural optimization for plate and shell structures is of great importance, especially in low-weight aerospace applications.

٤.١.٢ Direct Search Methods:

The general optimization problem is: minimize: $f(x_1 , x_2 , x_3 , \ldots x_n)$, of n real variables subject to the constraints : $g_i(x_1 , x_2 , x_3 , \ldots x_n) \leq b_i$ (i= ١ , ٢ , . . m).There is of course no loss of generality in assuming that all constraints are of less than or equal to variety. (The constraint $g(x) \geq$ ٠

can be written as $-g(x) \leq ٠$). Much effort has been devoted to devising direct search methods to locate the minimum of a function of n real variables. A direct search method is one that uses function values only. A number of methods have been suggested [١٠]. A function of two variables will be considered. Its contour lines are shown in Figure (٤.١), its minimum is at ($x_١^*$, $x_٢^*$). The crudest search method is the alternating variable search method. One starts at some point A and search in the direction of $x_١$ axis for a minimum in this direction and thus find B at which the tangent to the contour line is parallel to the $x_١$ direction. From B one then search in the direction of the $x_٢$ – axis and so proceed to C and then to D by searching parallel to the $x_١$ – axis… etc. In this way, one proceeds to the optimum point. It is clearly possible to extend the idea to function of n variables.

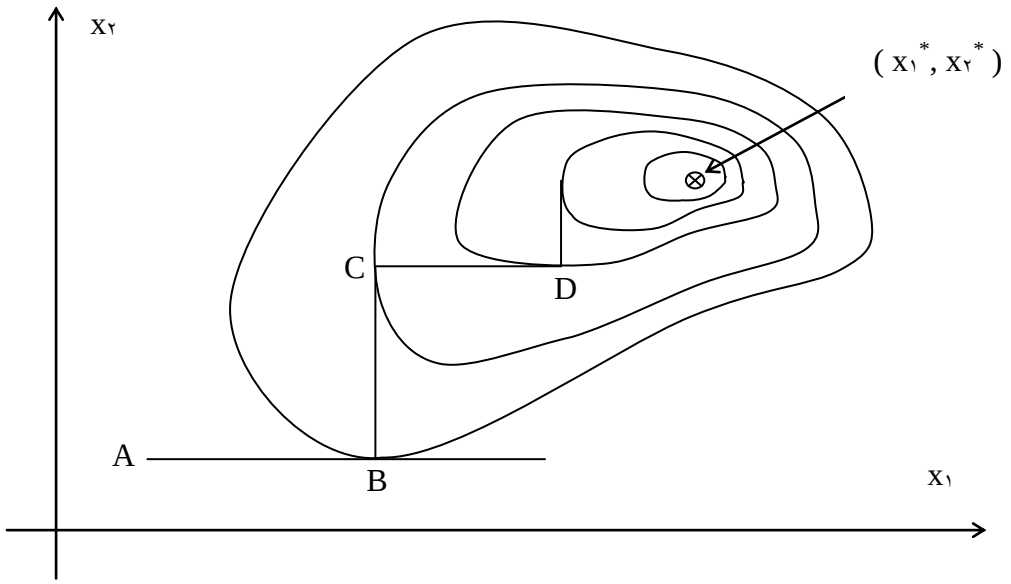

Figure (٤.١) Contour Lines for Function of Two Variables. [٤]

٤.١.٣ The Method of Hooke and Jeeves

In this method the search consists of a sequence of *exploration steps* about a *base point* which if successful are followed by *pattern moves.* The procedure is as follows: [٤]

(A) Choose an initial base point $\mathbf{b}_1$ and a step length hj for each variable xj; j=١, ٢, ..., n. The program written in this work uses a fixed step h for each variable

(B) Carry out an exploration about $\mathbf{b}_1$. The purpose of this is to acquire knowledge about the local behavior of the function. This knowledge is used to find a likely direction for the *pattern move* by which it is hoped to obtain an even greater reduction in the value of the function. The exploration about $\mathbf{b}_1$ proceeds as indicated.

(i) Evaluate f ($\mathbf{b}_1$).

(ii) Each variable is now changed in turn, by adding the step length. Thus one evaluates f ($\mathbf{b}_1+h_1\mathbf{e}_1$) where $\mathbf{e}_1$ is a unit vector in the direction of the x_1-axis. If this reduces the function, replace $\mathbf{b}_1$ by $\mathbf{b}_1+h_1\mathbf{e}_1$. If not, find f($\mathbf{b}_1-h_1\mathbf{e}_1$) and replace $\mathbf{b}_1$ by $\mathbf{b}_1-h_1\mathbf{e}_1$ if the function is reduced. If neither step gives a reduction leave $\mathbf{b}_1$ unchanged and consider changes in x_2, i.e. find f($\mathbf{b}_1+h_2\mathbf{e}_2$) etc. When one has considered all n variables, it is possible to have a new base point $\mathbf{b}_2$.

(iii) If $\mathbf{b}_2=\mathbf{b}_1$ i.e. no function reduction has been achieved, the exploration is repeated about the same base point $\mathbf{b}_1$ but with a reduced step length. In the present work, in which a structural optimization is performed using this method, it was found that reducing the step length to one half its former value is satisfactory.

(iv) If $\mathbf{b}_2 \neq \mathbf{b}_1$ one makes a *pattern move.*

(C) Pattern moves utilize the information acquired by exploration, and accomplish the function of the minimization by moving in the direction of the established "pattern". The procedure is as follows:

(i) It seems sensible to move further from the base point $\mathbf{b}_2$ in the direction $\mathbf{b}_2 - \mathbf{b}_1$ since that move has already led to a reduction in the function value. So one can evaluate the function at the next pattern point.

$$\mathbf{P}_1=\mathbf{b}_1+2(\mathbf{b}_2-\mathbf{b}_1) \qquad \text{----- (٤.١)}$$

In general

$$\mathbf{P}_i=\mathbf{b}_i+2(\mathbf{b}_{i+1}-\mathbf{b}_i) \qquad \text{----- (٤.٢)}$$

(ii) Then continue with exploratory moves about $\mathbf{P}_1$ ($\mathbf{P}_i$).

(iii) If the lowest value at step C(ii) is less than the base point $\mathbf{b}_2$ ($\mathbf{b}_{i+1}$ in general) then a new base point $\mathbf{b}_3$ ($\mathbf{b}_{i+2}$) has been reached. In this case repeat C(i). Otherwise abandon the pattern move from $\mathbf{b}_2$ ($\mathbf{bi}_{+1}$) and continue with an exploration about $\mathbf{b}_2$ ($\mathbf{b}_{i+1}$).

(D) Terminate the process when the step length has been reduced to a predetermined small value. The presentation of this method as a flow chart is shown in Figure (٤.٢) and Figure (٤.٣).

٤.١.٤ Dealing With Constraints

When applying the method of Hooke and Jeeves to the constrained optimization problem, one might suppose that it could be modified to take account of constraints. So, in the *modified* Hooke and Jeeves method it has been suggested that merely giving the objective function a very large value (in a minimization problem) will suffice whenever the constraints are violated. Certainly this idea has an intuitive appeal and is easy to program.

For each trial point one checks whether it lies within the constrained region or not. If so one evaluates the objective function in the normal

way. If not one gives the objective function a very large value. In this way, the search method will be directed back into the feasible region and hence towards the minimum point within the feasible region.

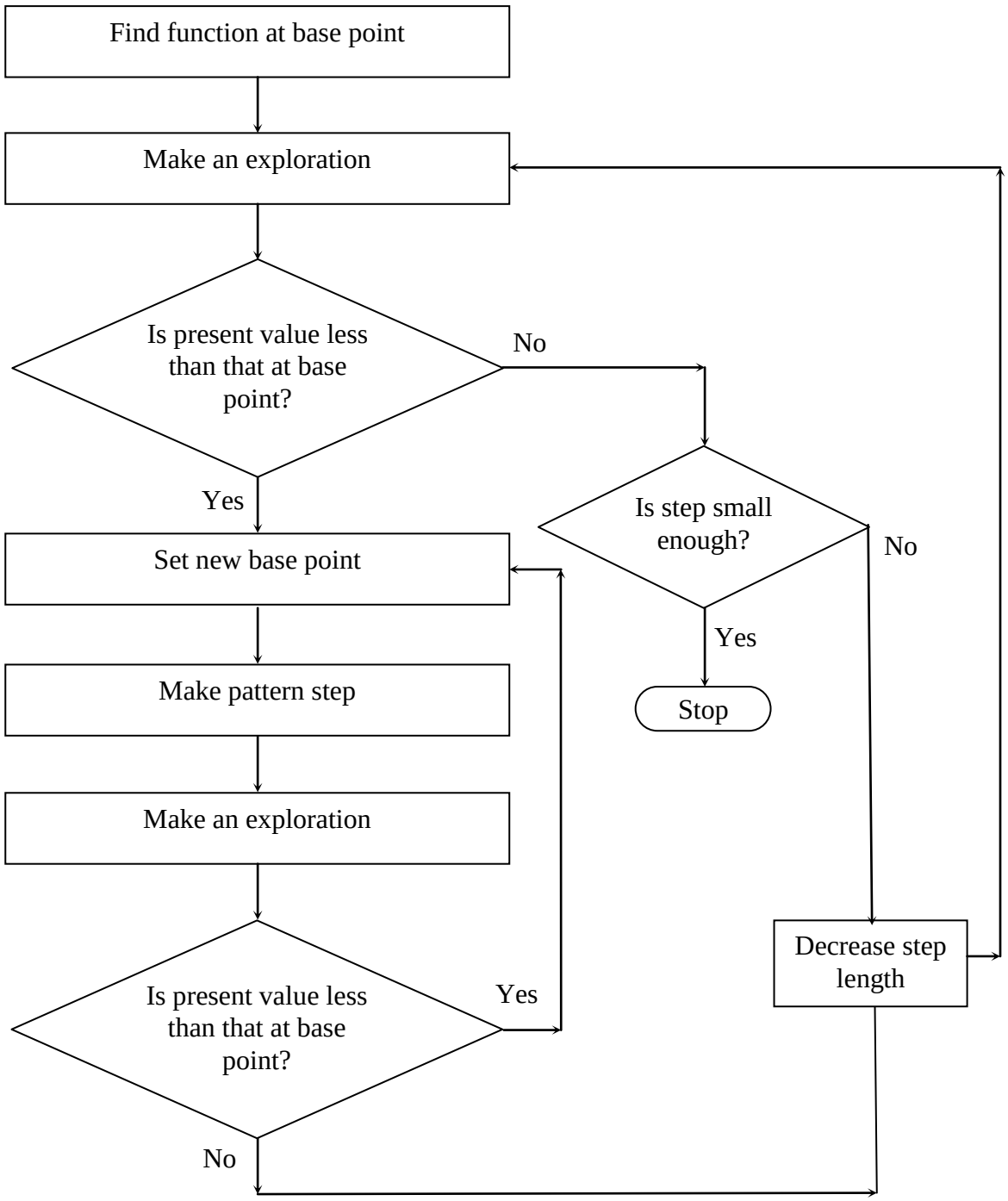

Figure (٤.٢) Flow Chart for Hooke and Jeeves Method [٤]

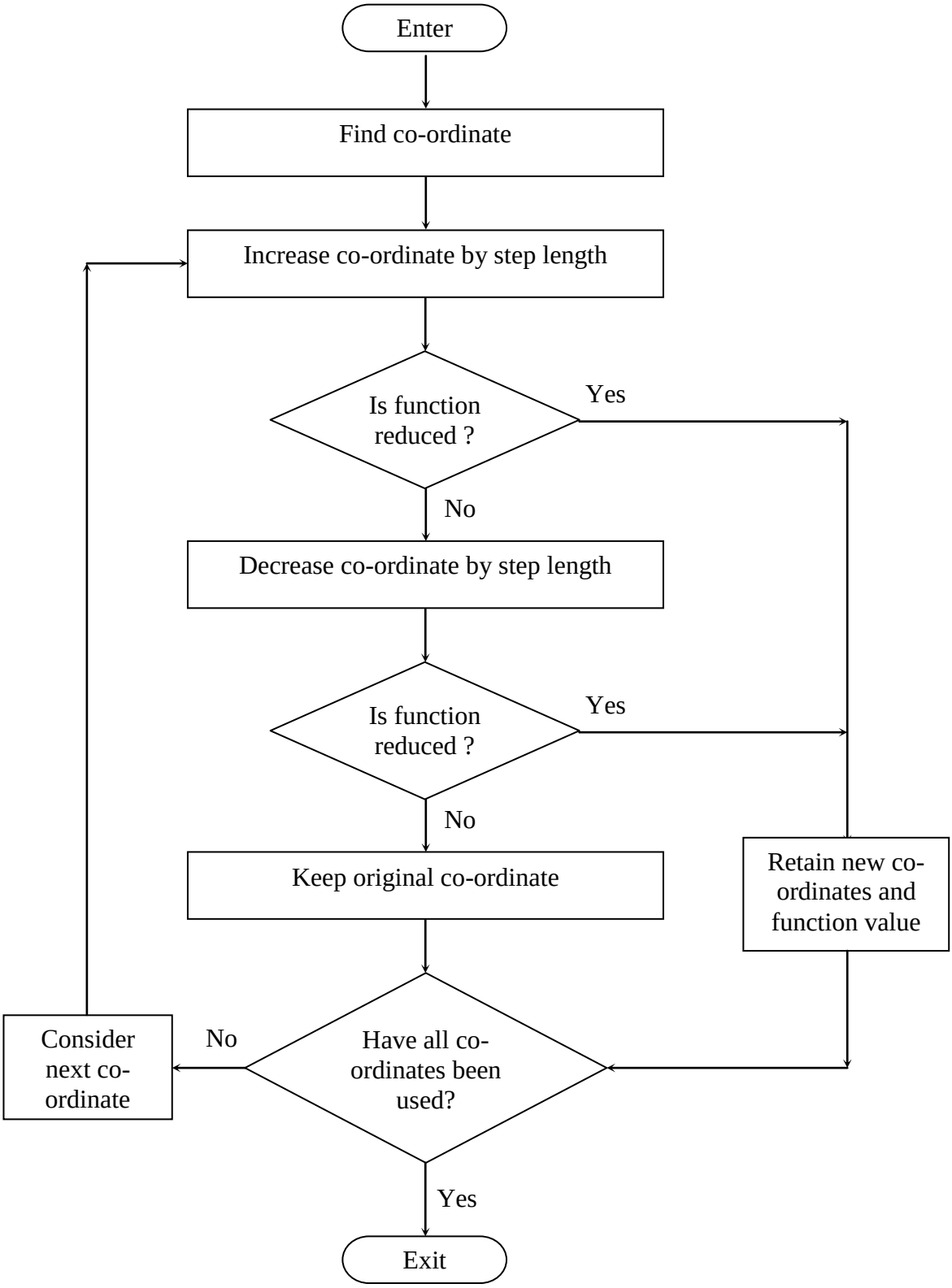

Figure (٤.٣) Flow Chart for an Exploration. [٤]

٤.٢ Plastic Design

٤.٢.١ General

In the structural analysis and design, the classical approach is based on the assumption that the stresses in the structure caused by the applied loads are within the elastic limit of the material used and thus deflections are small. The approach is, of course, widely used.

However, an alternative approach has gained increasing support recently. [٢٥] This new philosophy turns the problem on its head. It is obvious that any structure can be made to fall down (collapse) by applying loading of sufficient magnitude. The purpose of the new analysis is to find that magnitude. It requires knowledge of what happens at collapse and how structures behave when the stresses in the material exceed the elastic limit. This philosophy is embodied in the plastic methods of analysis and design. It is informative to examine the behavior of structures from zero load to failure because it is possible to show clearly the ideas behind the plastic methods.

٤.٢.٢ Elastic-Plastic Behaviour

Mild steel will be taken here as an example of elastic-plastic behavior of materials.

To achieve an understanding of relation between stresses and strains in both elastic and plastic ranges, laboratory tests must be accomplished [٢٥].

The simplest mechanical test is to apply a controlled tensile force to a long bar of material (Figure (٤.٤)). In the middle of the bar, remote from the clamps at each end, a state of pure uniaxial tension exists.

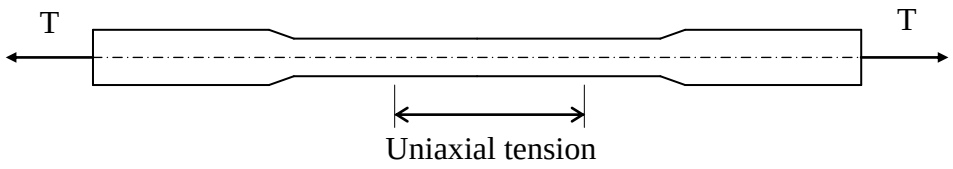

Figure (٤.٤) Uniaxial Tensile Specimen

If the extension of a mild steel specimen is measured (as strain) in this region and plotted against the applied force (expressed as a stress) the typical stress-strain curve shown in Figure (٤.٥) is obtained. At small strains, stress is directly proportional to strain (region OU). The material is elastic, and the slope, E, is the *Young's modulus.*

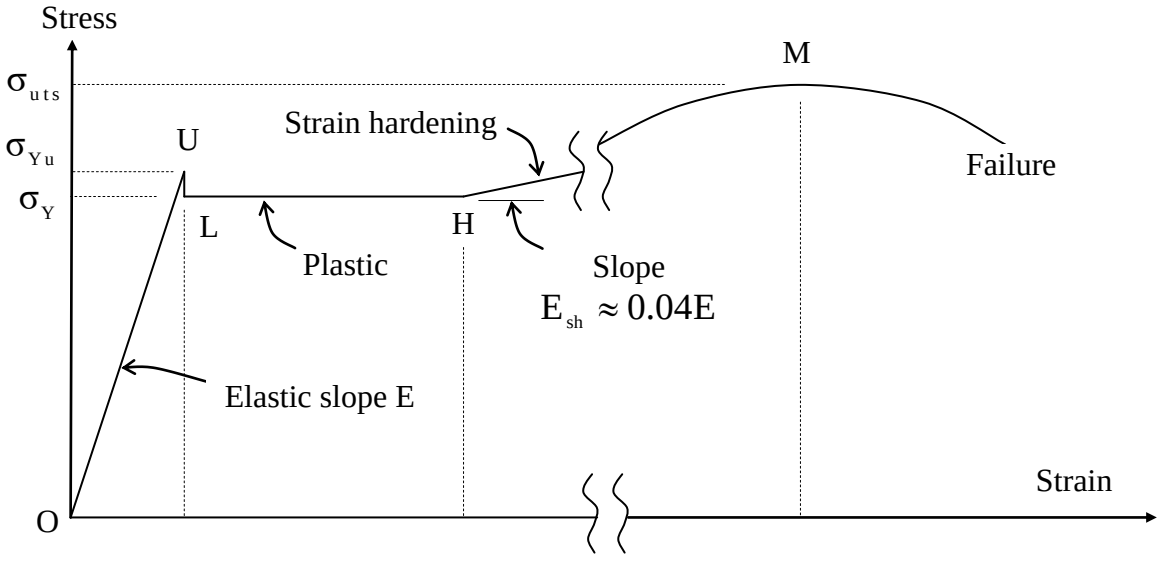

Figure (٤.٥) Stress-Strain Diagram. [٢٥]

On average E is about ٢٠٥ kN/mm^{٢}. The point U is the limit of proportionality between stress and strain. When this limit is reached there is a rapid drop in stress to the point L. U is called the *upper yield point*

with a corresponding stress σ_{Yu}. The magnitude of σ_{Yu} depends on the cross-sectional shape of the specimen and the type of equipment used to carry out the test. In many of the common structural steel sections which are hot rolled into shape, the residual stresses from the rolling process effectively remove point U. Hence the upper yield point is of no practical significance. The stress corresponding to point L is the *yield stress* σ_Y with a typical magnitude for mild steel of ٢٥٠ N/mm^2.

The strain at the yield stress is about ٠.٠٠١٢. When the strain is increased above this value it is found that no corresponding stress increase is required. The behavior in the region LH of the graph is called *plastic* (increase in strain without change in stress is called *plastic flow*). The end of plateau, H, is somewhat variable but a typical strain is ٠.٠١٤. The strain in the plateau is thus at least ten times the strain at the yield point.

After H, an increase in strain requires an increase in stress, but the relation is now non-linear. This is called *strain hardening.* The initial slope E_{sh} of this region is about ٤ per cent of Young's modulus, E. At a strain of at least ٠.٢, a ٢٠ per cent increase in the length of the specimen, the stress reaches its maximum value (point M). This stress is called the *ultimate tensile strength* σ_{uts} and is about ٤١٠ N/mm^2 for mild steel. Further increase in strain produces necking and eventually a cup and a cone fracture.

Careful tests have shown that the stress-strain curve for mild steel in compression is in fact identical to the one in tension up to the point of maximum stress, so that the complete graph is as in Figure (٤.٦). If the specimen is loaded to, say, point X and the load then removed, initially the change in strain is elastic (slope E) as shown by the solid line XY.

Ideal behavior will follow the solid line with compressive plastic flow occurring when the stress reaches σ_Y in the compressive sense. The actual behavior follows the broken line XY′ indicating an apparently reduced yield stress in compression. The divergence from the ideal path is called the *Bauschinger effect*.

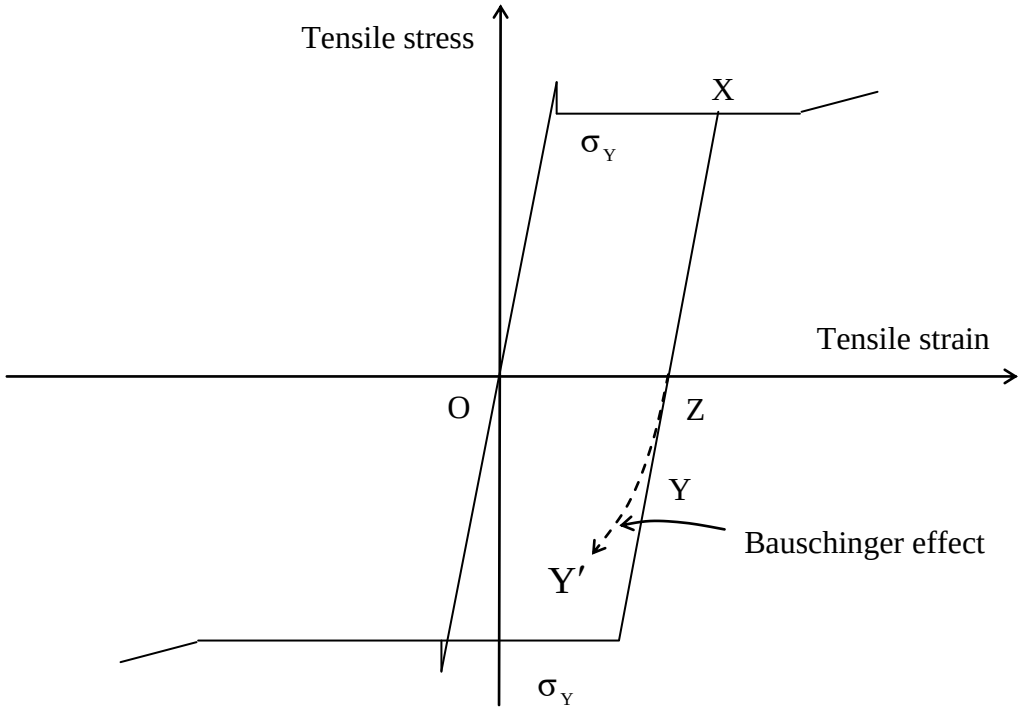

Figure (٤.٦) Bauschinger Effect

Perfect elastic-plastic behaviour is shown in Figure (٤.٧). Mild steel can be made to fit this by

(١) ignoring the upper yield point. This causes no problems; many structural members do not show it anyway.

(٢) ignoring strain hardening. This introduces some errors because many structures will have areas in the strain hardening region at collapse. However, the errors are small because of the small slope (E_{sh}) and are on the safe side since strain hardening represents an increase in strength.

(٣) ignoring the Baushinger effect. This causes errors but usually they are small. Figure (٤.٦) shows that when the stress is reduced to zero (point Z) there is little difference in the curves. In structures where full stress reversal is possible the errors can be significant. [٢٥] In the present optimal design formulation, the nature of the load is taken to be static and constant, i.e. there are no unloading cycles, and accordingly, Bauschinger phenomenon has no significant effect.

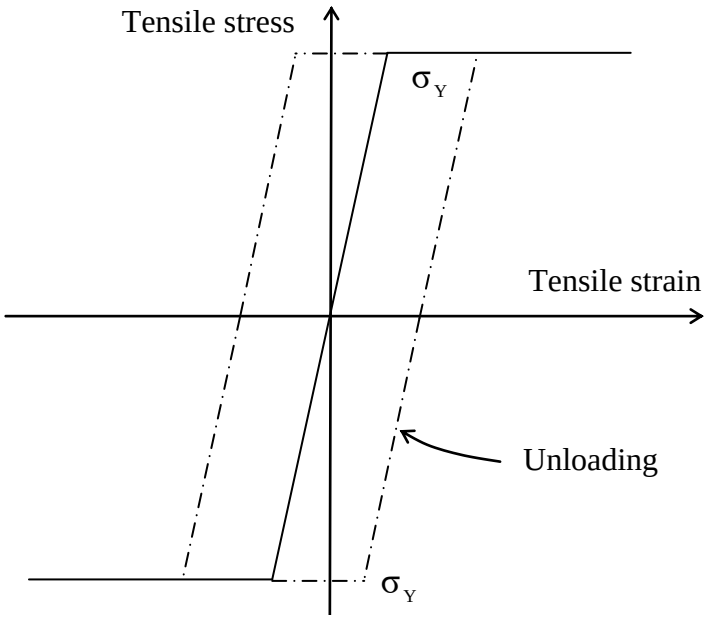

Figure (٤.٧) Perfect Elastic-Plastic Behaviour

Mild steel is not the only structural steel, various higher strength grades are in common use. Higher strengths are achieved at the expense of ductility as shown in Figure (٤.٨). In general, plastic analysis can be applied, with care, to structures made from these steels. The plastic design of plates and shells made of elastic-plastic material will be discussed in this chapter.

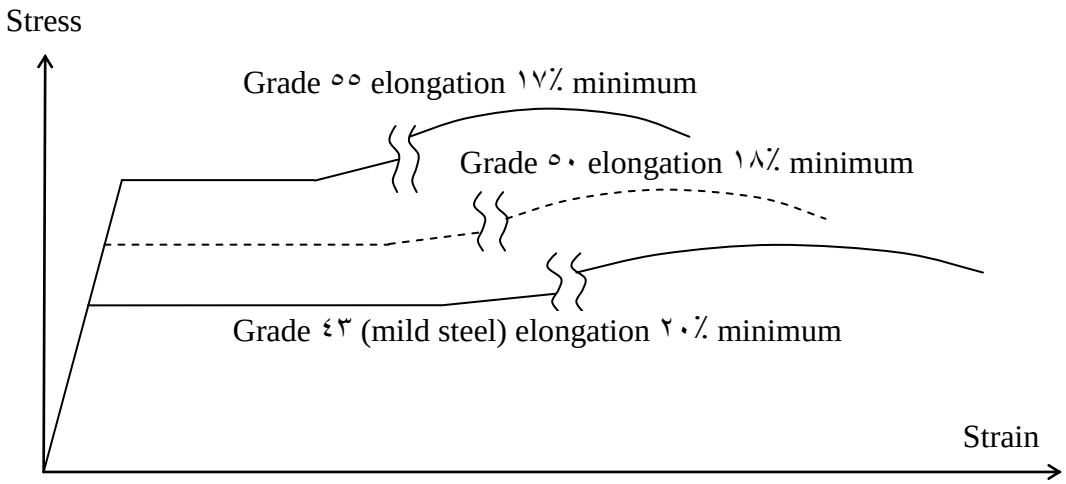

Figure (٤.٨) Stress-Strain Curves for Different Types of Steel

٤.٢.٣ Plastic Bending

Simple bending theory (based on elastic behavior) gives the following information about a general section under bending. If there is no yield in the material, there are straight line relationships for stress and strain over the whole depth of the section, as in Figure (٤.٩). The level at which the stress and strain are zero is the axis of zero strain. Stress and strain are proportional to distance (z) from this axis and for sagging there is maximum compression at the top and tension at the bottom. The maximum stress is given by

$$\sigma_{max} = \frac{M}{S}$$

where M = bending moment and S = elastic section modulus (minimum). (Notice that for an asymmetric section, as in Figure (٤.٩) with bending about the y axis, there are two possible values of the section modulus.)

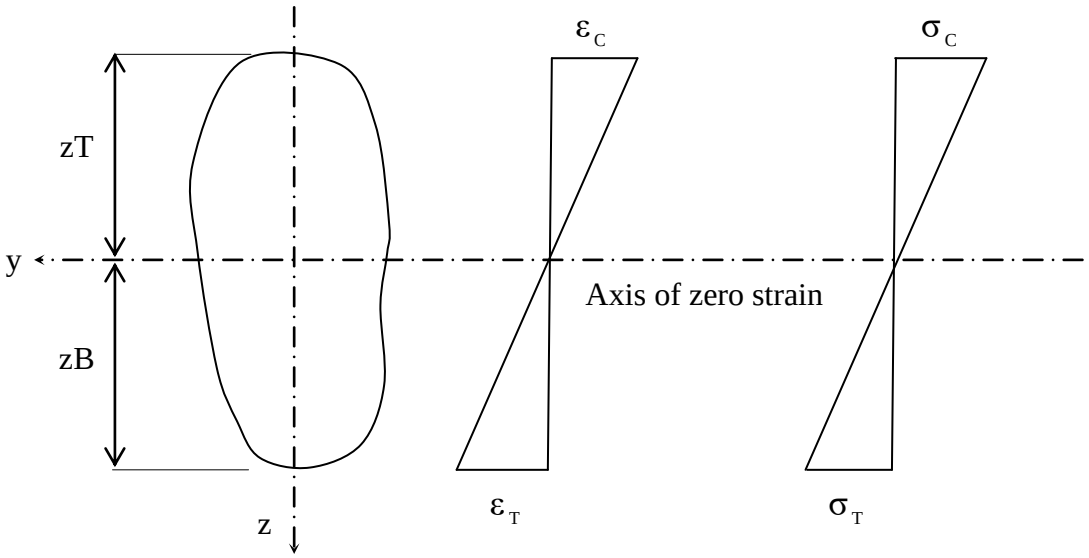

Figure (٤.٩) Elastic Stress and Strain

ST=I/zT and SB=I/zB where I is the second moment of area of the section about the y-axis. There will be different intensities of stress and strain at the top and bottom.

There will be elastic behavior until the maximum stress reaches the yield point. At this stage, of course, only material at the outside edge of the section yields. It has been shown in tests that the distribution of strains stays linear over the depth of the section after yield. [٢٥] (and the simple bending theory assumption of plane sections remaining plane is still valid). It is possible to find the stress at any position from the stress-strain curves as shown in Figure (٤.١٠) and (٤.١١). As the bending moment is increased, yielding spreads towards the axis of zero strain. The stress distribution shows two constant regions where yield has occurred (the stress is limited to the yield stress, but strain can be increased by plastic flow), joined by a linear (elastic) stress distribution.

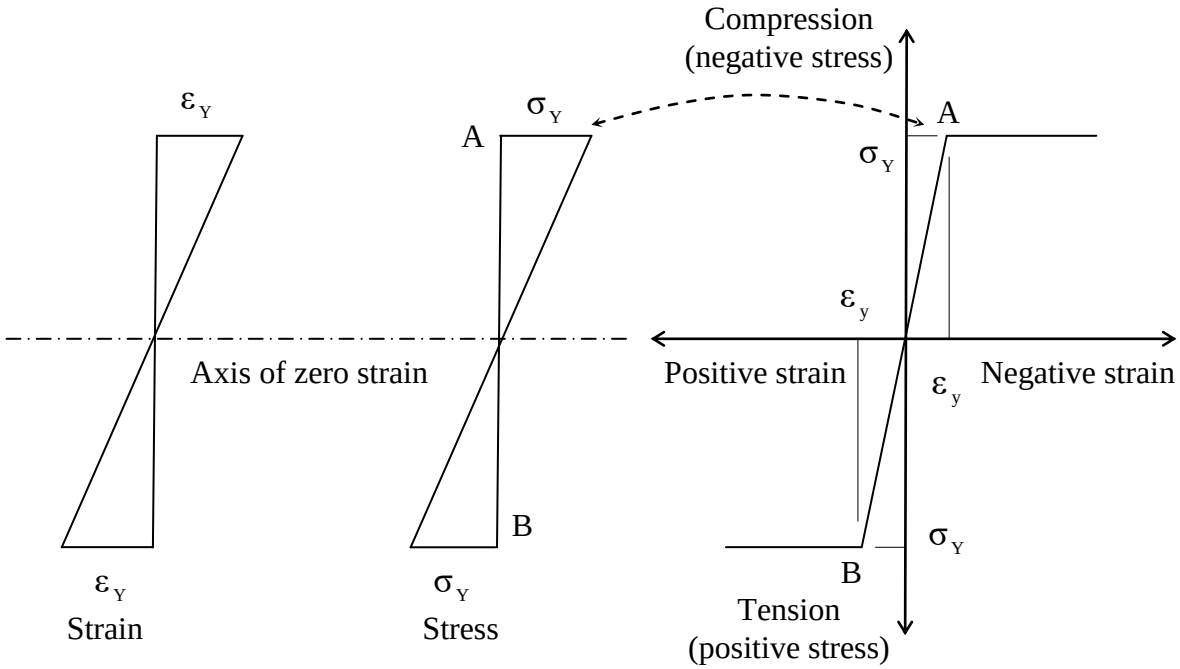

Figure (٤.١٠) Stress Distribution at Yield

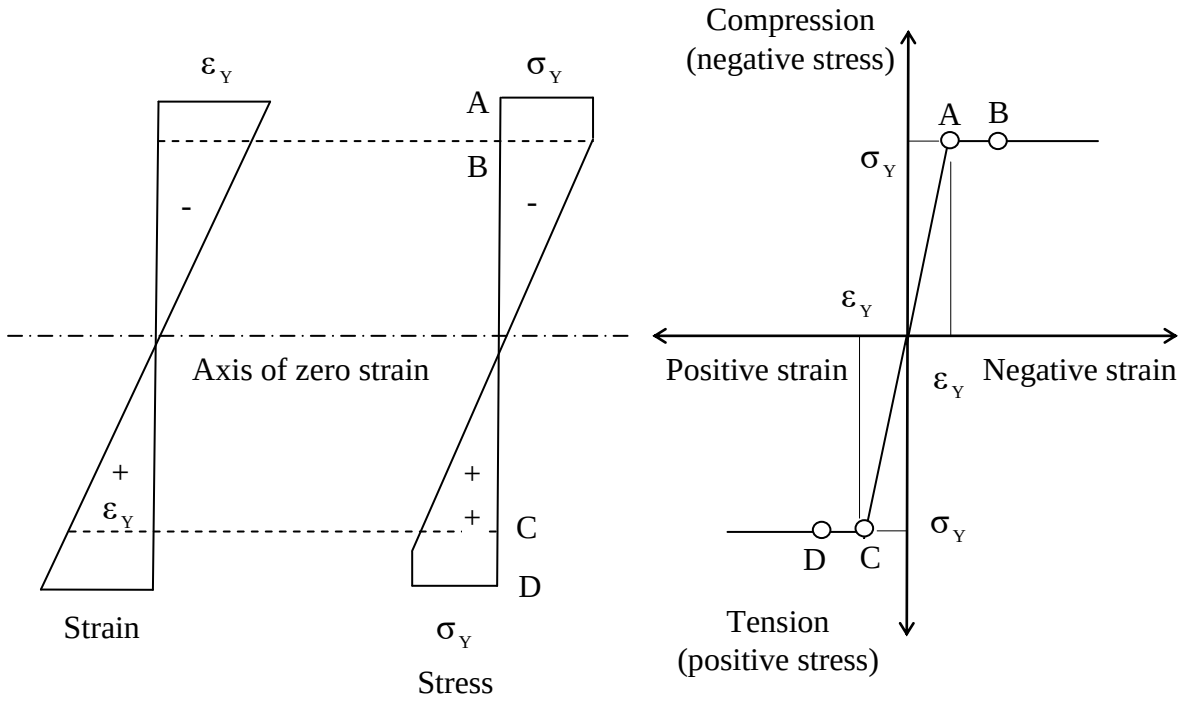

Figure (٤.١١) Stress Distribution after Yield

The logical conclusion is shown in Figure (٤.١٢) with constant stress to the axis of zero strain. With all the material yielding (in compression above and in tension below the axis of zero strain) the section behaves like a hinge because the strain can increase everywhere in the section without any change in stress.

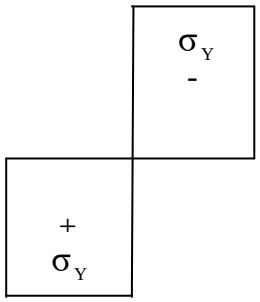

Figure (٤.١٢) Constant Yield Stress at Plastic stage

This hinge action is illustrated in Figure (٤.١٣). The section has become a *plastic hinge.* The plastic hinge is formed at a bending moment equal to the *plastic moment of resistance of* the section, which is the largest bending moment the section can carry. It is usually shortened to *plastic moment* and given the symbol M_p.

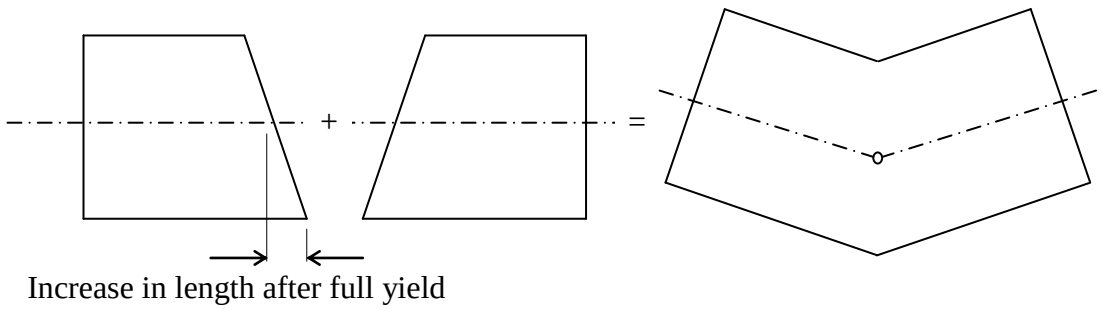

Figure (٤.١٣) Formation of Plastic Hinge

٤.٢.٤ Calculation of the Plastic Moment

٤.٢.٤.١ General

The load capacity of beams, frames, and plates is generally calculated according to plastic limit analysis. [٣] A general cross-section is shown in Figure (٤.١٤). The stress distribution due to the formation of a plastic hinge by bending about the y-axis is also shown. Since the hinge has been formed by bending only, horizontal equilibrium of the section requires that C = T, where C is the compressive force due to compressive yield above the axis of zero strain and T is the tensile force due to tensile yield below the axis.

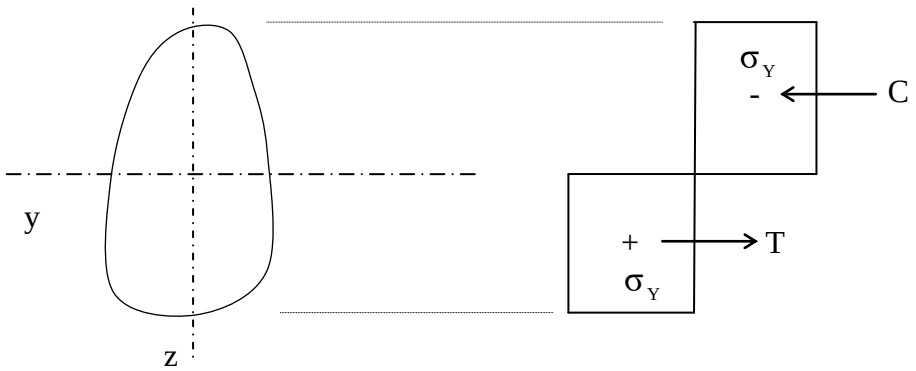

Figure (٤.١٤) Constant Stress Distribution

The area of section in compression is equal to the area of section in tension. Hence the axis of zero strain, when a plastic hinge forms, bisects the cross sectional area. This axis only coincides with the centroid of the section when the section is symmetric about the axis of zero strain.

٤.٢.٤.٢ Rectangular Section

In a rectangular section (Figure (٤.١٥)) bending about the y-axis, where the axis of zero strain is d/٢ from the top of the section,

$$C = T = \frac{bd}{2}\sigma_Y \qquad \text{----- (٤.٣)}$$

Since these forces are caused by a bending moment equal to M_p, taking moments about the axis of zero strain gives:

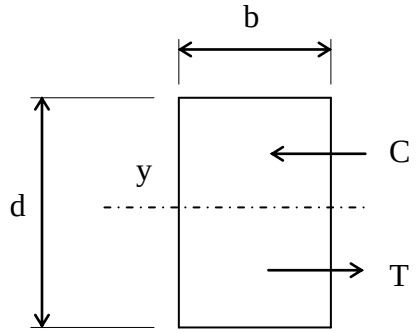

Figure (٤.١٥) Rectangular Section

$$M_p = C \times \frac{d}{4} + T \times \frac{d}{4} = 2 \times \frac{bd}{2}\sigma_Y \times \frac{d}{4}$$

that is

$$M_p = \frac{bd^2}{4}\sigma_Y \qquad \text{----- (٤.٤)}$$

This is usually written:

$$M_p = Z\sigma_Y \qquad \text{----- (٤.٥)}$$

where Z is called the *plastic modulus* of the section (differs from the section modulus S). Both the plastic and elastic moduli are geometric properties of the cross-section. The ratio of the plastic section modulus to the elastic section modulus is the shape factor of the section:

$$\text{shape factor} = \frac{Z}{S} \qquad \text{----- (٤.٦)}$$

For the rectangular section $S = bd^2/6$ so that:

$$\text{shape factor} = \frac{bd^2}{4} \Big/ \frac{bd^2}{6} = 1.5$$

Because the median surface of a shell exhibits at least one non-vanishing principal curvature, applied forces can be balanced

exclusively, from the very beginning of the loading process, by forces acting at every point of the median surface in the corresponding tangent plane. The shell is then said to act as a membrane. This situation occurs when the shell has a very small flexural rigidity, has supports with reactions in the tangent planes to the shell median surface at the boundary, and has discontinuities in, neither geometry (curvature, thickness) nor loading (concentrated loads). When the preceding conditions are not satisfied, flexural stresses arise in addition to membrane stresses. [٣٨]

٤.٢.٤.٣ Axial Force

In shell structures, cross sections may be exposed to high axial force and this will alter the plastic moment. The axial force, P, moves the axis of zero strain as in Figure (٤.١٦). To simplify the mathematics the stresses have been replaced by two equivalent distributions. [٢٥] The stresses in A are assumed wholly due to the axial force, that is

$$P = b\,z\,\sigma_Y \qquad \text{----- (٤.٧)}$$

The stresses in M are caused by the changed plastic moment M'_p

$$M'_p = 2\,\frac{(d-z)}{2} \times b \times \sigma_Y \left(\frac{d-z}{4} + \frac{z}{2}\right)$$

$$= (d-z) \times b \times \sigma_Y \left(\frac{d+z}{4}\right)$$

$$= \left(\frac{d^2 - z^2}{4}\right) b\,\sigma_Y$$

$$= \frac{b\,d^2}{4}\,\sigma_Y \left[1 - \left(\frac{z}{d}\right)^2\right]$$

From (٤.٤), $bd^2\sigma_Y/4$ is the plastic moment M_p of the rectangular section, so that

$$\frac{M'_p}{M_p} = 1 - \left(\frac{z}{d}\right)^2 \qquad \text{----- (٤.٨)}$$

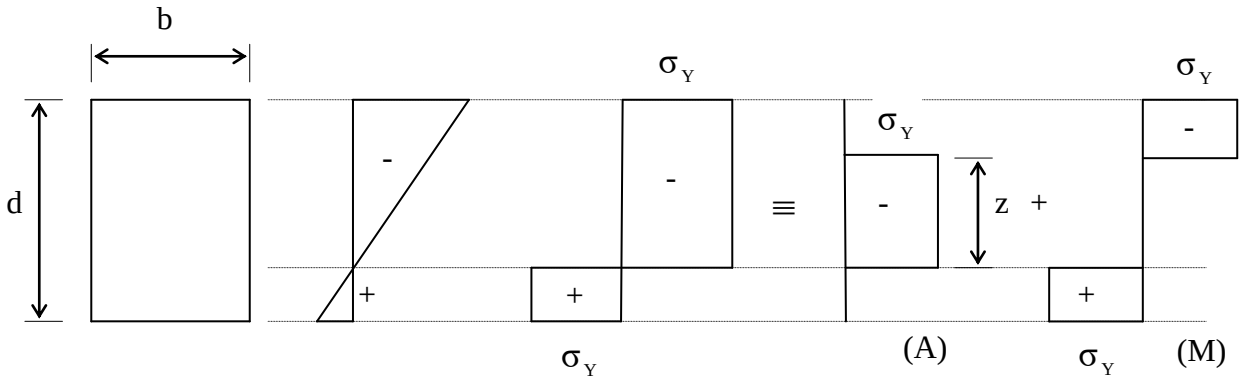

Figure (٤.١٦) the Equivalent Stresses

The maximum axial force N_p, where the section can carry ignoring buckling is called the *squash load* [٢٥] and is given by:

$$N_p = bd\sigma_Y \qquad \text{----- (٤.٩)}$$

so that

$$\frac{P}{N_p} = \frac{z}{d}$$

and

$$\frac{M'_p}{M_p} + \left(\frac{P}{N_p}\right)^2 = 1 \qquad \text{----- (٤.١٠)}$$

Equation (٥.١٠) shows that both tensile and compressive forces reduce the plastic moment because the reduction term is $(P/N_p)^2$. Equation (٤.١٠) is represented in Figure (٤.١٧)

Shells frequently have a large slenderness ratio (span-to-thickness ratio); the conservation of material normal to the median surface is well verified. Shear forces cause smaller reductions in plastic moment than axial forces, and need only be considered in the rare cases when they are exceptionally large. [٢٥]

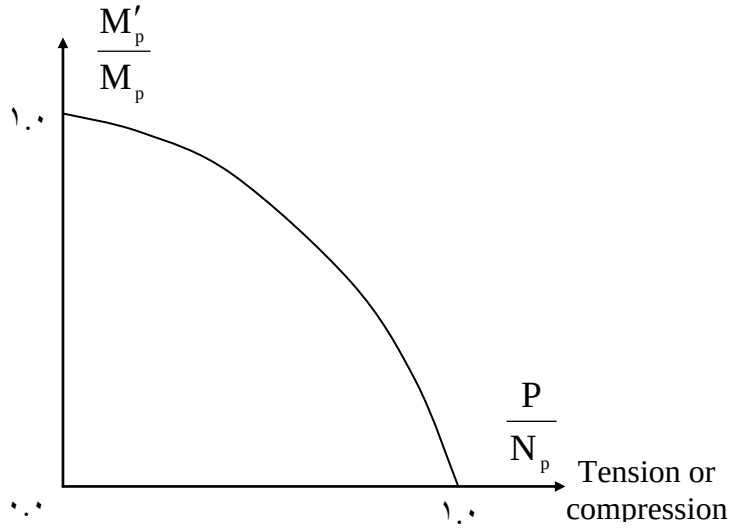

Figure (٤.١٧) Diagram for Equation (٤.١٠)

٤.٢.٤.٤ Approximations in Plastic Moment

To analyze the spread of yield through a section, a relationship must be found between bending moment and curvature for the section.

It is assumed that a short length of beam, length δx, which is initially straight, is bent into an arc of a circle as in Figure (٤.١٨). (This assumption is only true when the bending moments along the beam are constant, but the error is small when the moments vary provided that the deflection of the beam is small.). It has already been assumed that plane sections remain plane and the distribution of strain across the depth of the section is always linear as in Figure (٤.١٠), whatever is the distribution of stress

across the section. The arc which defines the axis of zero strain must remain δx long, while

length of top arc = $\delta x(1-\varepsilon_C)$

length of the bottom arc = $\delta x(1+\varepsilon_T)$

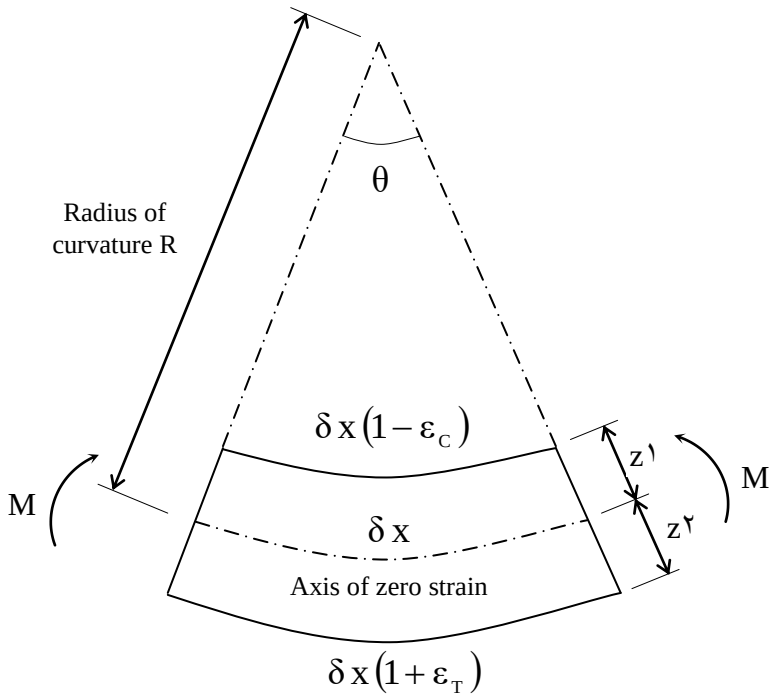

Figure (٤.١٨) Short Segment of a Beam under Bending. [٢٥]

From the geometry of Figure (٤.١٨)

$$R\theta = \delta x \qquad \text{----- (٤.١١)}$$

$$(R + z_2)\theta = \delta x(1+\varepsilon_T) \qquad \text{----- (٤.١٢)}$$

$$(R - z_1)\theta = \delta x(1-\varepsilon_C) \qquad \text{----- (٤.١٣)}$$

Substituting equation (٤.١١) into equations (٤.١٢) and (٤.١٣) gives:

$$(R + z_2) = R(1+\varepsilon_T) \qquad \text{----- (٤.١٤)}$$

$$(R - z_1) = R(1-\varepsilon_C) \qquad \text{----- (٤.١٥)}$$

Subtracting equation (٤.١٥) from equation (٤.١٤) gives:

$$(z_1 + z_2) = R(\varepsilon_C + \varepsilon_T) \qquad \text{----- (٤.١٦)}$$

The inverse of the radius of curvature, R, is defined as the curvature, χ, thus:

$$\text{curvature } \chi = \frac{\varepsilon_T + \varepsilon_C}{z_1 + z_2} = \frac{\text{range of strain}}{\text{depth of section}} \qquad \text{----- (٤.١٧)}$$

Curvature is simply a measure of bending deformation.

The ideal elastic-plastic moment curvature relationship is shown in Figure (٤.١٩ a). There is an elastic portion where an increase in curvature requires an increase in the moment causing the curvature. When the moment reaches the plastic moment, a plastic hinge forms and the curvature can increase without any change in the moment. This is the plastic rotation of the hinge. From simple bending theory, the slope of the elastic portion is EI.

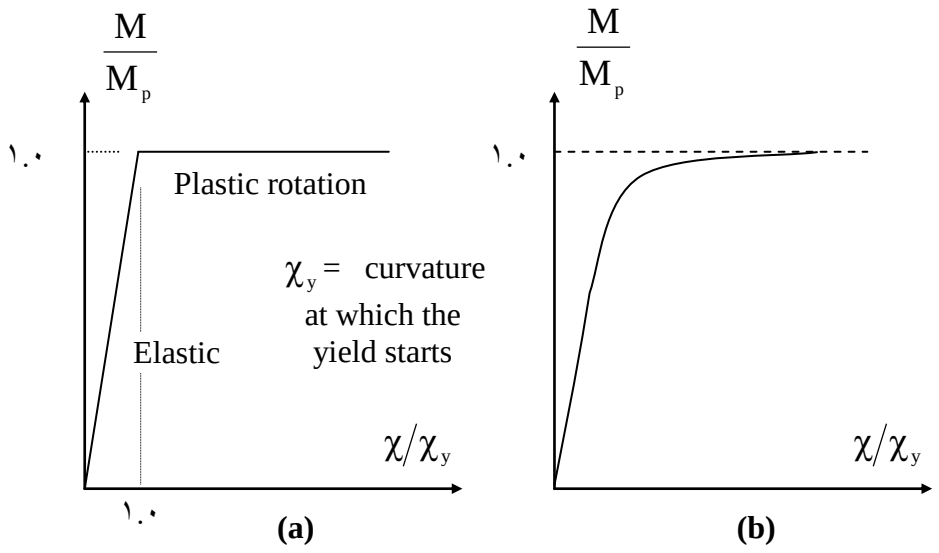

Figure (٤.١٩) Moment-Curvature Relationship

It is assumed in section (٤.٢.٣) that when a plastic hinge has formed, the whole of the critical section has yielded. This implies that just above and below the axis of zero strain there are strains equal to the yield strain, but of opposite sign. The only way that this and the assumption of plane

sections remaining plane can be valid, is for the strains to be very large at the top and the bottom of the section. Clearly this is physically impossible.

The spread of yield through the section is analyzed by assuming a distribution of stress as in Figure (٤.٢٠), with diminishing the size of the elastic region. At each stage the moment which causes the stress distribution and strains at the top and the bottom of the section can be calculated. This can be used to plot the actual moment-curvature relationship of the section. This has been done in Figure (٤.١٩ b) for the rectangular section, and as can be seen the actual curve is asymptotic to the ideal relationship. Practically there is always a small elastic region sandwiched in the middle of the section.

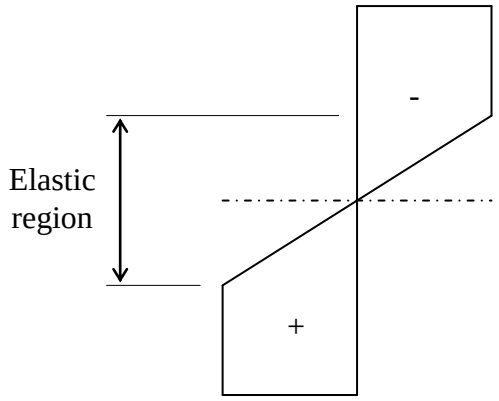

Figure (٤.٢٠) Assumed Stress Distribution

So far, only the critical section with highest bending moment has been considered, and it would appear that plastic flow is confined to that section. In fact, the bending moments at sections adjacent to the critical one are sufficient to cause yielding before the plastic hinge can form. The result is zones of plastic material around the critical section, as shown in Figure (٤.٢١). The extent of the zones depends on the type of loading. It is greater with distributed loads where the changes in bending moment are

more gradual, than with concentrated loads. The zones cause a gradual bend in the member, rather than a sharp kink which would result from a true plastic hinge. The fact that it is not practically possible to develop the full plastic moment of the section, is balanced by ignoring the hidden reserve in strength due to strain hardening.

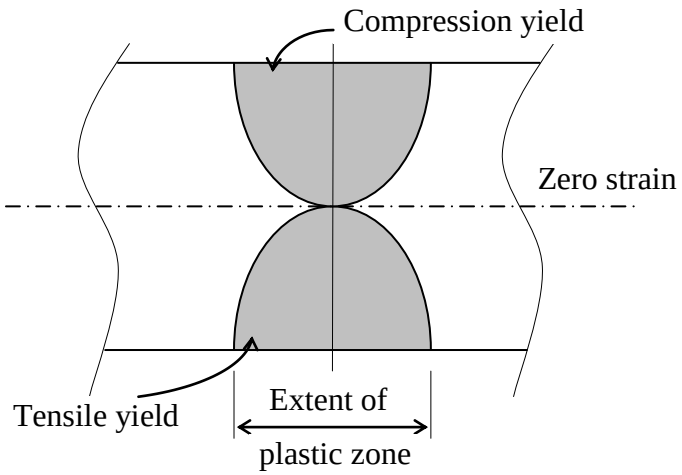

Figure (٤.٢١) Shape of Plastic Zone at Section with Highest B.M.

٤.٢.٥ Yield Condition

To formulate a reliable design technique, a yield criterion must be derived in terms of general, multi-axial stress resultants state. The yield criteria is given in terms of stress components. When the state of stress is a uniaxial tension or compression, the yield condition for most metals is:

$$\sigma = \pm \sigma_Y \qquad \text{-----} \quad (٤.١٨)$$

In a multiaxial state of stress, yielding will occur when a certain physical condition related to the state of stress will be satisfied. In uniaxial tension or compression, this condition must reduce to (٤.١٨). For metals, and particularly for mild steel, it has been observed that plastic deformations basically consist of slip in crystals. [٣٨] Hence, it has been thought that the maximum shearing stress determines the onset of yielding, which could

always occur for a *fixed* value of the maximum shearing stress. This is the Tresca's yield condition. The value of the maximum shear stress at yielding can be obtained, for instance, from a tensile test where:

$$\tau_{max} = \frac{\sigma}{2},$$

and hence,

$$\tau_{max,Y} = \frac{\sigma_Y}{2} \qquad \text{----- (٤.١٩)}$$

In a multiaxial state of stress with principal stresses $\sigma_1, \sigma_2, \sigma_3$, the magnitude of the maximum shearing stress is the largest among the three absolute values:

$$\frac{|\sigma_1 - \sigma_2|}{2}, \frac{|\sigma_2 - \sigma_3|}{2}, \frac{|\sigma_3 - \sigma_1|}{2}$$

Consequently, the yield condition is represented, in Cartesian orthogonal axes $(\sigma_1, \sigma_2, \sigma_3)$ by a hexagonal prism formed by the planes with equations:

$$\sigma_1 - \sigma_2 = \pm \sigma_Y \ , \ \sigma_2 - \sigma_3 = \pm \sigma_Y \ , \ \sigma_3 - \sigma_1 = \pm \sigma_Y$$

When one of the principal stresses vanishes, say, σ_3, the surface reduces to the hexagon obtained by intersecting the prism with the plane $\sigma_3 = ٠$ (figure (٤.٢٣-a)). The yield condition becomes

$$\max\left[|\sigma_1| \ , \ |\sigma_2| \ , \ |\sigma_1 - \sigma_2|\right] = \sigma_Y \qquad \text{----- (٤.٢٠)}$$

More refined tests have however shown [٣٨] that the circular cylinder circumscribed to the considered hexagonal prism was a more exact "yield surface" for most metals. this surface represents the yield condition of Maxwell, Huber, Hencky, and Von Mises, and usually it is called the "Von Mises yield condition" (Figure (٤.٢٢)). The equation of this surface is

$$\sigma_1^2+\sigma_2^2+\sigma_3^2-\sigma_1\sigma_2-\sigma_2\sigma_3-\sigma_3\sigma_1=\sigma_Y^2 \qquad \text{----- } (٤.٢١)$$

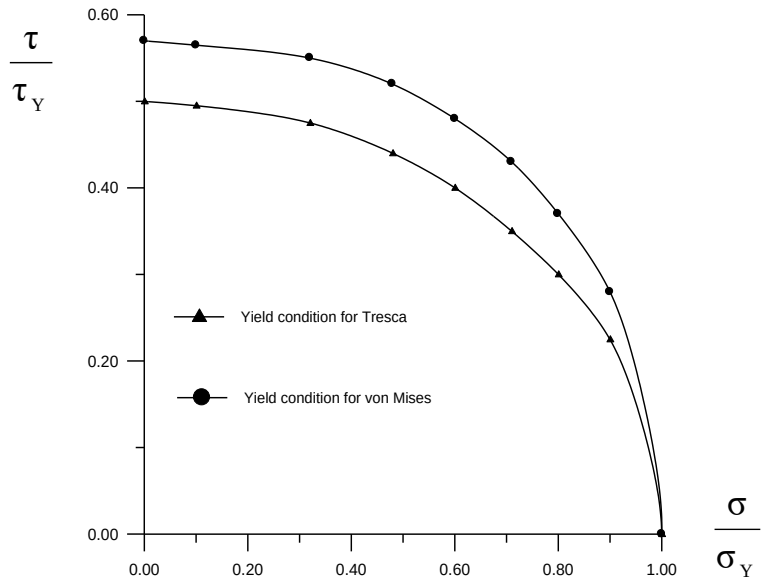

Figure (٤.٢٢) Tresca and Von Mises Yield Conditions. [٣٨]

For a state of plane stress as the case in the degenerated shell element ($\sigma_3=0$), condition (٤.٢٠) is represented by the ellipse of Figure (٤.٢٣ b) with the equation

$$\sigma_1^2+\sigma_2^2-\sigma_1\sigma_2=\sigma_Y^2 \qquad \text{----- } (٤.٢٢)$$

and since:

$$\sigma_1=\frac{\sigma_x+\sigma_y}{2}+\sqrt{\frac{1}{4}\left(\sigma_x-\sigma_y\right)^2+\tau_{xy}^2} \qquad \text{----- } (٤.٢٣)$$

$$\sigma_2=\frac{\sigma_x+\sigma_y}{2}-\sqrt{\frac{1}{4}\left(\sigma_x-\sigma_y\right)^2+\tau_{xy}^2} \qquad \text{----- } (٤.٢٤)$$

the following relation could be obtained:

$$\sigma_x^2+\sigma_y^2-\sigma_x\sigma_y+3\tau_{xy}^2=\sigma_Y^2$$

or

$$\left(\frac{\sigma_x}{\sigma_y}\right)^2+\left(\frac{\sigma_y}{\sigma_Y}\right)^2-\left(\frac{\sigma_x}{\sigma_Y}\right)\left(\frac{\sigma_y}{\sigma_Y}\right)+3\left(\frac{\tau_{xy}}{\sigma_Y}\right)^2=1 \qquad \text{----- (٤.٢٥)}$$

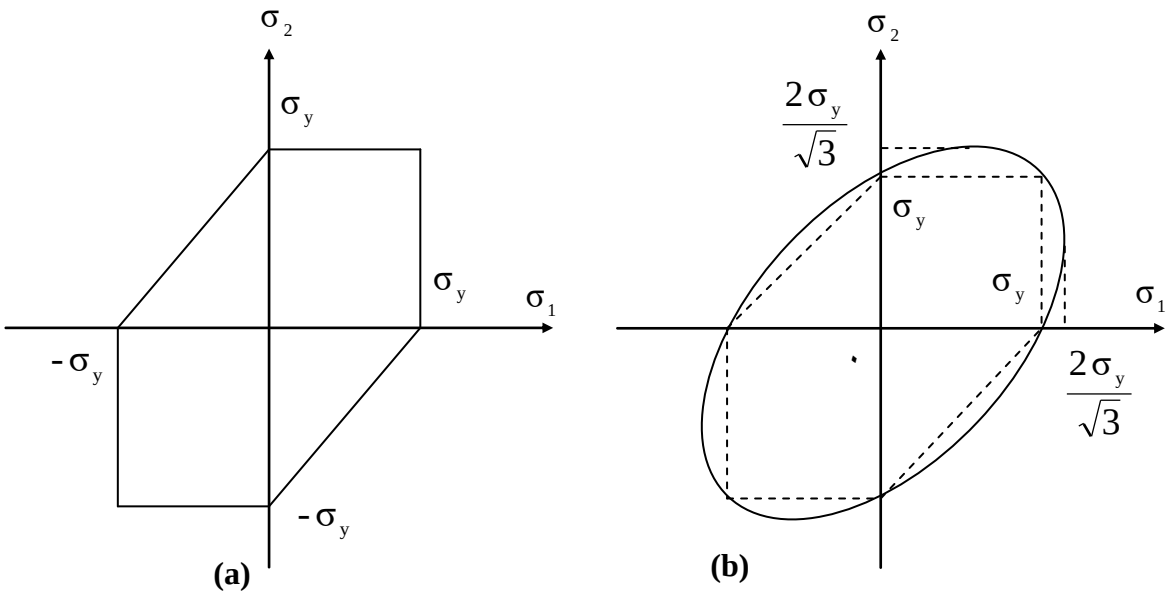

Figure (٤.٢٣) Yield Curves For Plane Stress
(a) Tresca Condition
(b) Von Mises Condition

The formula (٤.٢٤) does not account for the stress component τ_{xz} and τ_{yz} which are small in magnitude and can be neglected, while the normal stress component σ_z is already ignored.

Because moments are seen to be proportional to the stress components, the yield surface in the space of moments will have the same form as in the space of stress components. [٣٨], [١٧] i.e.

$$\left(\frac{M_x}{M_p}\right)^2+\left(\frac{M_y}{M_p}\right)^2-\left(\frac{M_x}{M_p}\right)\left(\frac{M_y}{M_p}\right)+3\left(\frac{M_{xy}}{M_p}\right)^2=1 \qquad \text{----- (٤.٢٦)}$$

Combination of (٤.١٠) and (٤.٢٤) and using the notations N_x and N_y for the axial stress resultant in x and y directions respectively, one can obtain the following criterion of yielding:

$$\left(\frac{M_x}{M_p}+\left(\frac{N_x}{N_p}\right)^2\right)^2+\left(\frac{M_y}{M_p}+\left(\frac{N_y}{N_p}\right)^2\right)^2-\left(\frac{M_x}{M_p}+\left(\frac{N_x}{N_p}\right)^2\right)\left(\frac{M_y}{M_p}+\left(\frac{N_y}{N_p}\right)^2\right)$$
$$+3\left(\frac{M_{xy}}{M_p}\right)^2=1 \qquad \text{----- (٤.٢٧)}$$

For a section with unit width and thickness t:

$$\left(\frac{4M_x}{\sigma_Y t^2}+\left(\frac{N_x}{\sigma_Y t}\right)^2\right)^2+\left(\frac{4M_y}{\sigma_Y t^2}+\left(\frac{N_y}{\sigma_Y t}\right)^2\right)^2-\left(\frac{4M_x}{\sigma_Y t^2}+\left(\frac{N_x}{\sigma_Y t}\right)^2\right)\times$$
$$\left(\frac{4M_y}{\sigma_Y t^2}+\left(\frac{N_y}{\sigma_Y t}\right)^2\right)+3\left(\frac{4M_{xy}}{\sigma_Y t^2}\right)^2=1$$

or

$$t=\left[\left(\frac{4M_x}{\sigma_Y}+\left(\frac{N_x}{\sigma_Y}\right)^2\right)^2+\left(\frac{4M_y}{\sigma_Y}+\left(\frac{N_y}{\sigma_Y}\right)^2\right)^2-\left(\frac{4M_x}{\sigma_Y}+\left(\frac{N_x}{\sigma_Y}\right)^2\right)\times\right.$$
$$\left.\left(\frac{4M_y}{\sigma_Y}+\left(\frac{N_y}{\sigma_Y}\right)^2\right)+3\left(\frac{4M_{xy}}{\sigma_Y}\right)^2\right]^{(1/4)} \qquad \text{----- (٤.٢٨)}$$

٤.٢.٦ Computer Program

A computer program is written in FORTRAN for optimal design of various types of shells and folded plates following the modified Hooke and Jeeves method. In the present work, at each exploration, an elastic-plastic geometrically nonlinear analysis, in which the thickness is constrained by equation (٤.٢٨), is performed. The process is continued as described in article (٤.١.٣) until the optimum (minimum volume of material) is reached. To achieve this task, two subroutines were written

and added to the analysis program, the first carries out the design process while the second performs auto generation of finite element mesh.

٤.٣ Load Factor

The objective of any design based on plastic theory must produce a structure with a specified load factor against collapse. The value of the load factor to be used is in itself a complex object and is always an issue of debate. It is worth while presenting the existing and proposed load factors.

The current British Standard, BS ٤٤٩ (١٩٦٩), allows design by plastic methods without stating explicitly the required load factor. BS ٤٤٩ is based mainly on elastic theory and it can be shown that the load factor for a single-span beam resulting from the elastic requirements varies with the end support conditions and type of loading. The minimum value is ١.٧٥ for a simply supported I-beam. It was argued [٢٥] that this value could be adopted for any structure. BS ٤٤٩ recognizes that it is highly unlikely that maximum wind load and maximum imposed load will occur simultaneously so that the load factor for such a load combination could be reduced. Consequently the commonly accepted load factors for design to BS ٤٤٩ are:

Imposed and dead load ١.٧٥

Wind and imposed and dead load ١.٤

Part of the limit state philosophy adopted in the B/٢٠ draft of the proposed new standard is to base load factor on the probability of occurrence of various load combinations. Consequently different collapse load factors are proposed for various loading condition. There is a further load factor in every case to allow for the possibility of variation in strength of the steel. This is done by using an effective yield stress equal

to σ_Y/١.٠٧٥. This increases the values of load factor by ٧.٥ per cent. Even so, the new proposed load factors are lower than those in BS ٤٤٩, reflecting the increase in confidence in the plastic methods of design.

The American specification for structural steel adopts a similar, but more detailed approach than BS ٤٤٩. It allows plastic methods of design and requires a collapse load factor of ١.٧ on live and dead load, and a reduced factor of ١.٣ when these loads act in conjunction with wind or earthquake loads.

CHAPTER FIVE

APPLICATIONS AND DISCUSSION

٥.١ General

In this chapter, some study cases are examined to compare the results obtained by the present elastic-plastic, geometrically nonlinear finite element analysis using the degenerated shell element with other theoretical and experimental results. A number of numerical examples have been analyzed by the developed program. The examples also serve as means to check the validity of the elastic-plastic representation of the material. Also, the examples demonstrate the applicability and capacity of the analysis method adopted in this research to a variety of three-dimensional plates and shells. From practical point of view, it is necessary to indicate that some approximations are involved in this method of analysis. These approximations are mainly due to: [٢]

١. Approximations included in the material modeling
٢. Approximations in the finite element modeling technique.
٣. Approximations introduced due to the type of procedure used in dealing with the nonlinear problem.

٥.٢ Nonlinear Analysis Applications

Convergence studies are usually carried out in finite element applications in order to select a suitable mesh with minimum number of elements that indicates a convergence in results.

٥.٢.١ Clamped Square Plate of Linear Hardening Material

A clamped square plate subjected to an increasing uniform load as described in Figure (٥.١) was analyzed by Moshaiov and Vorus [٢٤] and also by Owen and Figueiras. [٢٩], [٣٠] A linear strain hardening material was assumed. Due to symmetry of loading, geometry and boundary

conditions, only one quarter of the plate is analyzed using ٩ elements. Number of load increments is ٢٠ and ٦ layers are used to represent the material through the thickness. The thickness of the plate is h=٠.٢ and span L=٦.٠. The following properties of the plate material are used:

$$E_x = E_y = 30000.0, \upsilon = 0.3, \sigma_y = 30.0,\ H' = 300.0 \quad (\text{units MN, m})$$

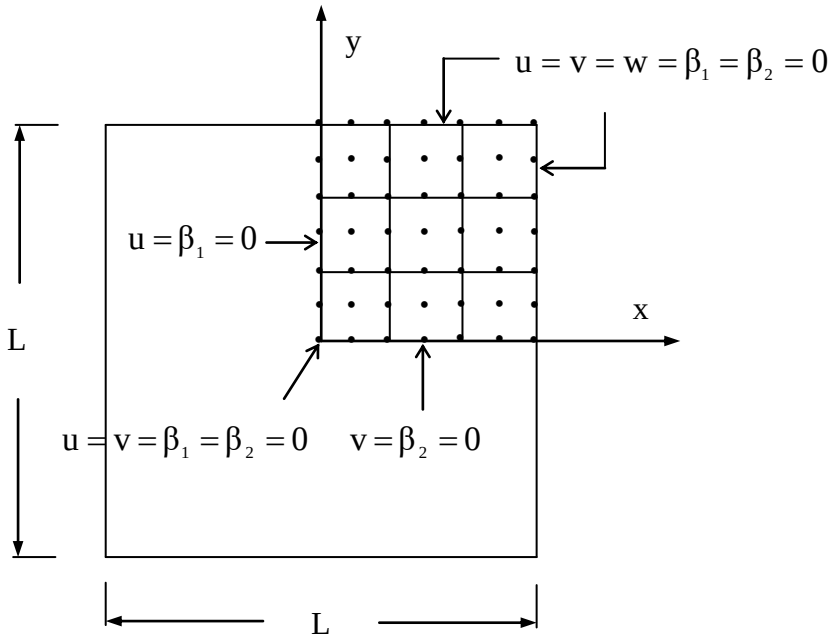

Figure (٥.١) Clamped Square Plate

The results of the deflection at the plate center vs. the uniformly distributed load are plotted in Figure (٥.٢). There is good agreement between the present results and those obtained by the boundary element method of Moshaiov and Vorus and also by the semiloof element by Owen and Figueiras.

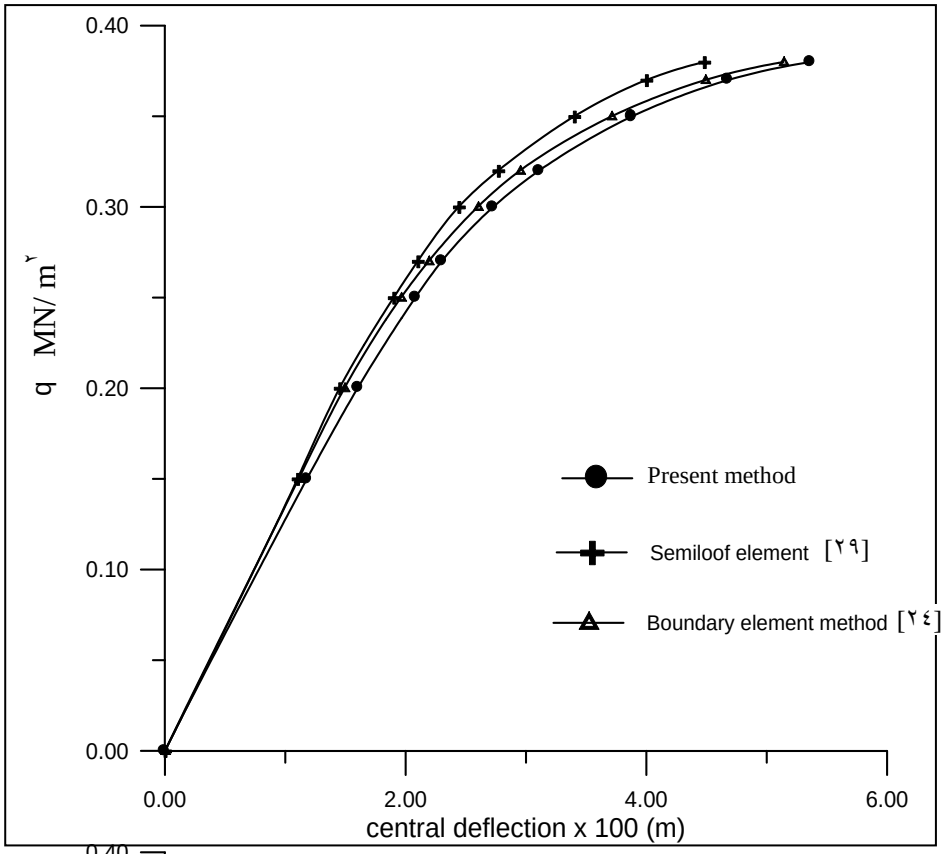

Figure (٥.٢) Load versus Central Deflection for Clamped Square Plate Subjected to Uniformly Distributed Load

Results for the same plate loaded by a central concentrated load are presented in Figure (٥.٣), together with those obtained by Owen and Figueiras.[٢٩] The nonlinear behaviour, following the linear elastic deflection is readily observed. Comparison of the results shows very good agreement between the curves in Owen and Figueiras study and those of the present study.

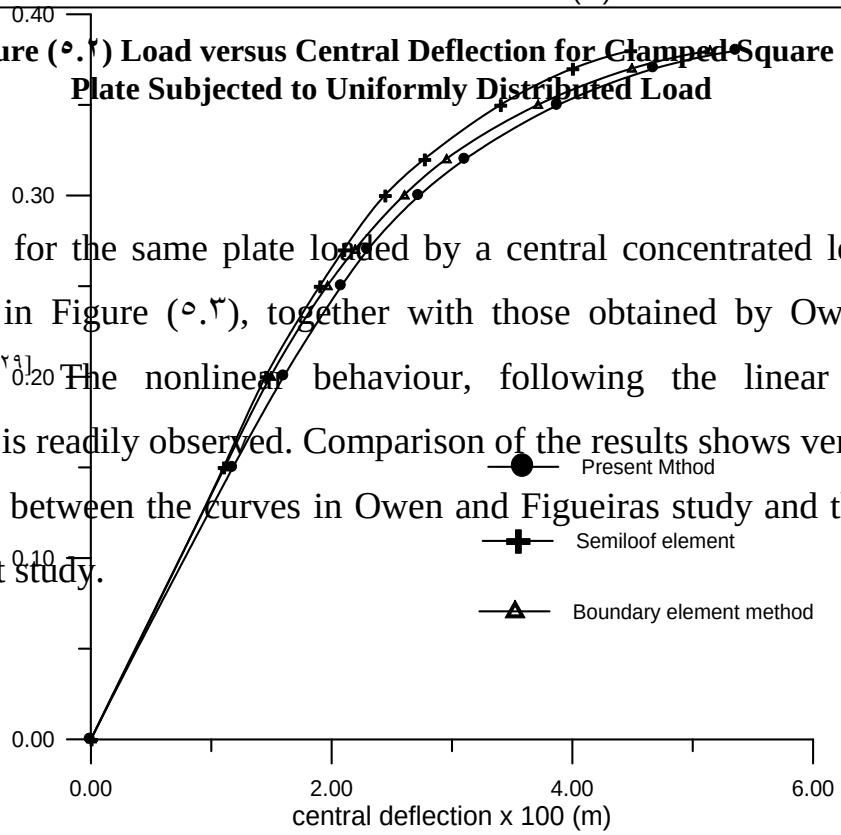

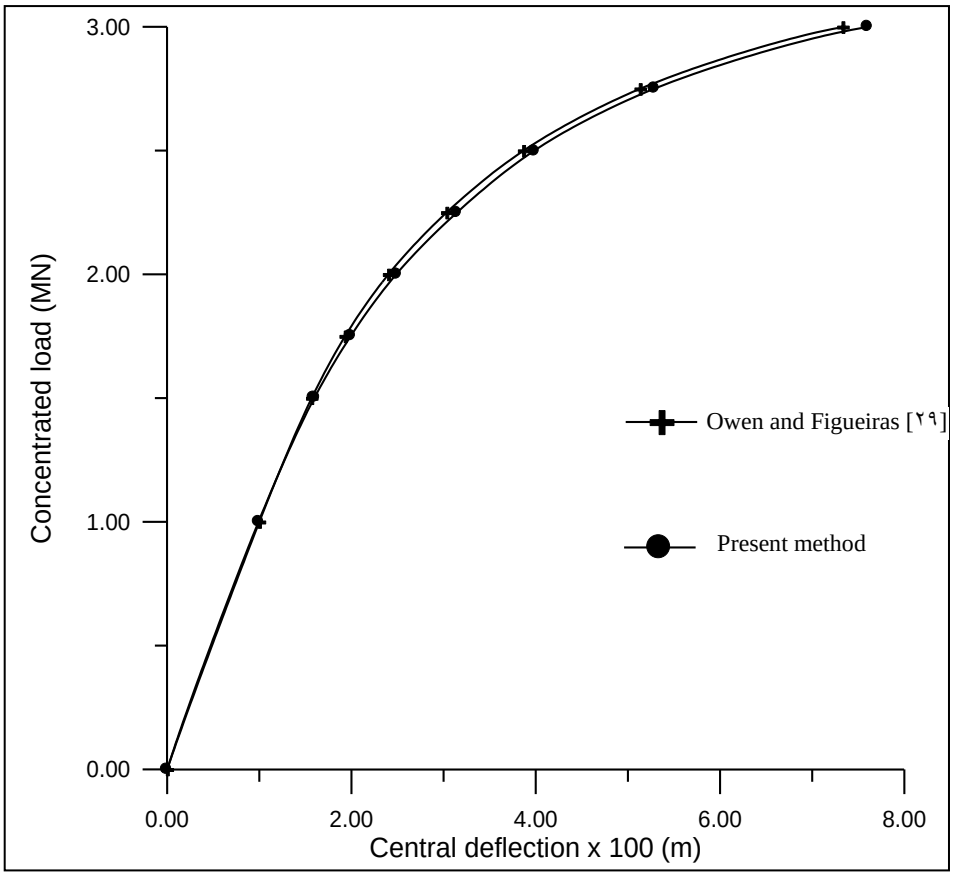

Figure (٥.٣) Load versus Central Deflection for Clamped Square Plate Subjected to Concentrated Load

٥.٢.٢ Clamped Circular Plate of Hardening Material Subjected to Uniform Load

This example of a clamped circular plate was investigated by Moshaiov and Vorus and also by Popov et al.[٢٤] as illustrated in Figure (٥.٤). Taking the symmetry of loading and geometry, a quarter of the plate is modelled by a mesh of ٥ nine-node degenerated shell element. The through-thickness behaviour of the plate is represented by ٦ equal layers and the number of load increments adopted in the solution is ٢٠. The plate has the following constants:

$E = 1.0 \times 10^4$ ksi (68950MPa), $\upsilon = 0.3, \sigma_y = 17$ ksi (117.2MPa),

$E_p = 3 \times 10^3$ ksi (20685MPa), plate thickness $2a = 1.0$in (25.4mm),

diameter $2R = 20.0$in (508 mm)

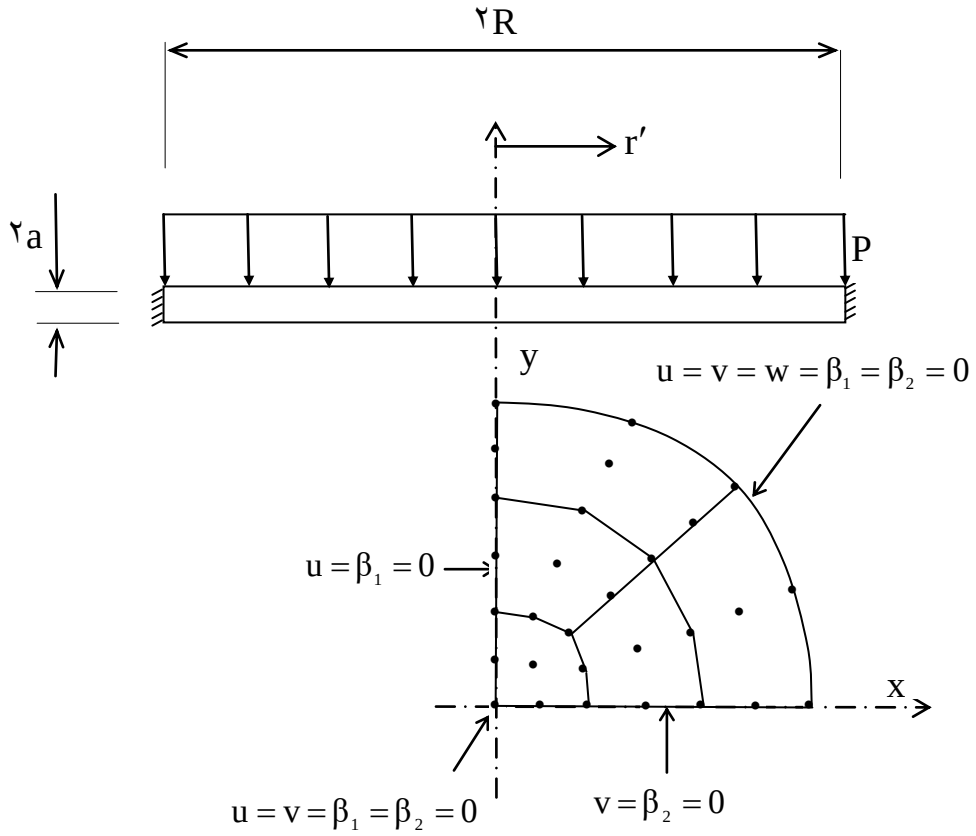

Figure (٥.٤) Clamped Circular Plate

Popov et al. considered a curvilinear hardening behaviour (see Figure (٥.٥)) while Moshaiov and Vorus approximated the above behaviour by a linear hardening material. The second approach is applied here.

The plate is subjected to uniform vertical load P= ٠.٥٦ ksi. The distribution of the deflections through the plate is plotted in Figure (٥.٦) together with that obtained by the two aforementioned groups of researchers. Good agreement is apparent. Also, it is noticed that at the centre of the plate, a region in which high bending moments are localized, the predicted deflection by the present method is higher than that found by the elastic-plastic boundary element method of Moshaiov and Vorus and that obtained by the curvilinear hardening approach of Popov et al.

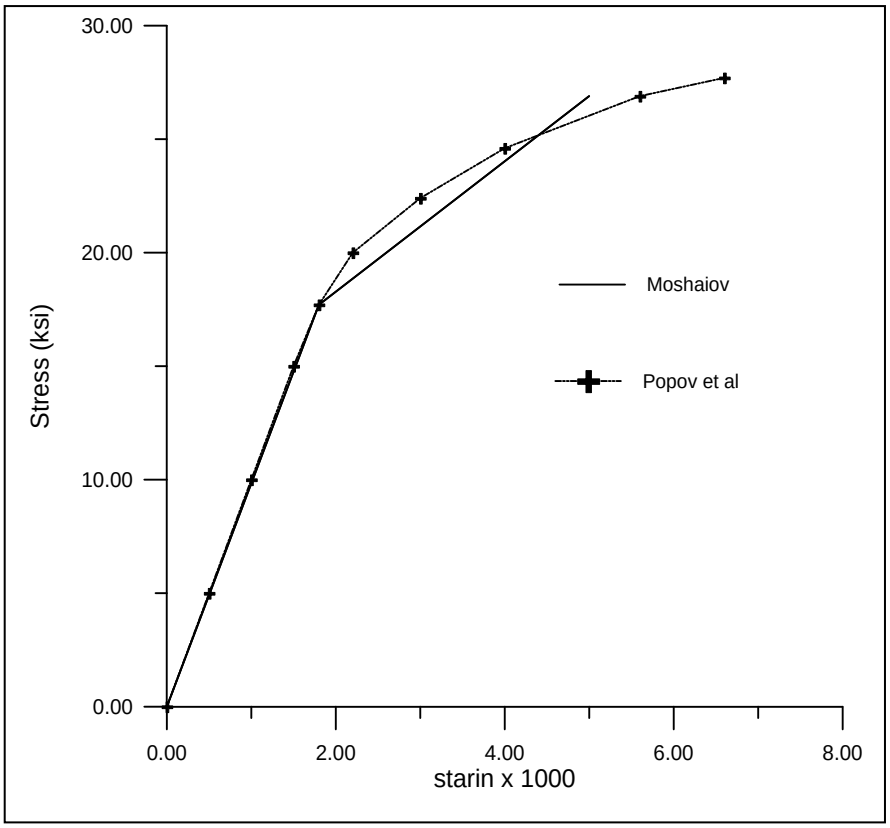

Figure (٥.٥) Uniaxial Stress Strain Curve. [٢٤]

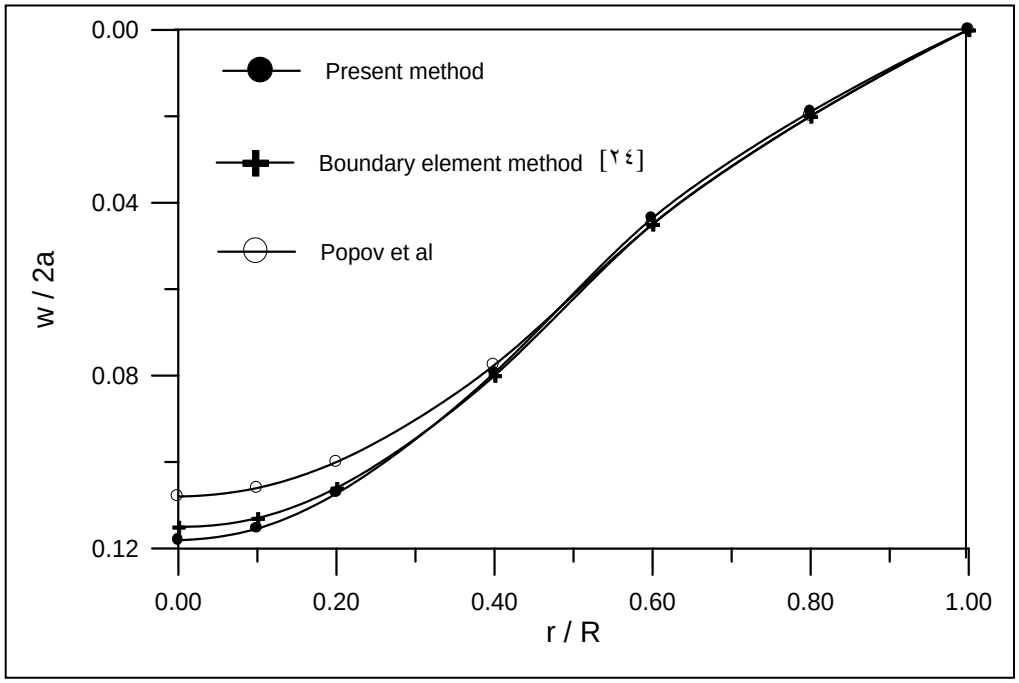

Figure (٥.٦) Distribution of Deflections for Circular Clamped Plate

٥.٢.٣ Clamped Quadratic Shell

The clamped quadratic shell shown in Figure (٥.٧) was analyzed by Owen and Figueiras [٢٩], [٣٠] under the action of self-weight and central point load.

The geometric details and the finite element idealizations are shown in Figure (٥.٧). One quadrant of the shell is discretized by ٩ finite elements and ٦ equal layers are taken through the thickness. The following material constants are used:

$$E_x = E_y = 30000.0, \upsilon = 0.3, \sigma_y = 30.0,\ H' = 300.0 \quad (\text{units MN, m})$$

Geometric characteristics: thickness h=٠.٢, span L=٦.٠

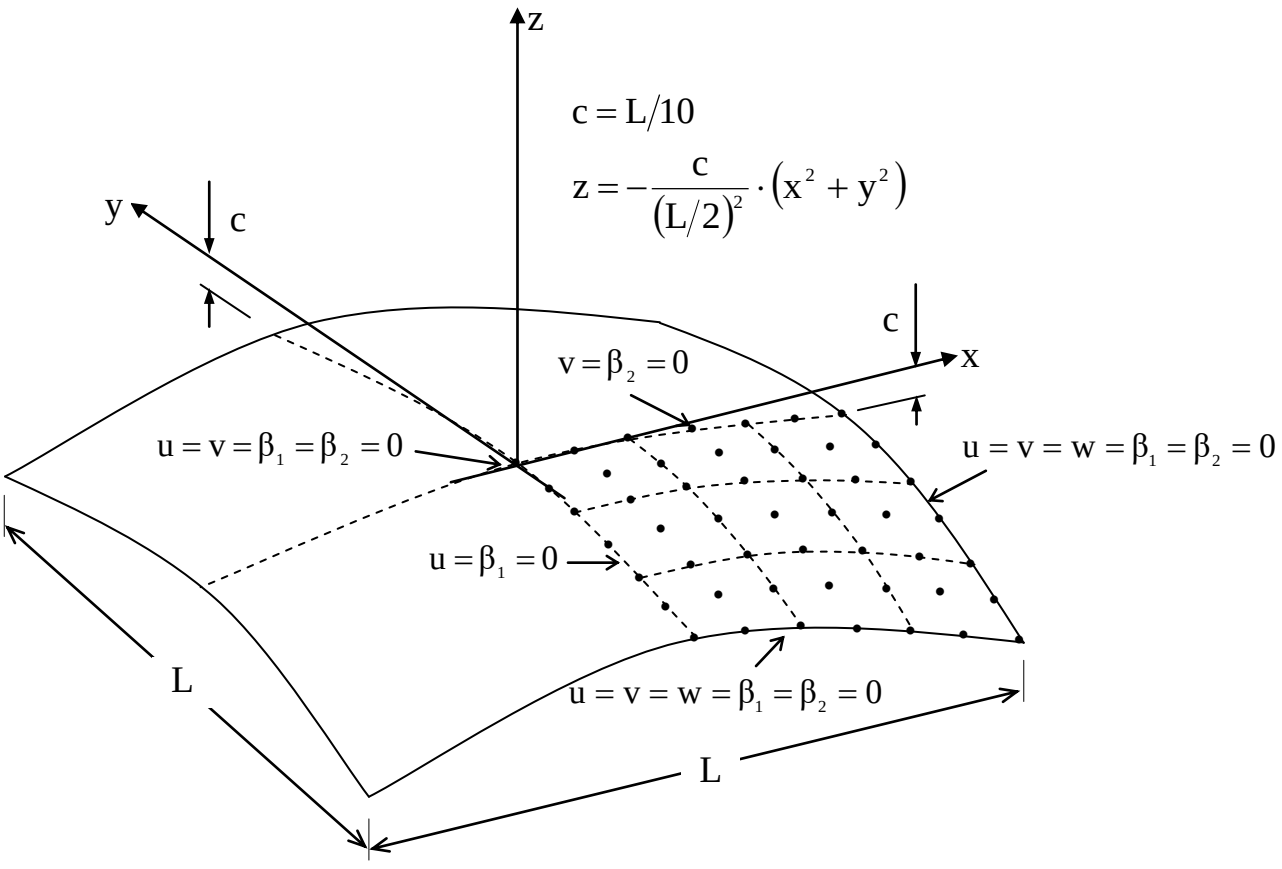

Figure (٥.٧) Clamped Quadratic Shell

The vertical displacement of the central point versus the concentrated load together with the results obtained by the layered approach by Owen and Figueiras is plotted in Figure (٥.٨). Figure (٥.٩) shows the corresponding results for the same shell loaded by self-weight, which varies by assuming a variable density. Good agreement is noticed between the results of the present study and those by Owen and Figueiras following the layered approach and semiloof element.

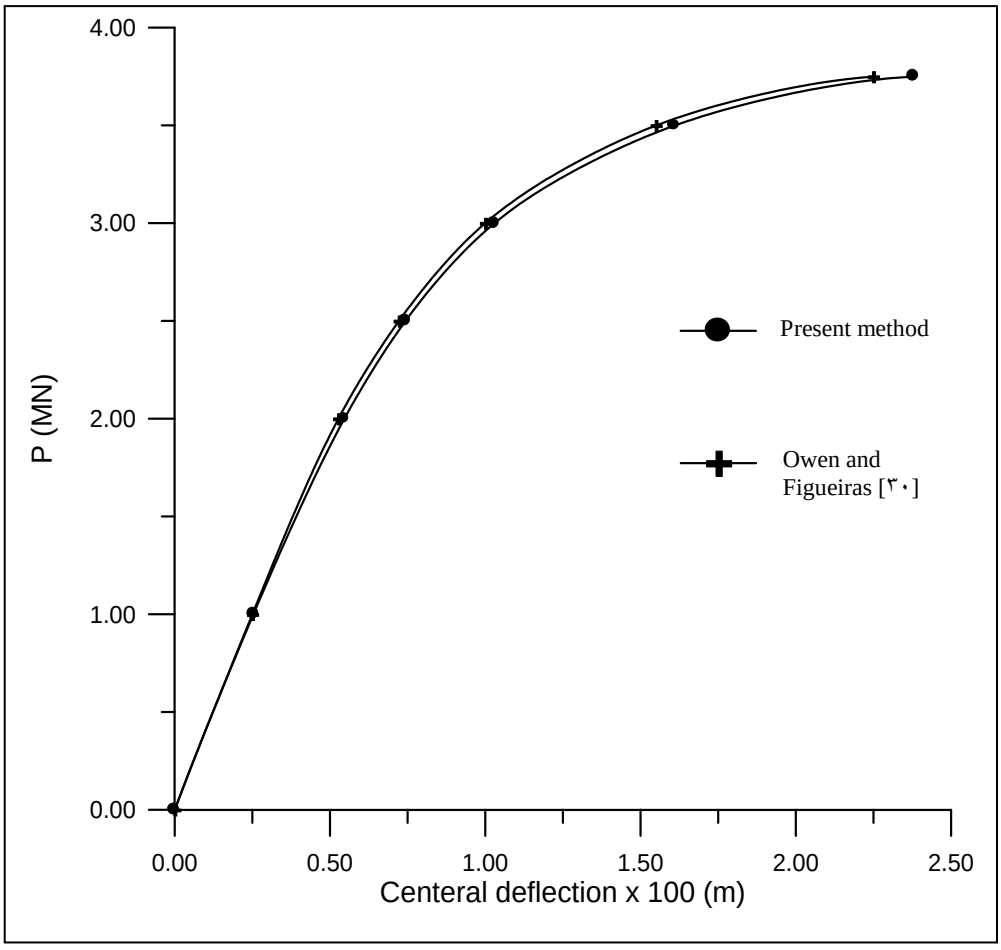

Figure (٥.٨) Load versus Central Deflection for Quadratic Shell Subjected to Concentrated Central Load

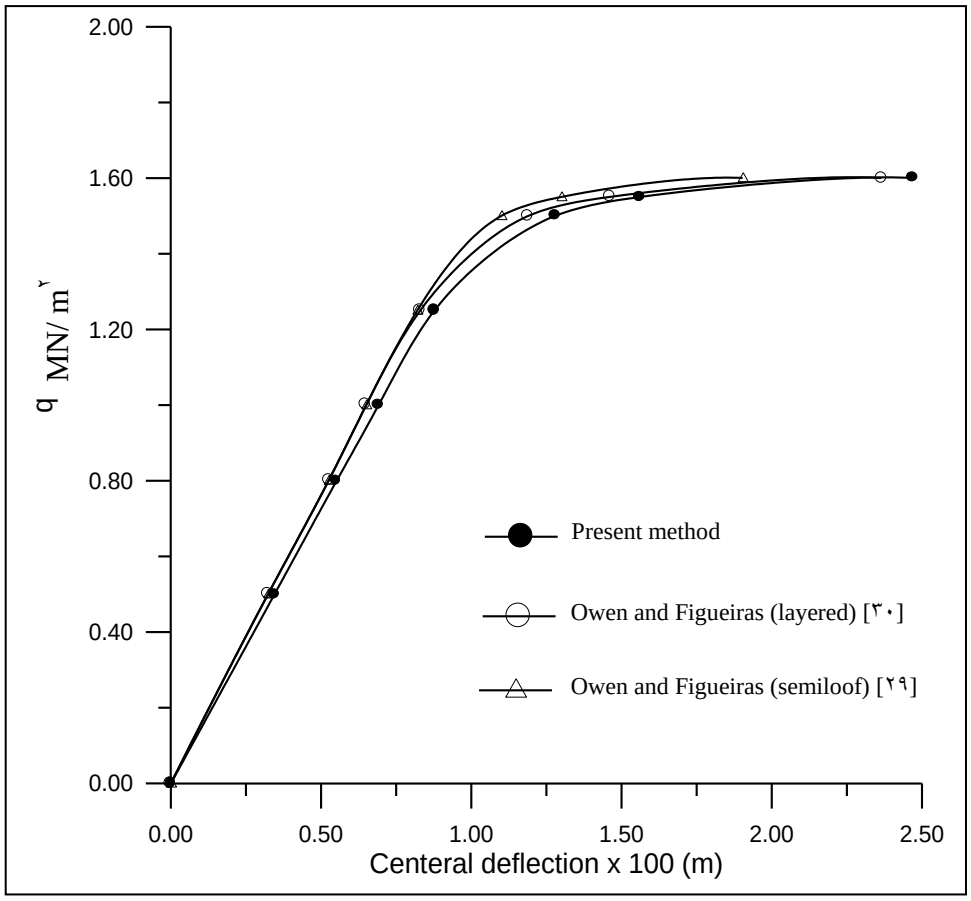

Figure (٥.٩) Load versus Central Deflection for Quadratic Shell Subjected to Self Weight

٥.٢.٤ Cylindrical Shell

The nonlinear analysis of the cylindrical shell shown in Figure (٥.١٠), subjected to self weight loading is undertaken. One-quarter of the shell is discretized by ٩ elements and for the layered approach, ٦ equal layers are taken through the depth. The following material and geometric constant are used in the solution:

$E = 21{,}000\ , \upsilon = 0.0 , \sigma_y = 4.1,\ H' = 0.0,\ L = 7.6,\ R = 7.6,\ h = 0.076,$

$\alpha = 40$ degrees (units MN, m)

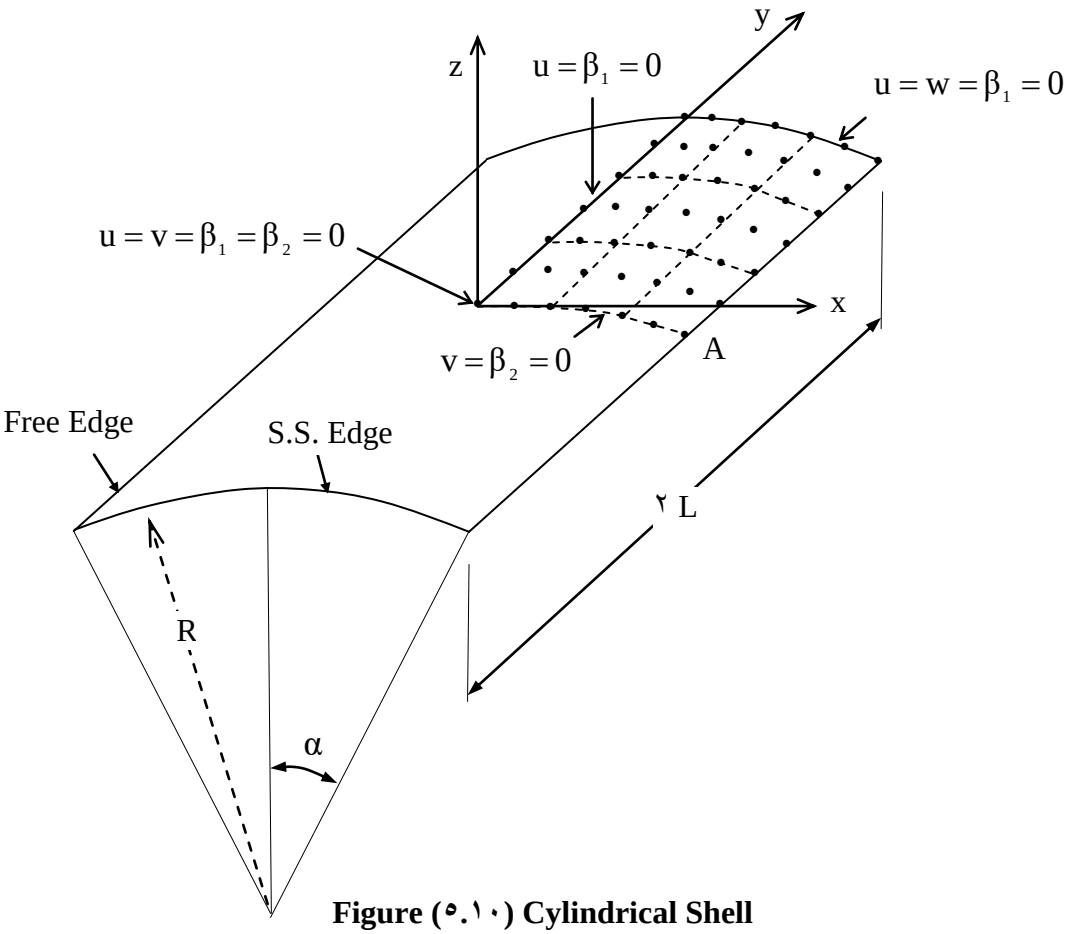

Figure (٥.١٠) Cylindrical Shell

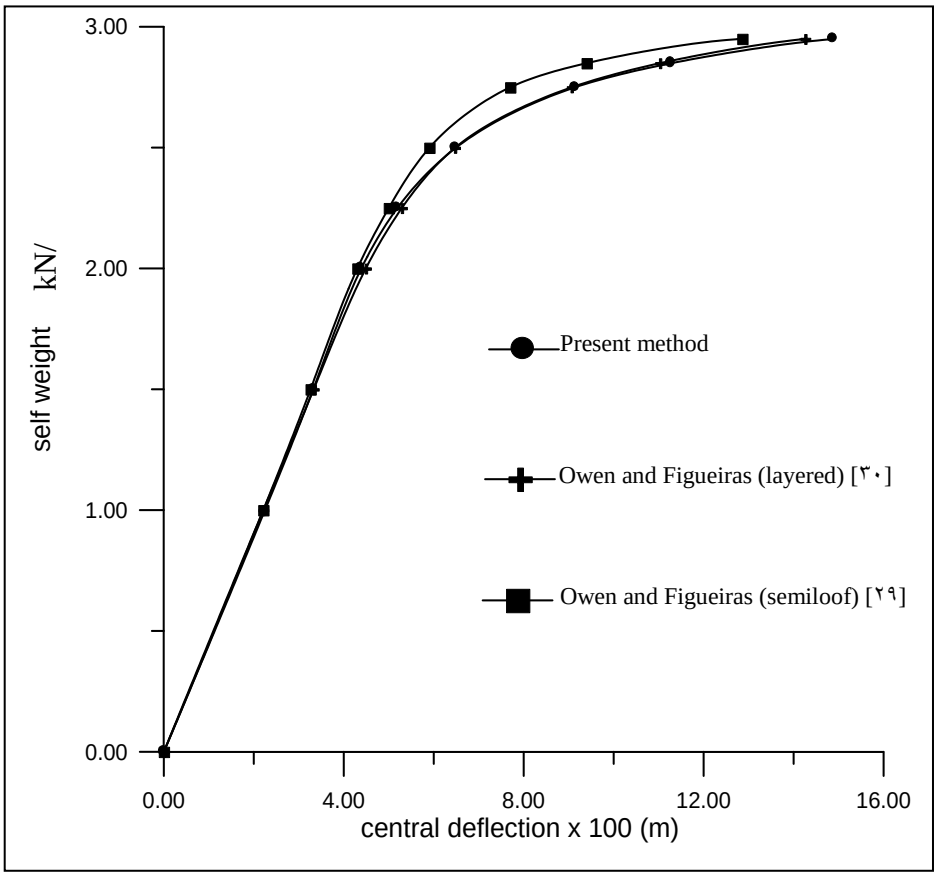

Figure (٥.١١) Load versus Deflection Curves for Cylindrical Shell Subjected to Self Weight

The plots of the vertical displacement of the central point of the free edge (A), versus the variable self-weight, which is simulated by variable density, are shown in Figure (٥.١١) together with those obtained by Owen and Figueiras [٢٩], [٣٠] for both layered approach and semiloof element. The present results compare well to those results.

٥.٢.٥ Folded Plate

A light gage simply supported folded plate was investigated by Nilson and then analyzed by Karkush [١٩]. The cross section of the adopted structure was trapezoidal. It consisted of five plates, as illustrated in Figure (٥.١٢.a). The bottom plate, of ٠.٩١٤ m width, was jointed to two ٤٥ degrees inclined plates of ١.٧٢٧ m width, which were in turn connected to two ٠.٤٥٧ m horizontal top plates. The plates have a thickness of ٠.٠٠٣ m. the load was applied as a vertical line loading along the lower fold lines. The material of the folded plates has the following properties: modulus of elasticity E = ٢٠٧ Gpa, $H' = 0$, yield stress σ_y =٤٠٠ MPa , Poisson ratio $\upsilon = 1/3$. A quarter of the folded plate, by utilization of symmetry property, was considered in the analysis and divided into nine elements as shown in Figure(٥.١٢.b).

The comparison of the results obtained was made for the load-vertical displacement curve of the upper free edge at midspan(point A) between those found by the present elastic-plastic, geometrically nonlinear analysis and those measured experimentally by Nilson and also those obtained by elasto-plastic, geometrically nonlinear analysis by finite strip method of Karkush [١٩] as illustrated in Figure (٥.١٣). The predicted vertical displacements by the present analysis are closer to those observed experimentally by Nilson than those of finite strip method and this indicates a very good performance of the present finite element analysis.

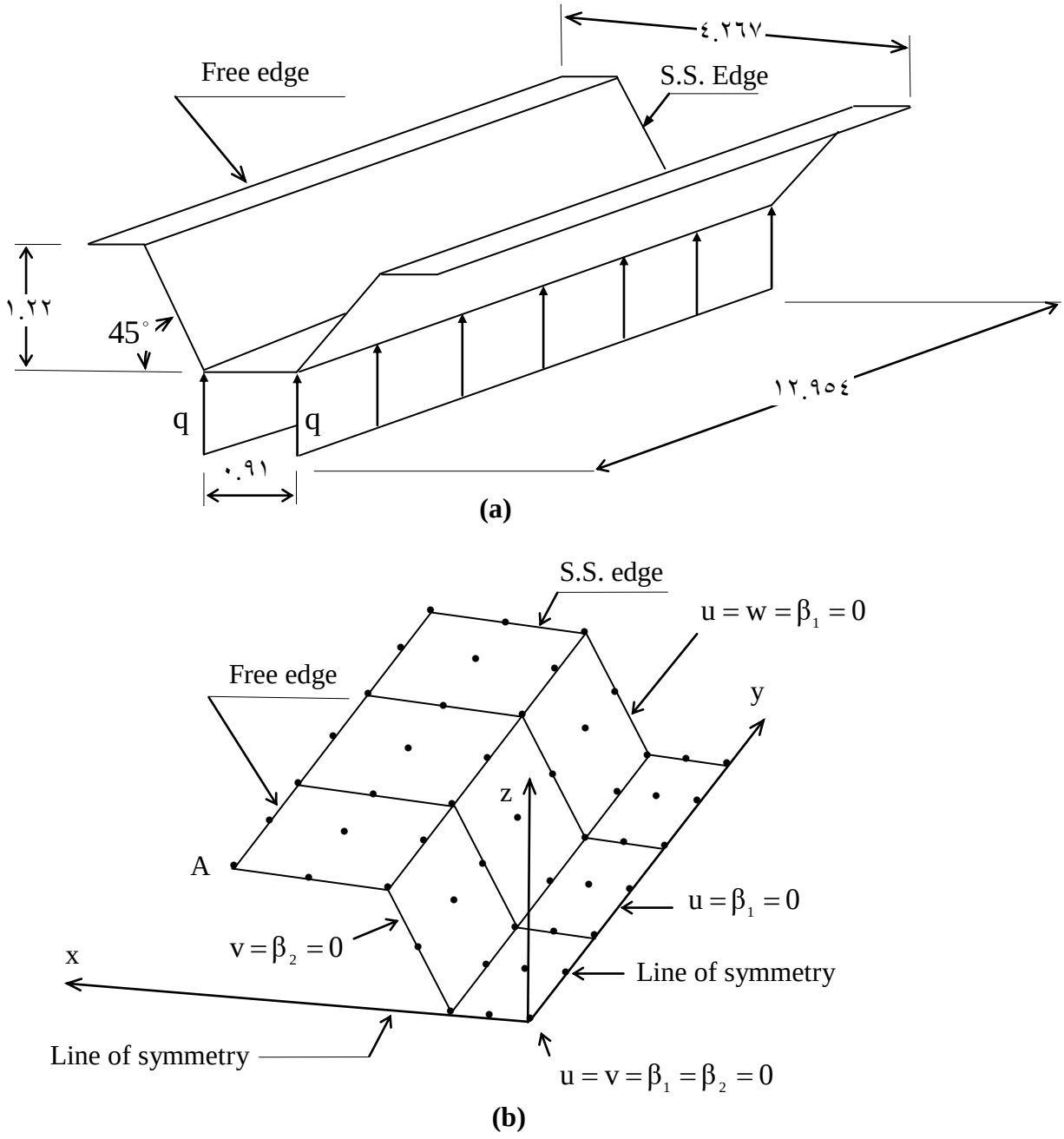

Figure (٥.١٢) Simply Supported Folded Plate

(a) Cross Section and Dimensions (b) Finite Element Idealization

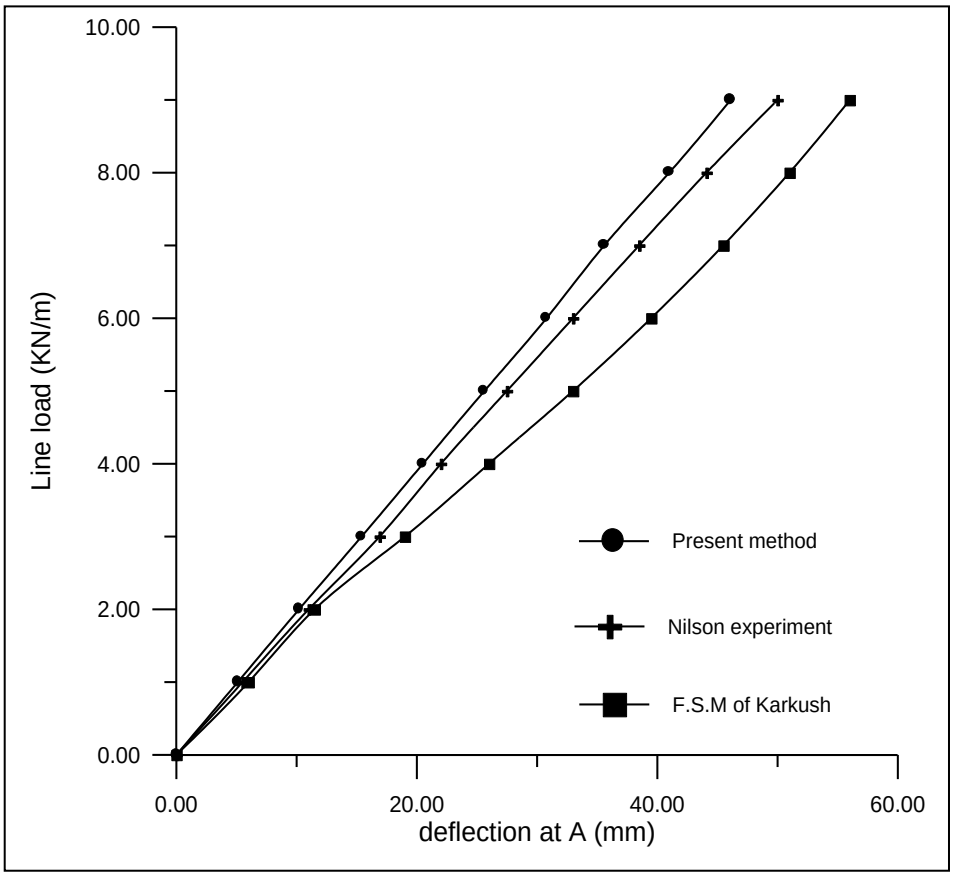

Figure (٥.١٣) Load-Deflection Curve for Folded Plate

٥.٣ Optimal Design Applications

٥.٣.١ Cylindrical Shell

The optimal design of cylindrical shell shown in Figure (٥.١٤) is investigated. The shell is exposed to uniformly distributed load of ٢.٠ kN/m^{٢} (in the radial direction). Nine elements and six equal layers through the thickness discretize a quarter of the shell, while the load is divided into ١٠ increments. The design variables are height H and thickness t. Volume $=\beta \times R \times t \times L \times 2.0$, where R is the radius of the shell $R = \left(H^2 + B^2\right)/\left(2.0 \times H\right)$ and β is the shell angle. The Initial values used are H=٢.٠٠٠, t=٠.٠٨٠ and the step length is ٠.١. The Constraints are $0.0 \le H \le B$ and $0.001 \le t \le 0.3$. The following material properties are used $E = 21{,}000, \upsilon = 0.0, \sigma_y = 4.1,\ H' = 0.0$ (all units are in MN, m)

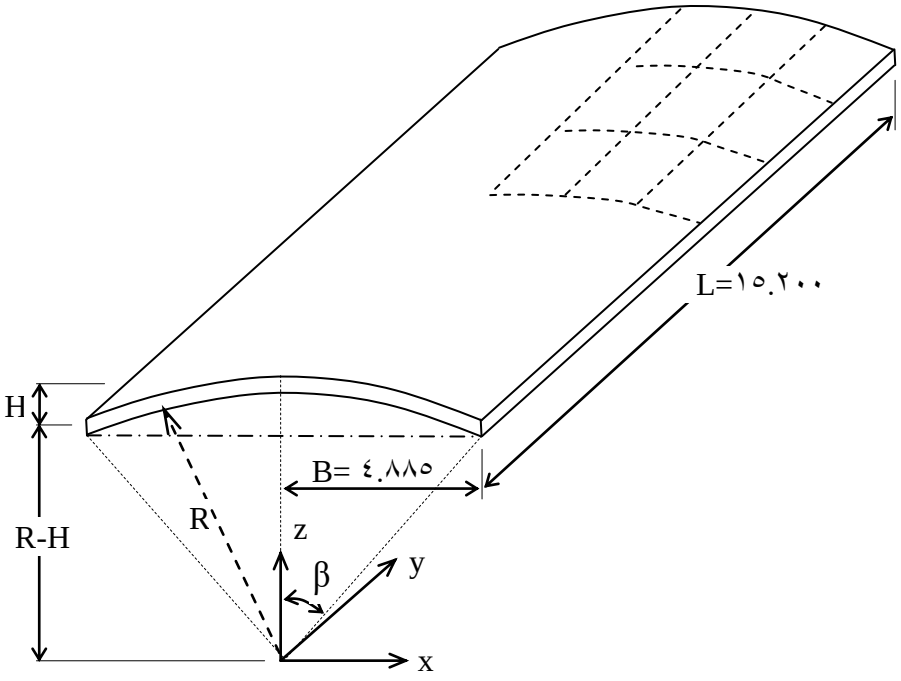

Figure (٥.١٤) Cylindrical Shell

The first case investigated is when the shell is clamped at curved edges and free at straight ones, where the optimum is reached after ٧ cycles in case of nonlinear analysis with volume=١٥.٢١١, H=١.٠٥٠ and t=٠.٠٩٩ (all units in meter).

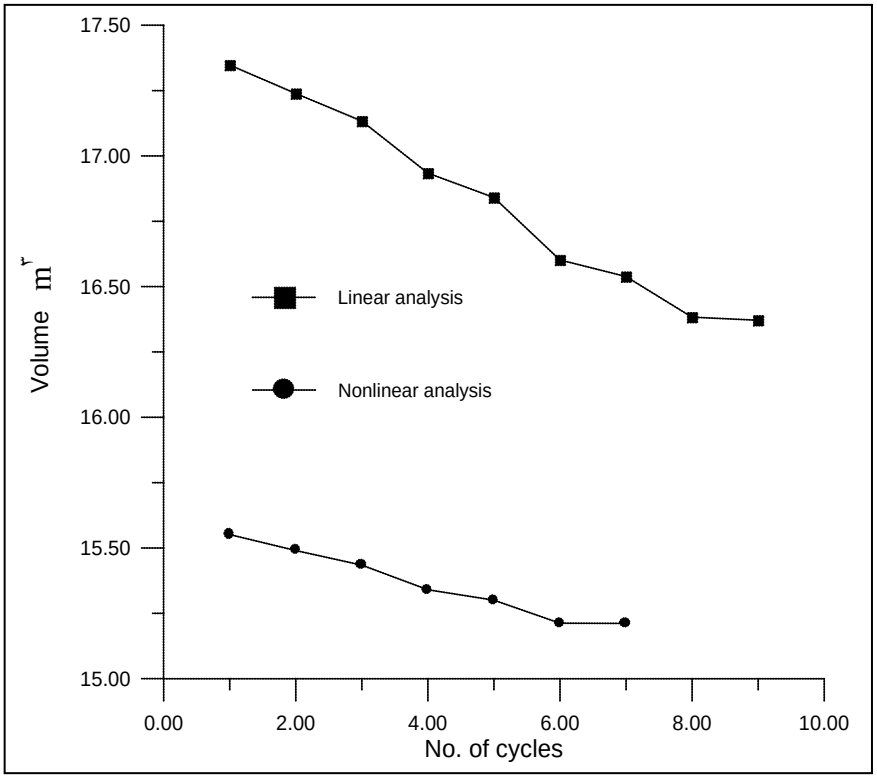

Figure (٥.١٥) Volume of Shell versus No. of Cycles for Cylindrical Shell of Clamped Curved Edges

For optimal design based on linear analysis, the results are volume=١٦.٣٧٠, H=٣.٥٠٠ and t=٠.٠٨٣ as illustrated in Figure (٥.١٥).

The search direction and consequently the optimal dimensions are not the same in the case of linear and nonlinear analysis. The reason is that the structural behaviour of the shell differs in case of nonlinear analysis due to redistribution of stresses in the plastic range. The same shell will now be examined to sustain the same loading when it is clamped at straight edges. Initial values are H=١.٠٠٠, t=٠.٠٢٥ and step length=٠.١, the optimization results for nonlinear analysis case are volume=٣.٩٤٤, H=١.٧٠٠ and t=٠.٠٢٥ obtained after ٦ cycles. In case of linear analysis the optimal volume is ٣.٩٩٥, H=١.٩٢٥ and t=٠.٠٢٤ obtained after ٧ cycles as shown in Figure (٥.١٦). When the same shell is simply supported at straight edges, using the same initial values and in case of nonlinear analysis after ٥ cycles, the volume is ٤.٠٤٦, h=١.٦٠٠ and t=٠.٠٢٥ while in case of linear analysis and after ٧ cycles, the optimal volume is ٤.١٥٢, H=١.٨٠٠ and t=٠.٠٢٦ as shown in Figure (٥.١٧).

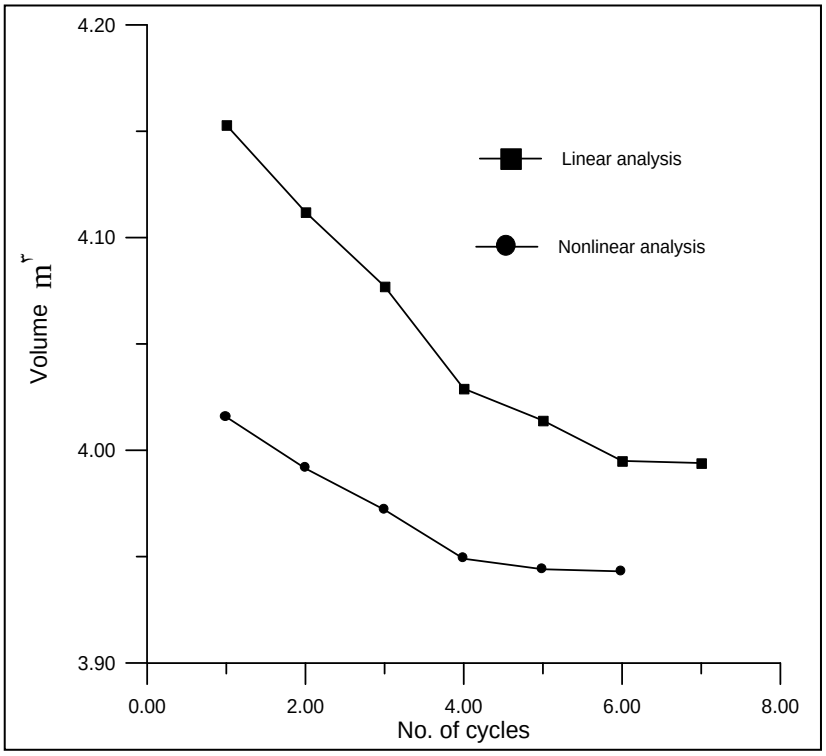

Figure (٥.١٦) Volume of Shell versus No. of Cycles for Cylindrical Shell of Clamped Curved Edges

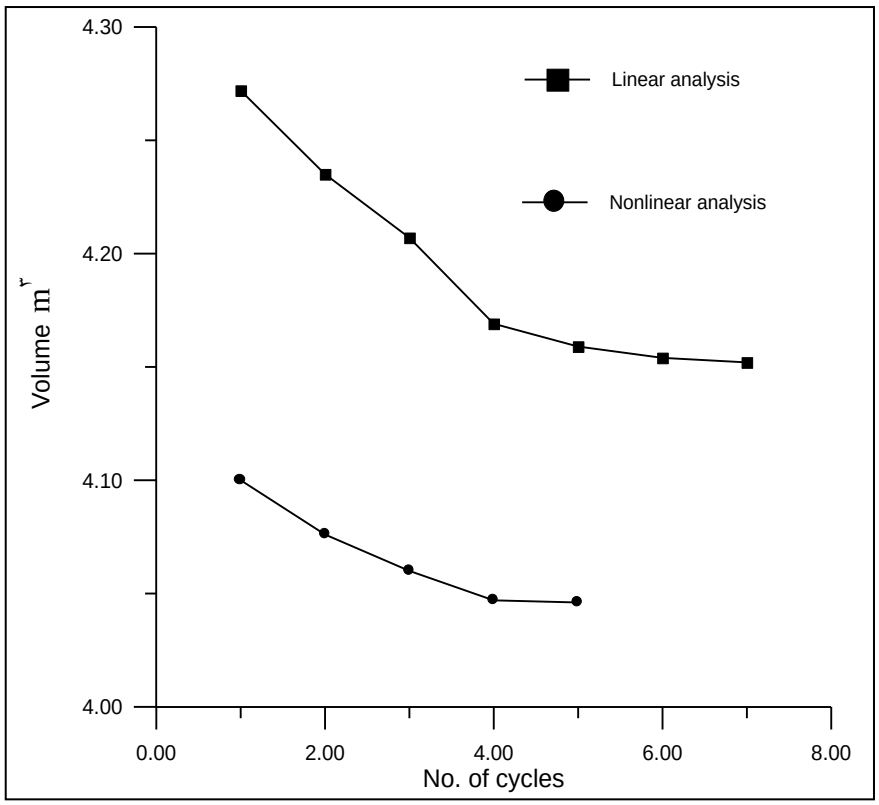

Figure (٥.١٧) Volume of Shell versus No. of Cycles for Cylindrical Shell of Simply Supported Straight Edges

٥.٣.٢ Spherical Shell

A clamped spherical shell of uniform thickness (t) is investigated. The shell is assumed to sustain a uniformly distributed load of ٢.٠ MN/m^{٢} in the radial direction.

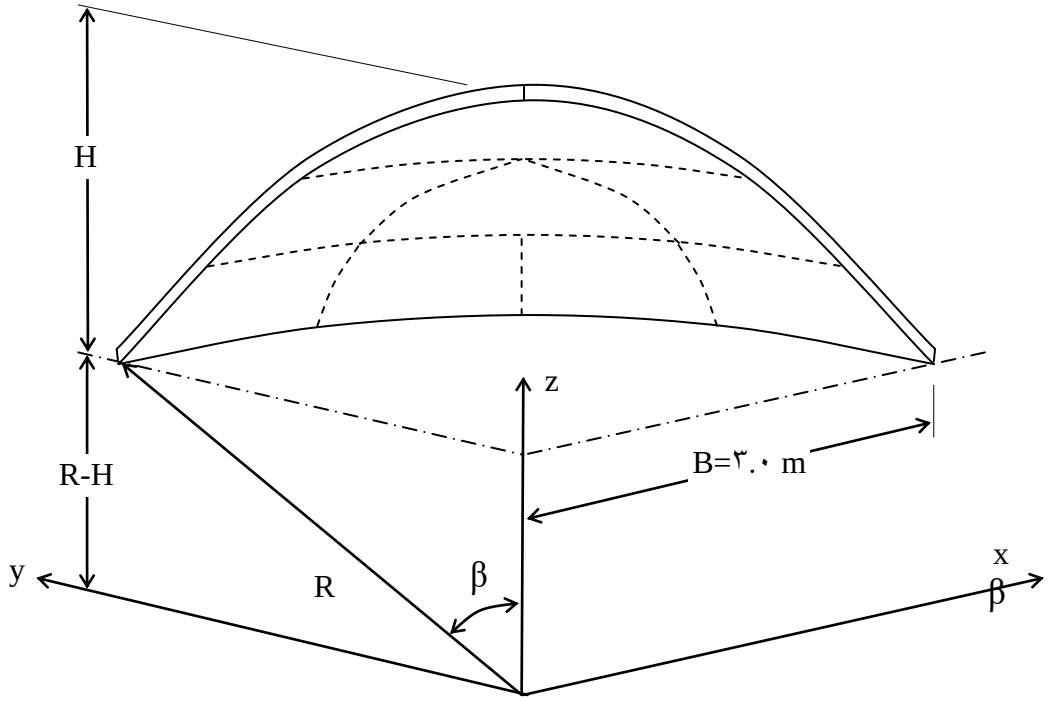

Figure (٥.١٨) Spherical Shell

A quarter of the shell is divided into ٨ elements and ٦ equal layers through the thickness as shown in Figure (٥.١٨). The following materials properties are used:

$$E_x = E_y = 30000.0, \upsilon = 0.3, \sigma_y = 30.0,\ H' = 300.0 \quad (\text{units MN, m})$$

The design variables are the height H and the thickness t. The volume of the spherical segment is $2\pi t R^2(1-\cos\beta)$, $R = (H^2 + B^2)/(2.0 \times H)$ where β is the shell angle. Initial values are H = ١.٠٠٠, t = ٠.١٣٥ and a step length of ٠.١. The constraints are: $0.0 \le H \le 3.0$ and $0.001 \le t \le 0.3$. In case of nonlinear analysis the optimal volume is ٤.٩٥٩, H=١.٣١٣ and t=٠.١٤٧ after ٥ cycles while in case of linear analysis the optimal volume is ٥.٣٣٠, H=١.٥٥٠ and t=٠.١٤٩ after ٥ cycles as shown in Figure (٥.١٩).

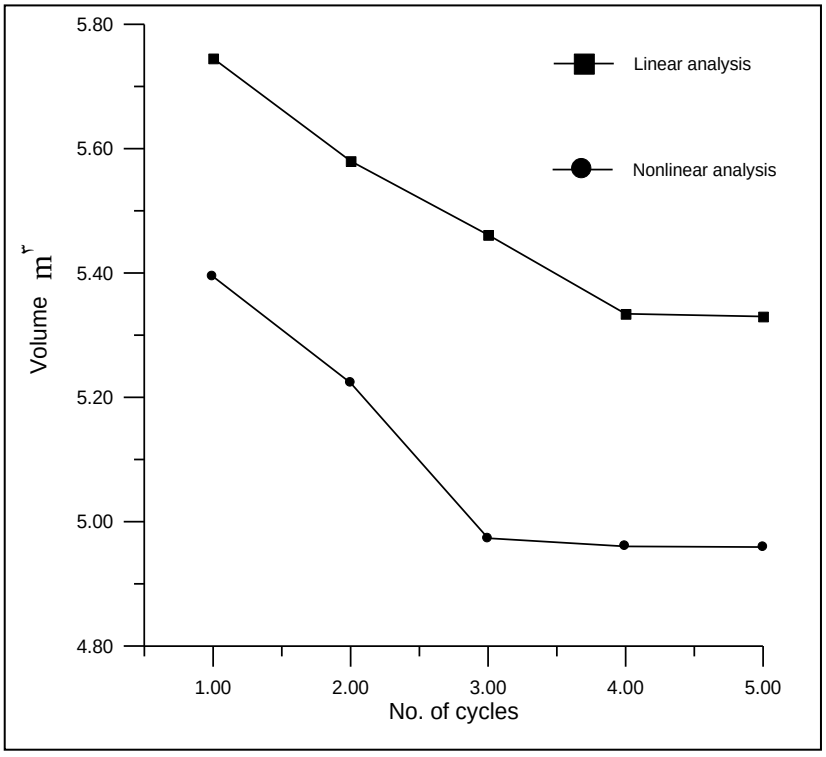

Figure (٥.١٩) Volume of Shell versus No. of Cycles for Clamped Spherical Shell

٥.٣.٣ Conical Shell

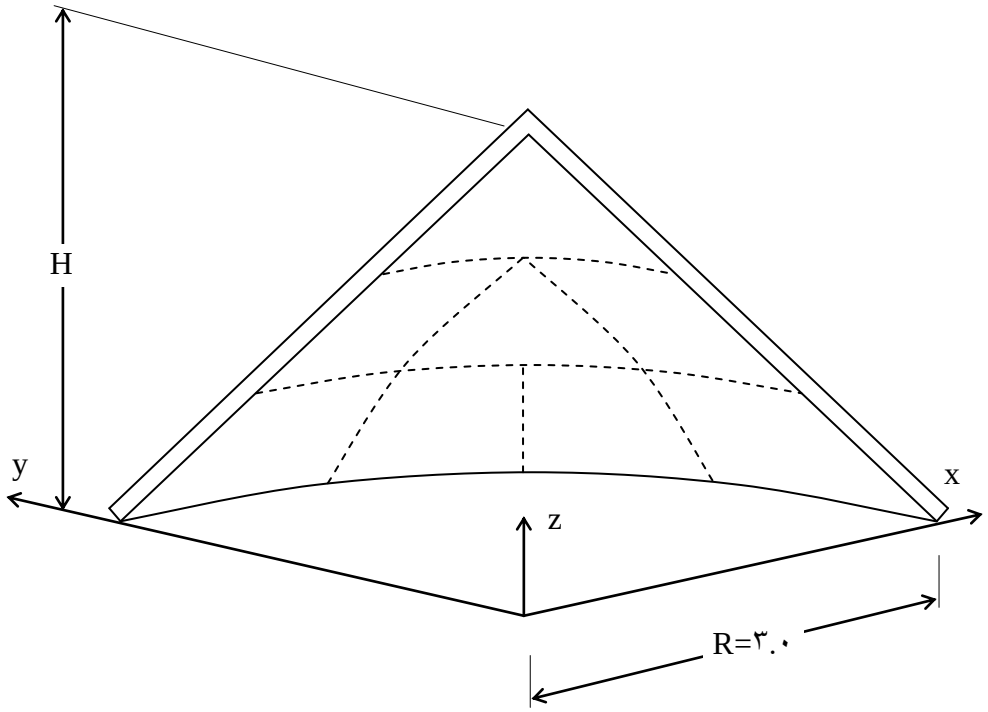

Figure (٥.٢٠) Conical Shell

The same finite element mesh, load, design variables, constraints, and materials properties are applied in the optimal design of conical shell of Figure (٥.٢٠). Volume $=\pi\times R\times t\times\sqrt{R^2+H^2}$. Initial values used are H=١.٠٠٠, t=٠.٣٠٠ and step length=٠.١. In case of nonlinear analysis and after ٨ cycles the optimization results are volume=٨.٠٧٧, H=١.٧٠٠ and t=٠.٢٤٩. In the optimal design based on linear analysis the optimization results are volume=٨.١٥٠, H=٢.٠٠٦ and t=٠.٢٣٩ obtained after ٨ cycles as shown in Figure (٥.٢١).

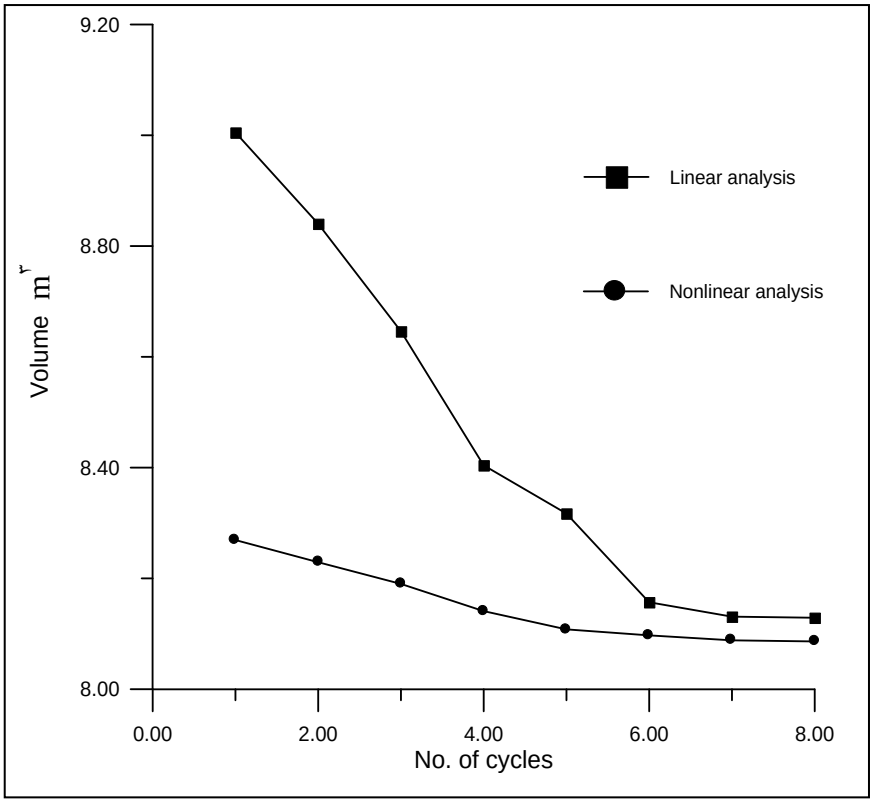

Figure (٥.٢١) Volume of Shell versus No. of Cycles for Clamped Conical Shell

The optimal ratio of rise to base radius for the conical shell is ١.٧٠٠/٣.٠ = ٠.٥٧ for optimal design based on nonlinear analysis, while in case of linear analysis, this ratio is ٢.٠٠٦/٣.٠ = ٠.٦٧. Parametric studies carried out by both Al-Azzawi and Rasheed [٢] showed that reinforced concrete conical shell would be with greatest stiffness (maximum load carrying capacity) with rise to base radius ratio of ٠.٥. The using of ratio of rise to base radius for conical shells in the range of ٠.٥ to ١.٠ is recommended in the Indian National Code because it can be considered as a desirable compromise between ultimate strength on the one hand and facility of construction on the other. In addition, it is noticed that the volume required to sustain the same loading is higher in case of conical shell than in case of spherical shell by about by ٣٧%, which indicates a greater stiffness of spherical shell.

٥.٣.٤ Folded Plate A

A simply supported folded plate shown in Figure (٥.٢٢) is subjected to line load of ٢٠٠ KN/m on the upper fold lines. Nine elements and six equal layers through the thickness (t) discretize a quarter of the plate. The line load is divided into ١٠ increments and the following materials properties are used: modulus of elasticity E = ٢٠٧ GPa, $H' = 0$, yield stress σ_y = ٤٠٠ MPa, Poisson ratio $\upsilon = 1/3$.Design variables: H, t, B١, B٢, B٣ Volume = $t \times \left(B_1 + \sqrt{B_2^2 + H^2} + B_3\right) \times 2 \times L$. Initial values are: H= ١.٠٠٠, t= ٠.٤٠٠, B١= ٠.٢٠٠, B٢= ٢.٠٠٠, step length =٠.١ Constraints: $0.0 \le H \le 3.0, 0.001 \le t \le 0.3, B_1 + B_2 + B_3 = 2.134, B_1 \ge 0.0$, $B_2 \ge 0.0$, $B_3 \ge 0.0$

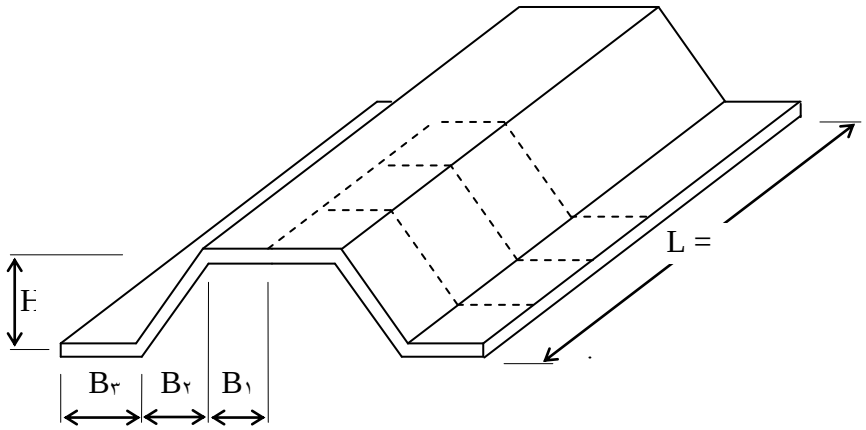

Figure (٥.٢٢) Folded Plate A

In case of nonlinear analysis, the optimisation results are volume=١١.٧١٣, H=١.١١٣, B١=٠.٠٠٦, B٢=١.٩١٩, B٣=٠.٢٠٩ and t=٠.١٨٦ obtained after ١٩ cycles. In case of linear analysis and after ١٠ cycles the optimization results are volume=١٥.٦٩٣, H=١.٢٠٠, B١=٠.٣٠٠, B٢=١.٦٠٠, B٣=٠.٢٣٤ and t=٠.٢٣٩ as shown in Figure (٥.٢٣) and Tables (٥.١) and (٥.٢).

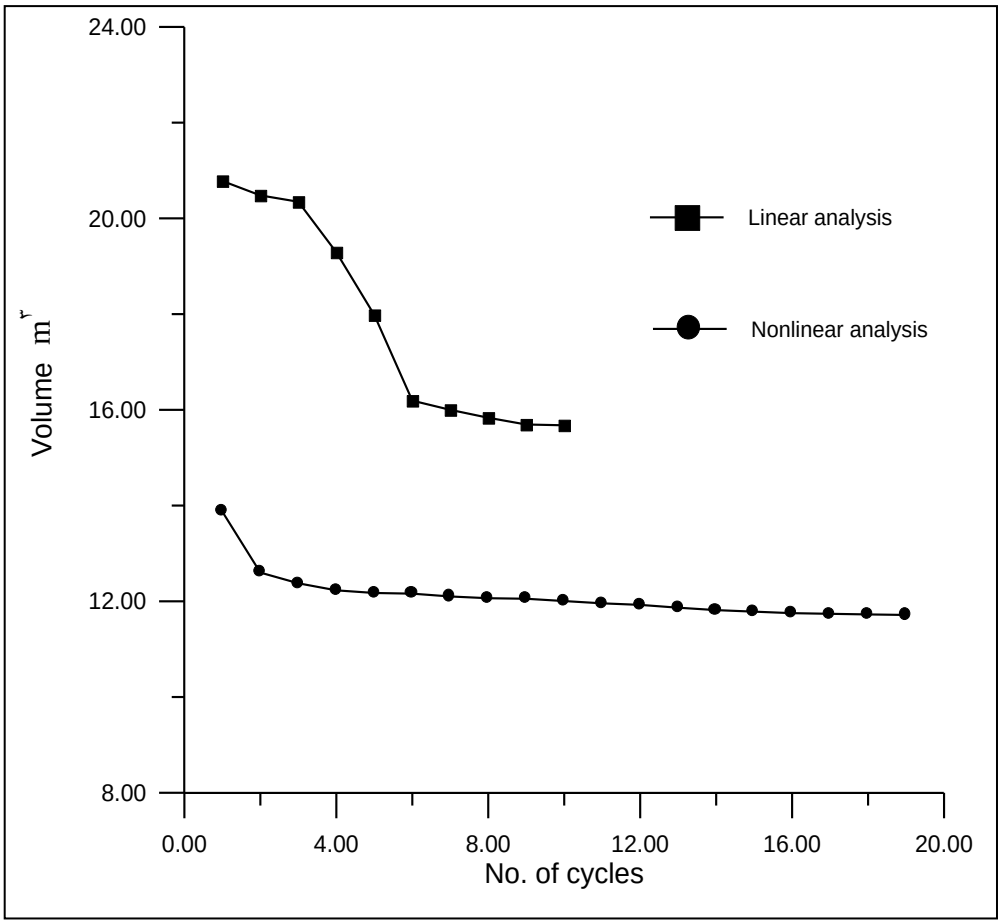

Figure (٥.٢٣) Volume versus No. of Cycles for Folded Plate A

Cycle No.	volume	H	B_1	B_2	B_3	t
١	١٣.٨٧٠	٠.٩٠٠	٠.١٠٠	٢.٠٠٠	٠.٠٣٤	٠.٢٣٠
٣	١٢.٣٧٤	٠.٩٠٠	٠.٠٥٠	١.٩٥٠	٠.١٣٤	٠.٢٠٤
٥	١٢.١٧٣	٠.٩٠٠	٠.٠٢٥	١.٩٥٠	٠.١٥٩	٠.٢٠٢
٧	١٢.١٠٠	٠.٩٢٥	٠.٠٢٥	٢.٠٠٠	٠.١٠٩	٠.٢٠٠
٩	١٢.٠٥٣	٠.٩٥٠	٠.٠٢٥	٢.٠٢٥	٠.٠٨٤	٠.١٩٨
١١	١١.٩٥٧	١.٠٢٥	٠.٠٢٥	٢.٠٥٠	٠.٠٥٩	٠.١٩٤
١٣	١١.٨٦٦	١.٠٧٥	٠.٠١٣	٢.٠٧٥	٠.٠٤٧	٠.١٩١
١٥	١١.٧٨٢	١.١٠٠	٠.٠١٣	١.٩٦٣	٠.١٥٩	٠.١٨٨
١٧	١١.٧٣٧	١.١٠٠	٠.٠٠٦	١.٩٣٧	٠.١٩٠	٠.١٨٧
١٩	١١.٧١٣	١.١١٣	٠.٠٠٦	١.٩١٩	٠.٢٠٩	٠.١٨٦

Table (٥.١) Optimization Results for Folded Plate A under Nonlinear Analysis

Cycle No.	volume	H	B_1	B_2	B_3	t
١	٢٠.٧٨١	١.٠٠٠	٠.١٠٠	١.٩٠٠	٠.١٣٤	٠.٣٣٧
٣	٢٠.٣٤٥	١.٠٠٠	٠.١٠٠	١.٧٠٠	٠.٣٣٤	٠.٣٢٦
٥	١٧.٩٧٩	١.١٠٠	٠.٢٠٠	١.٥٠٠	٠.٤٣٤	٠.٢٧٨
٧	١٥.٩٩٨	١.٢٠٠	٠.٣٠٠	١.٥٠٠	٠.٣٣٤	٠.٢٤٠
٩	١٥.٦٩٣	١.٢٠٠	٠.٣٠٠	١.٦٠٠	٠.٢٣٤	٠.٢٣٩

Table (٥.٢) Optimization Results for Folded Plate A under Linear Analysis

٥.٣.٥ Folded Plate B

By removing the horizontal bottom plates of folded plate A and using the same finite element discretization, load, and materials properties, the optimal design of folded plate B shown in Figure (٥.٢٤) is carried out.

Design variables: H, B_1, B_2, t. Volume $= t \times \left(B_1 + \sqrt{B_2^2 + H^2}\right) \times 2 \times L$.

Initial values: H= ١.٢٢٠, t= ٠.١٠٠, B_1= ٠.٠٤٥٧, B_2= ١.٦٧٧, step length =٠.١, Constraints: $0.0 \le H \le 3.0$, $B_1 \ge 0.0$ $0.001 \le t \le 0.3$, $B_1 + B_2 = 2.134$, $B_2 \ge 0.0$

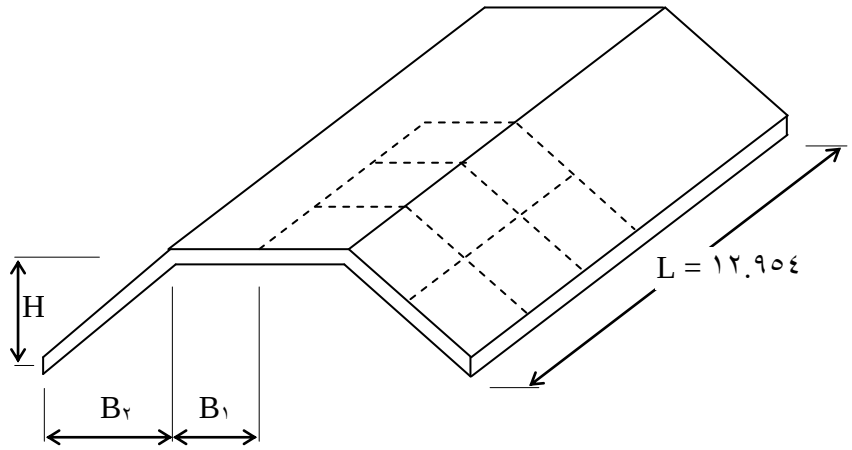

Figure (٥.٢٤) Folded Plate B

The optimization results based on nonlinear analysis are volume= ٥.٩٦٣, H=١.٣٩٥, B_1=٠.٧٠٧, B_2=١.٤٢٧, t=٠.٠٨٥ which were obtained after ٥ cycles. In case of linear analysis, after ٨ cycles the obtained

optimisation results are volume=٧.٥٦٤, H=١.٩٧, B_1=٠.٠٠٧, B_2=٢.١٢٧, t=٠.١٠٠ as illustrated in Figure (٥.٢٥) and Tables (٥.٣) and (٥.٤)

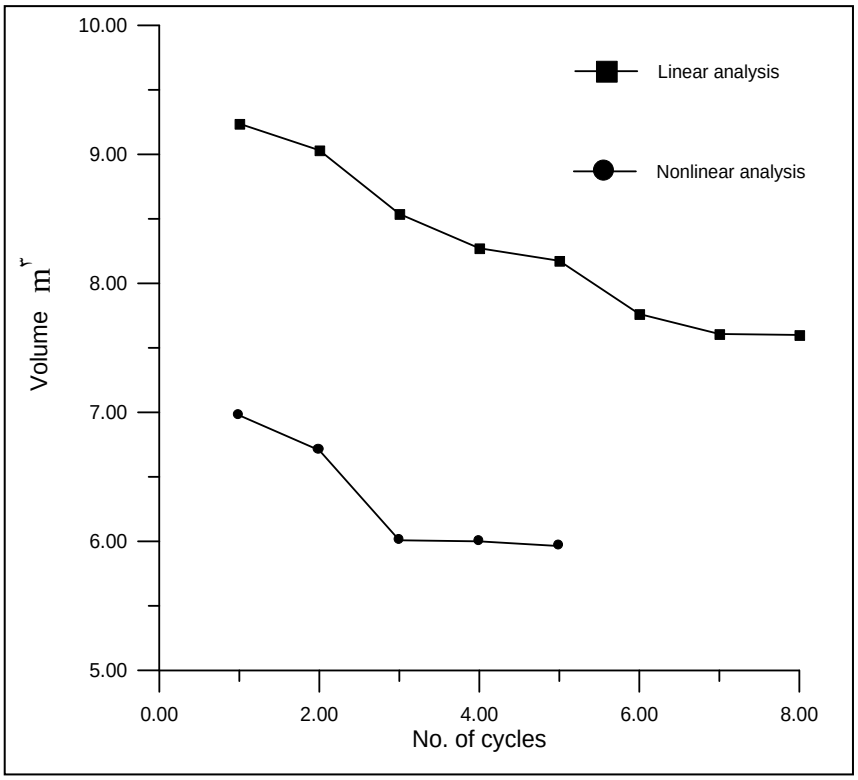

Figure (٥.٢٥) Volume versus No. of Cycles for Folded Plate B

Cycle No.	volume	H	B_1	B_2	t
١	٦.٩٧٦	١.٣٢٠	٠.٤٥٧	١.٦٧٧	٠.١٠٤
٣	٦.٠٠٨	١.٤٢٠	٠.٦٥٧	١.٤٧٧	٠.٠٨٦
٥	٥.٩٦٣	١.٣٩٥	٠.٧٠٧	١.٤٢٧	٠.٠٨٥

Table (٥.٣) Optimization Results for Folded Plate B under Nonlinear Analysis

Cycle No.	volume	H	B_1	B_2	t
١	٩.٢٣٨	١.٣٢٠	٠.٤٥٧	١.٦٧٧	٠.١٣٨
٣	٨.٥٣٨	١.٤٢٠	٠.٢٥٧	١.٨٧٧	٠.١٢٦
٥	٨.١٧٥	١.٥٢٠	٠.١٥٧	١.٩٧٧	٠.١١٩
٧	٧.٦٠٧	١.٩٢٠	٠.٠٥٧	٢.٠٧٧	٠.١٠٢

Table (٥.٤) Optimization Results for Folded Plate B under Linear Analysis

It is noticed that the optimal volume required to sustain the same load in case of folded plate B is less than in the folded plate A for both cases of linear and nonlinear analysis, which indicate a greater stiffness of this shape.

٥.٣.٦ Folded Plate C

By placing two vertical plates at both sides, the folded plate B takes the shape in Figure (٥.٢٦). Design variables: H_1, H_2 t, B_1, B_2. Volume = $t \times \left(H_1 + \sqrt{B_2^2 + H_2^2} + B_1\right) \times 2 \times L$. Initial values: H_1= ٠.٢٢٠, H_2= ١.٠٠٠, t= ٠.٢٥٠, B_1= ٠.٤٥٧, B_2= ١.٦٦٧, step length =٠.١. Constraints:

$0.0 \le H_1 + H_2 \le 3.0$, $0.001 \le t \le 0.3$, $B_1 + B_2 = 2.134$, $H_1 \ge 0.0$, $H_2 \ge 0.0$

$B_1 \ge 0.0$ $B_2 \ge 0.0$. The same material properties and loading conditions for the folded plates A and B are used.

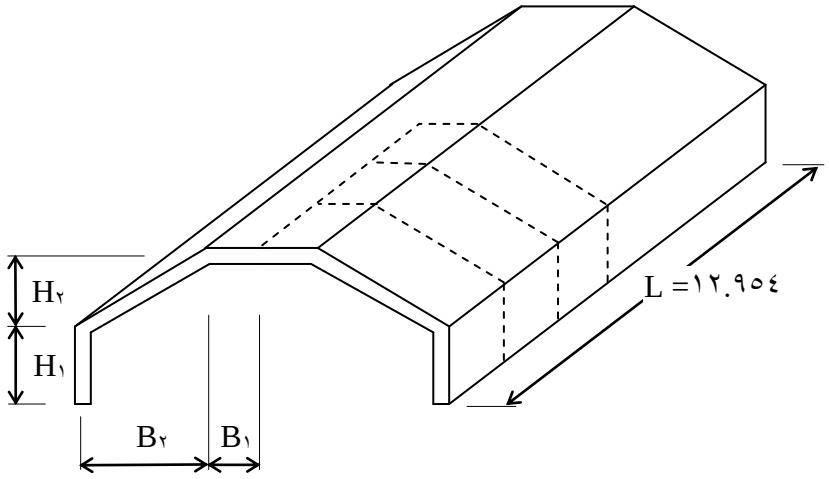

Figure (٥.٢٦) Folded Plate C

In case of nonlinear analysis the optimization results are: volume=٧.١٥٥, H_1=٠.٠٠١, H_2=١.٧٦٣, B_1=٠.٧٦٩, B_2=١.٣٦٥ and t=٠.٠٩٢ obtained after ٢١ cycles. In case of linear analysis and after ٣٠ cycles the optimization results are: volume=٨.٠٥٤, H_1=١.٩٢٠, H_2=٠.٨٠٠, B_1=٢.٠٥٧, B_2=٠.٠٧٧ and t=٠.٠٦٥ as shown in Figure (٥.٢٧) and Tables (٥.٥) and (٥.٦).

The optimal volume of folded plate C is greater than that of folded plate B for linear and nonlinear analysis, but it is smaller than that of folded plate A for both linear and nonlinear analysis. This indicates that the folded plate B is the most efficient in sustaining the same loading.

Cycle No.	volume	H_1	H_2	B_1	B_2	t
١	١٥.١٤٦	٠.٢٢٠	١.١٠٠	٠.٤٥٧	١.٦٧٧	٠.٢١٨
٣	١٤.٦٥٨	٠.٢٢٠	١.٢٠٠	٠.٦٥٧	١.٤٧٧	٠.٢٠٤
٥	١٢.٠٥٦	٠.١٢٠	١.٣٠٠	٠.٦٥٧	١.٤٧٧	٠.١٧٠
٧	٨.٦٠١	٠.٠٢٠	١.٥٠٠	٠.٩٥٧	١.١٧٧	٠.١١٥
٩	٧.٨٥٣	٠.٠٢٠	١.٧٠٠	٠.٦٥٧	١.٤٧٧	٠.١٠٣
١١	٧.٥٣٥	٠.٠٠٨	١.٧١٣	٠.٦٥٧	١.٤٧٧	٠.٠٩٩
١٣	٧.٤٧١	٠.٠٠٨	١.٧١٣	٠.٦٨٢	١.٤٥٢	٠.٠٩٨
١٥	٧.٤١٥	٠.٠٠٨	١.٧٣٨	٠.٦٩٤	١.٤٤٠	٠.٠٩٧
١٧	٧.٢٤٨	٠.٠٠١	١.٧٣٨	٠.٧٥٧	١.٣٧٧	٠.٠٩٤
١٩	٧.١٩١	٠.٠٠١	١.٧٥٠	٠.٧٨٢	١.٣٥٢	٠.٠٩٣
٢١	٧.١٦	٠.٠٠١	١.٧٦٣	٠.٧٦٩	١.٣٦٥	٠.٠٩٢

Table (٥.٥) Optimization Results for Folded Plate C under Nonlinear Analysis

Cycle No.	volume	H_1	H_2	B_1	B_2	t
١	٢٠.٣٥٧	٠.٣٢٠	١.٠٠٠	٠.٤٥٧	١.٦٨٠	٠.٢٨٨
٣	١٨.٧٤٢	٠.٣٢٠	١.١٠٠	٠.٥٥٧	١.٥٧٧	٠.٢١٤
٥	١٦.٤٤٣	٠.٥٢٠	١.٢٠٠	٠.٦٥٧	١.٤٧٧	٠.٢٠٦
٧	١٥.٨٠٦	٠.٧٢٠	١.٣٠٠	٠.٩٥٧	١.١٧٧	٠.١٧٨
٩	١٥.٤١٧	٠.٦٢٠	١.٢٠٠	٠.٩٥٧	١.١٧٧	٠.١٨٢
١١	١٣.٧١	٠.٧٢٠	١.٢٠٠	١.٣٥٧	٠.٧٧٧	٠.١٥١
١٣	١٣.٢٥٥	٠.٧٢٠	١.١٠٠	١.٤٥٧	٠.٦٧٧	٠.١٤٧
١٥	١١.٢٦٤	٠.٩٢٠	١.٠٠٠	١.٨٥٧	٠.٢٧٧	٠.١١٤
١٧	١٠.٩٠١	٠.٩٢٠	١.١٠٠	١.٩٥٧	٠.١٧٧	٠.١٠٥
١٩	١٠.١٥٨	١.٠٢٠	١.١٠٠	٢.٠٥٧	٠.٠٧٧	٠.٠٩٤
٢١	٩.٥٦٨	١.١٢٠	١.٣٠٠	٢.٠٥٧	٠.٠٧٧	٠.٠٨٢
٢٣	٩.٢٧٦	١.٢٢٠	١.٢٠٠	٢.٠٥٧	٠.٠٧٧	٠.٠٨٠
٢٥	٨.٨١٣	١.٥٢٠	١.١٠٠	٢.٠٥٧	٠.٠٧٧	٠.٠٧٢
٢٧	٨.٣٩٥	١.٨٢٠	١.٠٠٠	٢.٠٥٧	٠.٠٧٧	٠.٠٦٦
٢٩	٨.١٠٤	٢.٠٢٠	٠.٨٠٠	٢.٠٥٧	٠.٠٧٧	٠.٠٦٤

Table (٥.٦) Optimization Results for Folded Plate C under Linear Analysis

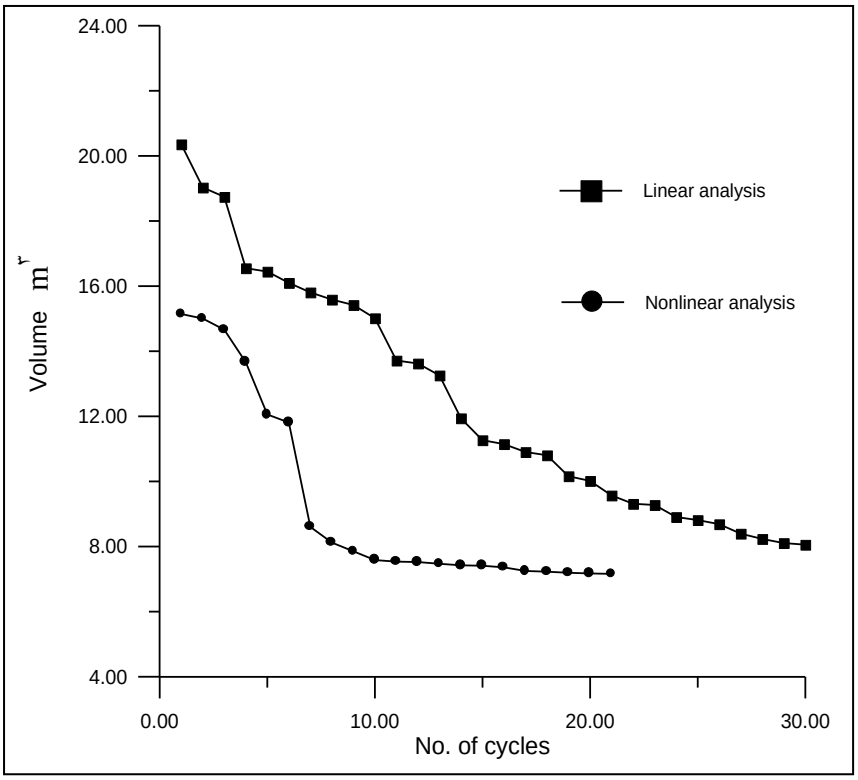

Figure (٥.٢٧) Volume versus No. of Cycles For Folded Plate C

٥.٣.٧ Folded Plate-Saw Teeth

A folded plate has the shape of saw teeth (Figure (٥.٢٨)) and sustains a uniformly distributed load of ٥٠.٠ kN/m^{٢}. A quarter of the structure was discretized by ١٢ elements and ٦ equal layers through the thickness (t) and ١٠ increments were used for the load. The following materials properties were used:

$$E_x = E_y = 30000.0, \upsilon = 0.3, \sigma_y = 30.0,\ H' = 300.0 \quad (\text{units MN, m})$$

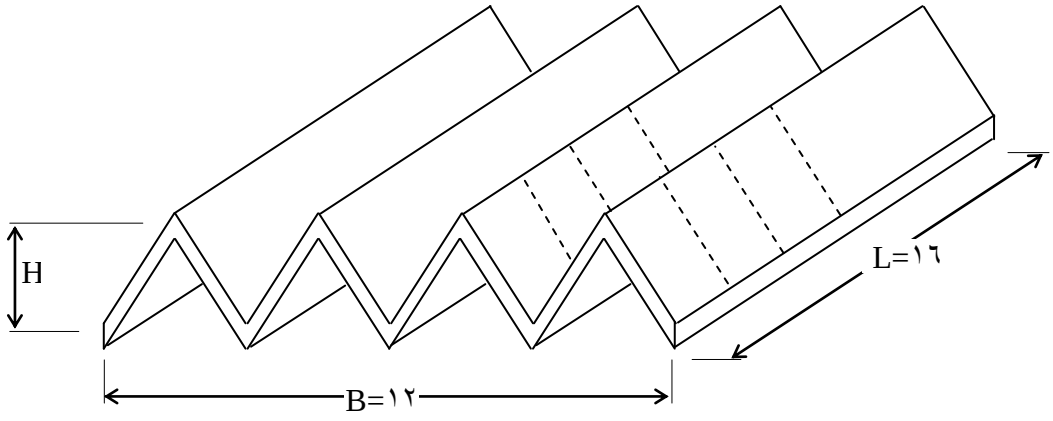

Figure (٥.٢٨) Folded Plate-Saw Teeth

Design variables: H, t. Volume $= t \times \left(\sqrt{(B/8)^2 + H^2}\right) \times 8 \times L$. Constraints: $0.0 \le H \le 3.0,\ 0.001 \le t \le 0.3$. The folded plate is investigated for two cases. The first case is when the folded plate has no intermediate supports. The initial values: H = ١.٠٠٠, t = ٠.٢٠٠, step length = ٠.١. In this case and for clamped edges, the optimization results are: volume=٤١.٠٨٨, H=٠.٦٠٦, t=٠.١٩٨ obtained after ٦ cycles for nonlinear analysis, while in case of linear analysis and after ٩ cycles the results are volume= ٤٥.٦٨٨, H=٢.٥٠٠ and t=٠.١٢٢ as illustrated in figure (٥.٢٩). For a simply supported case and in optimization based on nonlinear analysis, the results are volume=٥٢.٢١٧, H=١.٨٠٠ and t=٠.١٧٤ after ٧ cycles of optimization, while for linear analysis the optimal dimensions of the folded plate are volume=٥٦.٨٥٦, H=٢.٤٠٠, t=٠.١٥٩ after ٨ cycles as shown in Figure (٥.٣٠)

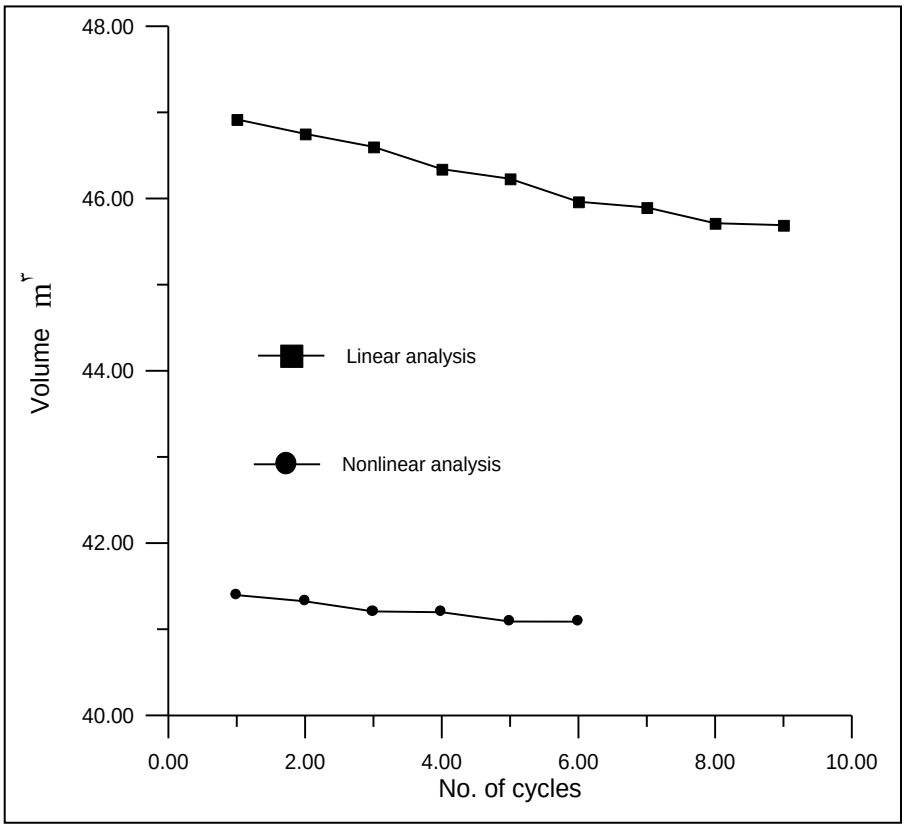

Figure (٥.٢٩) Volume versus No. of Cycles for Folded Plate (Saw Teeth) of Clamped Edges without Intermediate Supports

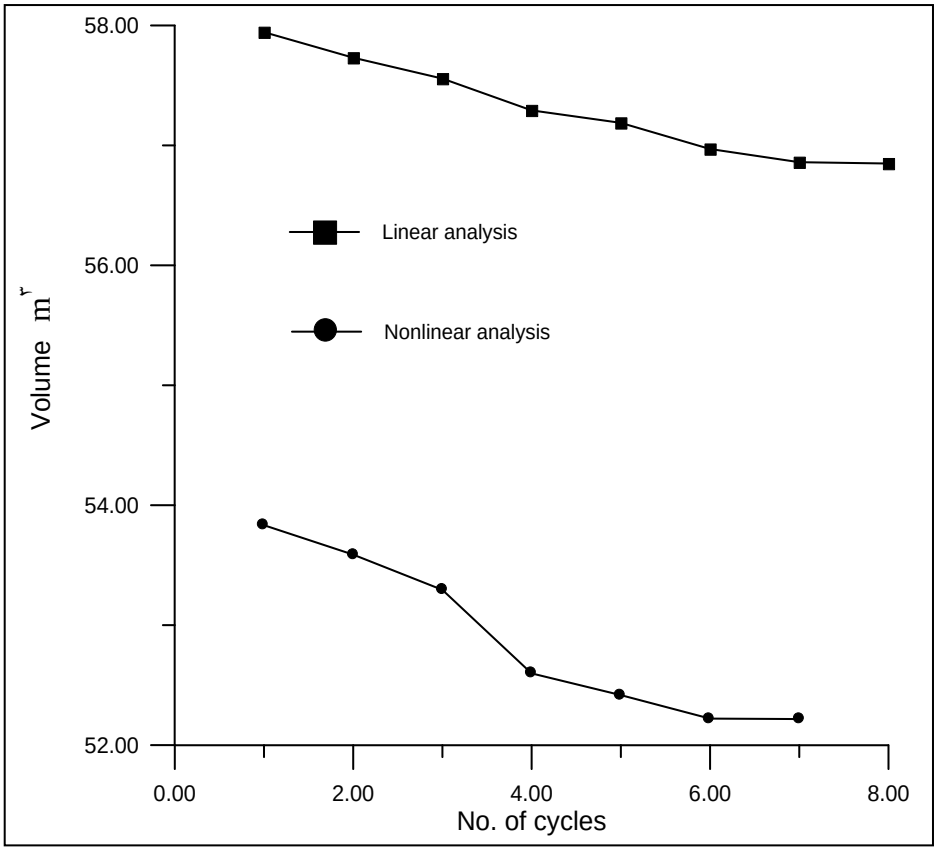

Figure (٥.٣٠) Volume versus No. of Cycles for Folded Plate (Saw Teeth) of Simply Supported Edges without Intermediate Supports

The second case considered is when the folded plate has intermediate supports i.e. continuous folded plate. The folded plate is assumed to sustain the same uniformly distributed load of ٥٠ kN/m^{٢}. The initial values used are: H=١.٠٠٠, t=٠.٠٢٥ and step length of ٠.١. When the folded plate is of clamped edges, then in case of nonlinear analysis and after ٧ cycles the optimal dimensions are volume=٤.٢٩٩, H=٠.٢٧٥ and t=٠.٠٢٢ while in case of linear analysis the optimization results are volume= ٤.٤٦٦, H=٠.٣٥٠ and t=٠.٠٢٧ after ٦ cycles as shown in Figure (٥.٣١). When the same folded plate is simply supported and in case of nonlinear analysis the optimization results are: volume=٦.١٩٣, H=٠.٣٥٠ and t=٠.٠٣١ obtained after ٧ cycles, while in case of linear analysis and after ٦ cycles the optimization results are volume=٦.٣٣٦, H=٠.٣٥٠, t=٠.٠٣٢ as illustrated in Figure (٥.٣٢). The effect of intermediate supports is clear in reducing the optimal volume of the folded plate.

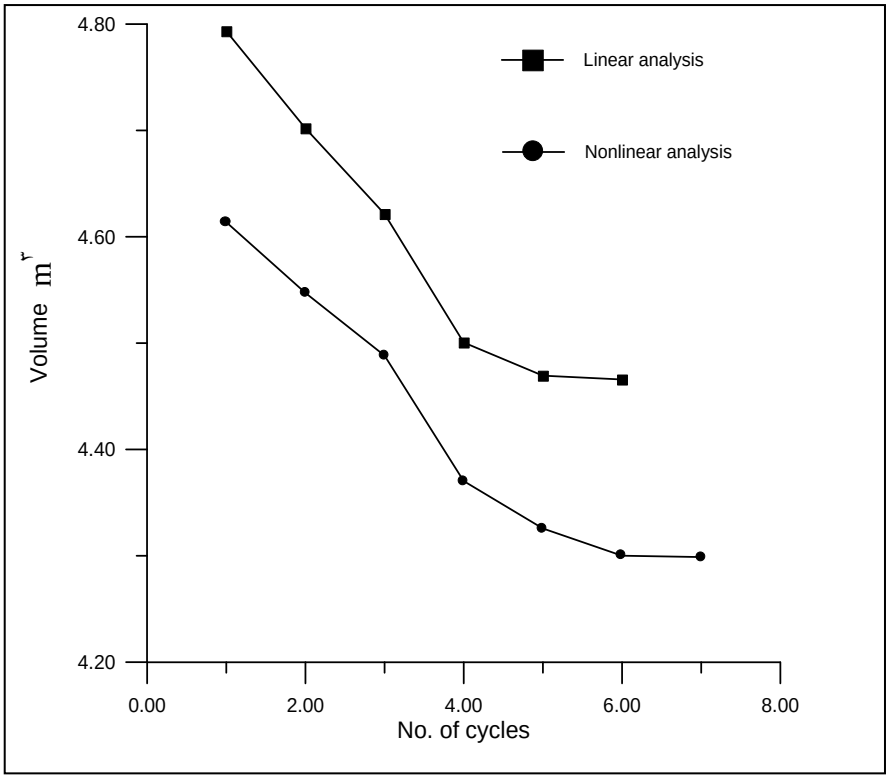

Figure (٥.٣١) Volume versus No. of Cycles for Folded Plate (Saw Teeth) of Clamped Edges with Intermediate Supports (Continuous)

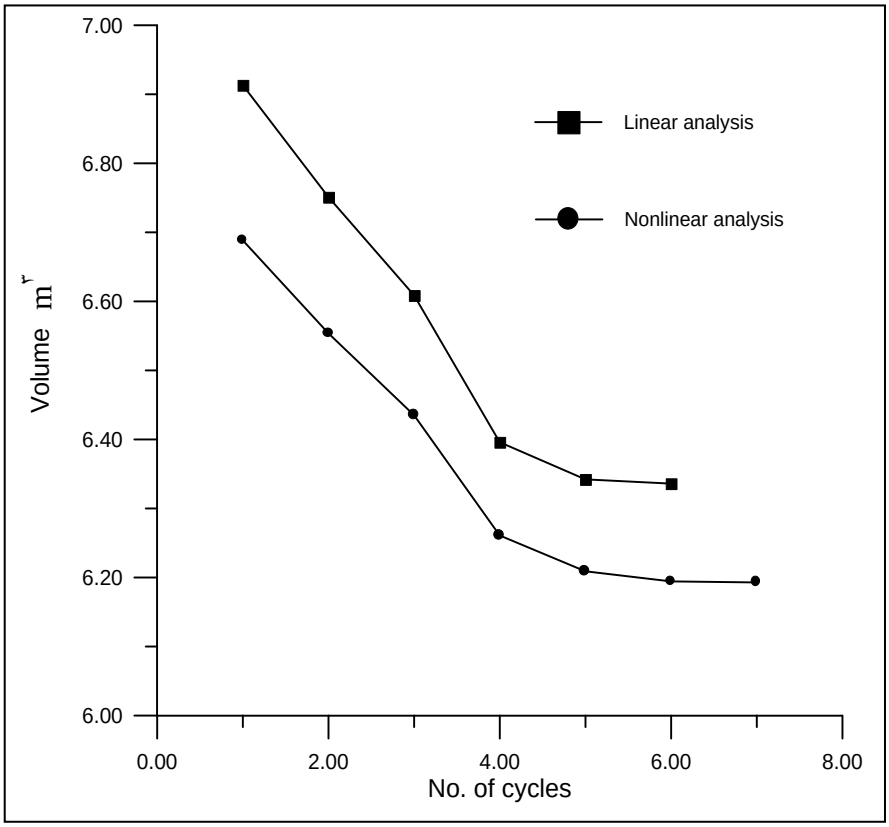

Figure (٥.٣٢) Volume versus No. of Cycles for Folded Plate (Saw Teeth) of Simply Supported Edges with Intermediate Supports (Continuous)

CHAPTER SIX

CONCLUSIONS AND RECOMMENDATIONS

٦.١ Conclusions

The main conclusions in the present study are as follows:

١. The present method of elastic-plastic analysis is capable to predict the nonlinear response of plates and shells in a good manner with maximum difference in deflection of ٧٪ compared to previous studies.

٢. In studying the nonlinear behaviour through the shell thickness, layered approach is seemed to be suitable for general shell structures.

٣. The nonlinear constrained optimization problem is solved by using the modified Hooke and Jeeves method. It has been shown that this method is efficient, easy to be programmed and can be used in general nonlinear constrained optimization.

٤. In structural optimization by the modified Hooke and Jeeves method, an appropriate initial step length must be used to reduce the computational time. The numerical applications have shown that a step length of ٠.١ to ٠.٢ times the smallest design variable (thickness exclusive) is suitable for most cases.

٥. For the optimal design of the considered single bay cylindrical shell, the best rise/bay width ratio ranges from ٠.٣-٠.٤.

٦. For the considered multi-bay folded plates without intermediate supports, the optimal rise/bay width ratio ranges from ٠.٦ to ٠.٨.

When interior supports are introduced, this ratio will decrease to about ٠.١.

٧. In the case of single-bay simply supported folded plates, the optimal design will be obtained when the folded plate takes a shape near to a cylindrical shell.

٨. The optimal shape of a clamped spherical segment is that of rise/ base radius ratio which ranging ٠.٤ to ٠.٦

٩. The rise/ base radius ratio that determines the optimal shape of a clamped conical shell lies in the range of ٠.٥-٠.٧. To sustain the same loading the optimal volume in this case is ٣٧٪ higher than that in the case of a spherical shell. This indicates a greater stiffness of spherical shell.

٦.٢ Recommendations for Future Research

As an extension of the present work, the following topics are suggested:

١. Optimum design studies of reinforced concrete plate and shell structures including both material and geometric nonlinearities. A case in which the percentage of reinforcement steel will be an additional design variable.

٢. Using a different type of element in the nonlinear analysis problem like a flat shell element or using a different nonlinear analysis technique like the closed form solutions and carrying out an optimal design based on that formulation.

٣. Optimal design of plates and shells based on dynamic nonlinear analysis such as aircraft, marine and space structures, also in thin walled structures exposed to the dynamic effects such as earthquake and blast loading.

٤. An experimental study on metal plates or shells is recommended to be done to ensure the accuracy of material modelling, nonlinear response and optimal design procedures.

٥. As underground structures, the optimal design of plate and shell foundations need to be carried out following the nonlinear behaviour. Special technique must be introduced for the soil and interface layer.

٦. Formulation of optimal design of general plate and shell structures that are exposed to cyclic loading considering the material and geometrical nonlinearities.

٧. The optimal design of general composite or laminated plates and shells; depending on elastic-plastic geometrically nonlinear analysis, need to be investigated. The thicknesses of different internal layers may be considered as design variables.

٨. Implementing a different optimization technique other than the modified Hooke and Jeeves method, e.g. gradient based methods and comparing the results with those obtained in the present work.

٩. Optimal design of stiffened plates and shells based on elastic-plastic and geometrically nonlinear analysis. The dimensions of stiffeners may be incorporated as design variables.

REFERENCES

[١] Ahmed M., Sekhon G.S. and Singh D. (٢٠٠٢) **"Finite Element Simulation of Axisymmetric Sheet Forming Operations Using Shell Element"**, Department of Applied Mechanics, New Delhi, Vol. ٨٤, pp. ١٦١- ١٦٤.

[٢] Al-Azzawi A. A. (٢٠٠٠) **"Finite Element Analysis of Thin and Thick Reinforced Concrete Shell Foundations"**, Ph.D. thesis, University of Baghdad, Baghdad, Iraq.

[٣] Bazant Zdenek P. (٢٠٠٣) **"Asymptotic Matching Analysis of Scaling of Structural Failure Due to Softening Hinges. I: Theory"**, Journal of Engineering Mechanics, Vol. ١٢٩, PP. ٦٤١-٦٥٠.

[٤] Bunday B. D. (١٩٨٤) **"Basic Optimization Methods"**, School of Mathematical Sciences, University of Bardford, Edward Arnold Pty Limited, Australia.

[٥] Chia C.-Y. (١٩٨٠) **"Nonlinear Analysis of Plates"**, University of Babylon, Springer-Verlag, London, U.K.

[٦] Ciarlet P. G. and Coutand D. (١٩٩٩) **"A Minimization Problem Arising in Nonlinear Thin Shell"**, GDR ١١٥١ (CNRS), Laboratory of Numerical Analysis, Paris University, France.

[٧] Colliat J.B., Ibrahimbecovic A., Davenne L. (٢٠٠٤) **"Nonlinear Thermomechanical Analysis of Cellular Structures in Flat Shell Context"**, Laboratory of Mechanics and Technology (LMT), France.

[٨] Cruz J. R. (١٩٩١) **"Optimization of Composite Sandwich Cover Panels Subjected to Compressive Loadings"**, National Aeronautics and Space Administration, Washington, NASA TP-٣١٧٣.

[٩] Dippery R.E., Jr. and Srivastava D. (١٩٩٩) **"Pressure Vessel Design Using Boundary Element Method With Optimization"**, Kettering University, Michigan, USA, No. XIV, pp. ٢٦٧-٢٧٢.

[١٠] Fujikubo M., Yao T., Abdul Rahim M., Murakami Y. (١٩٩٣) **"Elastoplastic Optimal Design of Frame and Truss Structures Using Repeated Sensitivity Analysis"**, Proceedings of the Third International Offshore and Polar Engineering Conference, Vol. ٤, pp. ٥٣٨-٥٤٤.

[١١] Gorji M. (١٩٨٥) **"Nonlinear Analysis of Plates with Plastic Orthotropy"** Journal of Structural Engineering, Vol. ١١١, No. ١٠, paper No. ٢٠٠٩١, pp. ٢٢١٤-٢٢٢٥.

[١٢] Gosling P.D. and Roy I.M. (٢٠٠٣) **"An Elasto-Plastic Total Lagrangian Shell Formulation for Large Displacements"**, School of Engineering and Geoscience, University of Newcastle, Newcastle, NE١ ٧RU, U.K.

[١٣] Gotsis P. K. (١٩٩٢) **"Structural Optimization of Thin Shells Using Finite Element Method**" National Aeronautics and Space Administration, Washington, NASA TM-١٠٥٩٠٣

[١٤] Hinton E. and Owen D.R.J. (١٩٨٤) **"Finite Element Software for Plates and Shells"**, Department of Civil Engineering, University College, Swansea, Pineridge Press Limited, U.K.

[١٥] Hossain S.J., Latifa S., Sinha P.K. (٢٠٠٤) **"A Doubly Curved Element for Laminated Composite Shells Undergoing Finite Rotation"**, Department of Aerospace Engineering, Indian Institute of technology, Kharagpur, W.B.-٧٢١٣٠٢, India.

[١٦] Huang H. - C. (١٩٨٩) **"Static and Dynamic Analysis of Plates and Shells"**, Department of Civil Engineering, University of Swansea, Springer-Verlag, London, U.K.

[١٧] Jaeger L. G. (١٩٦٤) **"Elementary Theory of Elastic Plates"**, Library of Congress Catalog Card No. ٦٣-١١٦١٠, Pergamon Press Limited, London.

[١٨] Kansara K. (٢٠٠٤) **"Development of Membrane, Plate and Flat Shell Elements in Java"** M.Sc. thesis, Virginia Polytechnic & State University, Blacksburg, Virginia, U.S.A.

[١٩] Karkush M. O. (١٩٩٨) **"Nonlinear Behavior of Folded Plate Structures"**, M.Sc. thesis, University of Babylon, Iraq.

[٢٠] Kerja I. and Schmidt R. (٢٠٠٤) **"Plastic Ductile Damage Evolution and Collapse of Plates and Shells"**, Aachen University of Technology, Germany.

[٢١] Kruzelecki J. and Trzeciak P. (١٩٩٩) **"Optimal Design of Rotationally Symmetric Shells for Inelastic Buckling under Hydrostatic Pressure"**, Cracow University of Technology, Poland.

[٢٢] Lund E. and Stegmann J. (٢٠٠٤) **"Structural Optimization of Composite Shell Structures using a Discrete Constitutive Parameterization"**, Institute of Mechanical Engineering, Aalborg University, Denmark.

[٢٣] McGowan D. M. and Anderson M. S. (١٩٩٧) **"Development of Curved-Plate Elements for the Exact Buckling Analysis of Composite Plate Assemblies Including Transverse Shear Effect"**, American Institute of Aeronautics and Astronautics, U.S.A.

[٢٤] Moshaiov A. and Vorus W. S. (١٩٨٦) **"Elasto-Plastic Plate Bending Analysis by a Boundary Element Method With Initial Plastic Moments"**, Int. J. Solids Structures, Vol. ٢٢, No. ١١, pp. ١٢١٣-١٢٢٩.

[٢٥] Moy S.S.J. (١٩٨٥), **"Plastic Methods for Steel and Concrete Structures",** Department of Civil Engineering, University of Southampton, Macmillan Publishers Limited, U.K.

[٢٦] Nasr M. N. B. and Pereira R. N. (١٩٩٥) **"Stability Analysis of Plates and Doubly Curved Shallow Shells using Finite Element Methods and Applications of MSC/NASTRAN"**, Technology Institute of Aeronautics, Brazil.

[٢٧] Nath Y. and Sandeep K. (٢٠٠٠) **"Nonlinear Analysis of Doubly Curved Shell: An Analytical Approach"**, Sadhana, India, Vol. ٢٥, Part ٤, pp. ٣٤٣-٣٥٢.

[٢٨] Ostwald M. (١٩٩٦) **"Multicriteria Optimization of Sandwich Cylindrical Shells under Combined Loads with Core of Different Mechanical Properties"**, Poznan University of Technology, Institute of Applied Mechanics, Poland.

[٢٩] Owen D. R. J. and Figueiras J. A. (١٩٨٣) **"Elasto-Plastic Analysis of Anisotropic Plates and Shells by the Semiloof Element"** International Journal for Numerical Methods in Engineering, Vol. ١٩, pp. ٥٢١-٥٣٩.

[٣٠] Owen D. R. J. and Figueiras J. A. (١٩٨٣) "**Anisotropic Elasto-Plastic Finite Element Analysis of Thick and Thin Plates and Shells**" International Journal for Numerical Methods in Engineering, Vol. ١٩, pp. ٥٤١-٥٦٦.

[٣١] Owen D.R.J. and Hinton E. (١٩٨٠) **"Finite Elements in Plasticity: Theory and Practice"**, Pineridge Press Limited, Swansea, U.K.

[٣٢] Papadrakakis M., Lagaros N. D., Tsompanakis Y. and Plevris V. (٢٠٠١) **"Large Scale Structural Optimization: Computational Methods and Optimization Algorithms"**, Archives of Computational Methods in Engineering. Vol. ٨, pp. ٢٣٩-٣٠١.

[٣٣] Rahmatalla S. (٢٠٠٠) **"A ٤-node Geometrically Nonlinear Degenerated Shell Element for Fabric Modeling"**, Virtual Soldier Research, The University of Iowa, U.S.A.

[٣٤] Reddy J. N. and Huang C. L. (١٩٨١) **"Nonlinear axisymmetric Bending of Annular Plates with Varying Thickness"** Int. J. Solids and Structures, Vol. ١٧, pp. ٨١١-٨٢٥.

[٣٥] Rich J. E. (١٩٩٧) **"Design Optimization Procedure for Monocoque Composite Cylinder Structures Using Response Surface Technique"** M.Sc. thesis, Virginia Polytechnic Institute and State University, U.S.A.

[٣٦] Rigo P. (٢٠٠١) **"Least Cost Structural Optimization Oriented Preliminary Design"**, The Society of Naval Architects and Marine Engineers, Michigan, USA, Paper ١٠.

[٣٧] Rozvany G. I.N. and Olhoff N. (٢٠٠٠) **"Topology Optimization of Structures and Composite Continua"**, ProceedingS of the NATO Advanced Research Workshop, held in Budapest, Hungary.

[٣٨] Save M.A. and Massonnet C.E. (١٩٧٢) **"Plastic Analysis and Design of Plates, Shells and Disks"**, North Holland Publishing Company-Amsterdam, London.

[٣٩] Sofistik (٢٠٠٢) **"Nonlinear Analysis of Plates and Shells"**, University of California, Berkeley, USA.

[٤٠] Stegmann J., Rauhe J.C., Rosgaard L. and Lund E. (٢٠٠١) **"Shell Element for Geometrically Nonlinear Analysis of Composite Laminates and Sandwich Structures"**, Institute of Mechanical Engineering, Aalborg University, Denmark.

[٤١] Sze K.Y. and Kim Y.H. (٢٠٠٢) **"Curved Quadratic Triangular Degenerated and Solid-Shell Elements"**, Department of Mechanical Engineering, The University of Hong Kong, Hong Kong.

[٤٢] Tong D., Williams R. L. and Agrawal S. K. (١٩٩٨) **"Optimal Shape Control of Composite Thin Plates with Piezoelectric Actuators"** Journal of Intelligent Material Systems and Structures, Vol. ٩, pp. ٤٥٨-٤٦٧.

[٤٣] Uchiyama M. and Yamada S. (٢٠٠٠) **"Nonlinear Buckling Simulation of Imperfect Shell Domes Using a Hybrid Finite Element Formulation and the Agreement with Experiment"**, Fourth International Colloquium on Computation of Shell & Spatial Structures, Chania-Crete, Greece.

[٤٤] Wang J.T., Johnson T.F., Sleight D.W. and Saether E. (٢٠٠١) **"Cryogenic Tank Structure Sizing with Structural Optimization Method"**, the American Institute of Aeronautics and Astronautics, Inc., No. ١٧

[٤٥] Zhiming Y. (١٩٩٥) **"Nonlinear Analysis and Optimization of Shallow Shells of Variable Thickness"**, School of Architectural Engineering. Computers and Structures, Vol. ٥٥(٢), pp. ٣٢٥-٣٣١.